FORM, SCALES AND OPTIMALITY IN THE BASIN LANDSCAPE AND ITS CHANNEL NETWORK

by

Ede Jorge Ijjász-Vásquez

Ingeniero Civil, Escuela de Ingenieria de Antioquia, 1987

Matemático, Universidad Nacional de Colombia, 1988

S.M. Civil Engineering, Massachusetts Institute of Technology, 1990

Submitted to the Department of Civil and Environmental Engineering in Partial
Fulfillment of the Requirements for the Degree of
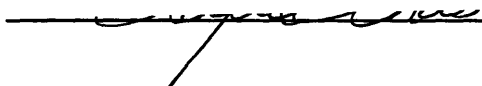
DOCTOR OF PHILOSOPHY

at the

MASSACHUSETTS INSTITUTE OF TECHNOLOGY

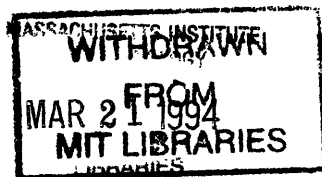February, 1994

Signature of Author_____
Department of Civil and Environmental Engineering
December 21, 1993

Certified by _____
Rafael L. Bras
Thesis Supervisor

Accepted by _____
Joseph Sussman, Chairman
Departmental Committee on Graduate Studies

Form, Scales and Optimality in the Basin Landscape and its Channel Network

by

Ede Jorge Ijjász-Vásquez

ABSTRACT

Based on data provided by Digital Elevation Maps (DEM), this work studies the basin landscape, its form and scales, the relationship to concepts of optimality in the channel network organization, issues of network growth, scaling properties in the geometry of the network and the spatial distribution of hydrologic variables in river basins.

The large amount of data in DEMs allows the study of the distribution of contributing area (a surrogate variable for mass) and energy in the basin. It is found that these distributions at the link level follow a power-law with common scaling slopes of 0.43 and 0.9 across different basins in the U.S. In order to study the physical processes leading to such organization, a simple model of landscape simulation and channel network growth is presented. The model is based on the observed scaling relationship between slopes and areas in the basin $S \sim A^{-\theta}$ and is called the Slope-Area model. It is shown that not only the spatial but also the temporal properties of the simulated structure present fractal distributions, which is common to self-organized critical systems.

Three principles of energy expenditure and their implications for the three-dimensional structure of river basins are examined. A random search algorithm to find the optimal channel network (OCN) that drains a given area is presented. OCNs are shown to reproduce common geomorphological characteristics of actual river basins. In order to predict the level of optimal energy for a basin at DEM resolution, a connection was made with the Slope-Area model because of the size restrictions present in the random search algorithm. It is shown how the basin in its evolution tends towards states of minimum energy expenditure linking OCNs with evolution models.

The implications of minimum energy expenditure on the shape of competing drainage sub-units that try to optimally allocate space among them in order to drain a given area were studied. It is shown that OCNs elongate with size and reproduce the observed behavior in actual basins known as Hack's law.

The planar geometry and planar oscillations of river courses are studied. The geometric scaling of rivers is shown to be self-affine and the scaling behavior is common across different basins. It is also shown that the parameter θ used in the Slope-Area model affects not only the vertical profile of rivers and energy distribution in the basin but it also influences the structure of the network and the tortuosity of rivers. The self-affine scaling of actual rivers is reproduced only when the appropriate value of θ is used in the model

2

showing the connection between the vertical dimension of the basin, the organization of energy and the planar form of rivers.

The spatial organization of energy, mass and slope in river basins is studied with the multifractal formalism. This analysis goes one step beyond the study of the geometric form of rivers and looks into important hydrologic variables. It is shown that the distribution of these variables has a multifractal scaling with a common spectrum across different basins.

The issue of hillslope and channel scales in the basin is also studied, given its importance in hydrologic applications of DEMs. Based on the behavior of the mean slope of points with common values of contributing area, four regions are identified in the basin. These regions are in increasing order of area: (1) convex hillslopes where diffusive sediment transport processes dominate, (2) concave hillslopes, (3) a region where hillslope and channel nodes with the same contributing area coexist but which can be differentiated using a threshold criteria previously proposed in the SIBERIA model of landscape evolution, and (4) channels with a large contributing area.

Finally, the convergent/divergent nature of hillslopes compared to the aggregate organization of the channel network is studied. The relationship with an observed break in the power-law behavior of the distribution of areas at small scales is analyzed. A landscape evolution model that takes into account the divergent geometry of hillslopes is presented.

Thesis Supervisor: Dr. Rafael L. Bras
Title: William E. Leonhard Professor of Civil and
                      Environmental Engineering

3

Acknowledgments

It is impossible to thank all the people who have helped me on the journey that ends with this work. To all those omitted my special gratitude.

I would like to thank my thesis and academic advisor, Professor Rafael L. Bras, for his guidance, advice and understanding. His words, and in many occasions his silence, helped understand and learn the art of scientific inquiry. Professor Ignacio Rodriguez-Iturbe is thanked for his enthusiasm, his avalanches of research avenues and his joy for discovery. I learned from him not to reinvent the wheel but to look at other areas of science for possible answers to our problems in hydrology. The other members of my doctoral committee: Professors Peter Eagleson, David Tarboton and Dan Rothman have contributed in various ways to this work. I would like to thank Professor Dara Entekhabi for his words of encouragement when I needed them the most. To all my other professors, and especially Maria de Losada, my gratitude and admiration.

The Parsons Lab is a place like no other at MIT because of its people. Many useful discussions with my friend Glenn Moglen have influenced this work. Jorge Ramirez and Pedro Restrepo are thanked for their help during the first semester at MIT. From the old crowd: Hari Rajaram, Garry Willgoose, Shafik Islam, Nalin Wikramanayake and many others, my gratitude. From recent generations, I would like to thank Stephen Tay, Lynn Reid, Fernando Miralles-Wilhelm, Elfatih El-Tahir, Vivek Kapoor, Kaye Brubaker, Guido Salvucci, Ying Fang, Kevin Johnson, Roseanna Neupauer, Shu-guang Li, Jeng-Jong Lee, Roland Springer, Mark French, Kelly Hawk, Steve Luis, Joshua Joseph, Cheo Lee, Margaret Talbott, Karsten Trulsen and everybody else.

My thanks to Elaine Healy for always keeping a smile and the dream alive of an office in a tropical island; to Carole Salomon for many laughs and good stories about Cartagena; and to Pat Dixon for always having a helping hand extended.

Finally, I have no words to thank my parents, Elod and Mercedes, and my sister, Enna, for their love, support and encouragement. This work would not have been possible without their love. I dedicate this thesis to them.

"Uncertainty is fruitful...
so long as it is accompanied
by the wish to understand"
                    Antonio Machado

                              "Every valley has been made
                        by its river, and the proportion
                        between valleys is the same as
                        that between river and river"
                                    Leonardo da Vinci

"When the river is flooded,
it's because it is raining,
and if you hear it making noise,
it's because it is carrying stones"
Traditional *vallenato* song.
Northern Part of Colombia.

                        "But then..." I ventured to remark,"
                     you are still far from the solution..."
                     "I am very close to one," William said,"
                                   but I don't know which."
                     "Therefore you don't have a single answer
                                        to your questions?"
                   "Adso, if I did I would teach theology in Paris."
                   "In Paris do they always have the true answer?"
                     "Never," William said," but they are very
                                     sure of their errors."
                   "And you," I said with childish impertinence,
                                     "never commit errors?"
                   "Often," he answered." But instead of conceiving
              only one, I imagine many, so I become the slave of none."
                           Umberto Eco, *The Name of the Rose.*

Table of Contents

7

List of Figures

11

13

14

List of Tables

Chapter 1

Introduction

1.1. Scope

The geometrical structure of river networks and the
properties of catchment landscapes have fascinated
hydrologists and geomorphologists for many years. Two
challenging avenues of research in the study of river basins
are, first, the understanding of the non-linear physical
processes that drive the system towards the current state of
the basin and generate the intricate forms of the network,
and, second, the analysis of the relationship between form
and hydrologic response. Furthermore, as the National
Research Council mentions in its report on opportunities in
the hydrologic sciences:

> " The search for an invariance property across
> scales as a basic hidden order in hydrologic
> phenomena, to guide development of specific
> models and new efforts in measurements is one
> of the main themes of hydrologic science"
> (National Research Council, 1991, p.197).

Scales, form and processes are the main themes of the present
work.

One key element of this work is the large amount of data
on the landscape of catchments now available through digital
elevation maps (DEM) which provide elevations in a grid,
usually 30m to a side. The ability to handle data at this

resolution allows us to move one step down in the level of aggregation of the analysis. From Horton's studies based on streams and Shreve's framework based on links, this work will move to the analysis of the network and the basin landscape at the scale of pixels. One of our objectives is to develop new characterizations of river basins that could be used both to understand and to infer the physical processes that lead to the observed behavior and to check the results of catchment evolution and channel network simulation models. We will look at the spatial organization, distribution and scaling of variables like contributing area (as a surrogate for flow), slope and energy, which are not topological but physically based and govern the geomorphic and hydrologic processes in the basin.

We will also develop in this work various models of landscape evolution and channel network growth with the purpose of obtaining some understanding of the physical processes and the non-linear interactions in the river basin, viewed as a dynamical system. Although these models can be perceived as very simplistic, the goal is to gain some predictive understanding of the key variables and the essential physics that could help in the development of more comprehensive models which require higher levels of complexity. The simplicity of the models to be presented will also permit the simulation of basins in large domains necessary in scaling studies.

1.2. Outline

We will try to present in this section a global description of the main questions to be studied in this work and the interrelationships between the various chapters in this report.

Chapter 2 is a literature review and analysis of previous work on the area of fluvial geomorphology. We have concentrated in this chapter only on those pieces of research that have been most influential on the questions posed and the results presented in later chapters. The review of previous work related to methods and tools developed in other areas, like physics and biology, is presented in the individual chapter where such tools are used.

Chapter 3 presents the characteristics of the data set of river basins to be used in this work, the data structure developed by Tarboton et al. (1989b) to analyze DEMs and a review of the handling procedures and general properties of DEMs.

Chapter 4 examines the distributions of mass and energy in river basins. These distributions are found to have a power-law behavior invariant over many spatial log-scales. This is one of the properties of self-organized critical systems. These are dynamical systems that evolve towards states characterized by fractal distributions in space and time. The question of whether the physical system behind the

evolution of the landscape has some of these fractal properties motivated the development of a simple model to be presented in chapter 5. Another result in chapter 4 is the existence of a break in the power-law behavior of the cumulative distribution of contributing areas at small scales. This fact will be used later in chapters 11 and 12, where processes at the hillslope scale are studied.

Chapter 5 presents a simple model of landscape simulation and channel network growth called the Slope-Area model. The model is based on the scaling relationship between slopes and areas observed in river basins. The simplicity of the model allows the analysis of large simulation domains and the study of spatial and temporal properties over various log-scales. It is found in chapter 5 that the simulated landscapes exhibit the three scaling properties commonly associated with self-organized critical systems.

Chapter 6 studies river networks from a different perspective. In this chapter we present an optimization method that allows the study of network structures, where three principles of energy expenditure originally proposed by Rodriguez-Iturbe et al. (1992b) hold true. These networks are called Optimal Channel Networks (OCN). The optimization method is analogous to the random search algorithm used in the classical traveling salesman problem. The structure of networks obtained by minimizing the energy expenditure reproduce common geomorphological measures, like Horton's

laws and the power-law distribution of areas studied in chapter 4. One of the implications of this chapter is that these measures are not the result of a random process but there is instead an important optimization component in network structures.

The optimization approach to the study of river networks only examines what should be the final equilibrium state of the network and not the processes that drive the system towards that state. In order to understand the relationship between evolution and energy minimization, chapter 7 takes the Slope-Area model and the OCN model described in chapters 5 and 6 and analyzes their relationship in terms of energy expenditure. It is shown that the values of total energy in networks simulated with these two models are very similar. An argument explaining how the landscape in its evolution prefers states of minimum energy expenditure is presented. This observation provides a way to examine the hypothesis that actual river systems optimize energy expenditure. Given that the random search procedure used in chapter 6 to construct OCNs is computer intensive, the largest domains that can be studied are of the order of 10^4 pixels. This size is about two orders of magnitude smaller than basins at the available resolution of DEMs. The Slope-Area model is used then as an intermediate step to check the optimal value of energy in large domains. Networks are simulated inside the domain of actual basins, using the Slope-Area model. The total energy expenditure of the simulated and the actual

networks are shown to be very similar, indicating that river basins appear to organize in states of minimum energy expenditure.

The OCN formalism is used in chapter 6 to analyze the internal structure of the optimal network given the domain it has to drain. Chapter 8 will examine instead the consequences of the optimality criteria when the dimensions and proportions of independent drainage sub-units are adjusted to drain optimally a larger area. The connection between optimal organization and Hack's law, a scaling relationship that quantifies the observation that river basins change their shape and become longer and narrower with size, is examined in this chapter. It is shown that the hypothesis that attributes the scaling behavior of Hack's law to the fractal nature of rivers is not entirely correct because of the elongation and change of shape of basins with size. It is proposed in chapter 8 that this elongation may be the result of optimal configurations of competing sub-basins.

Chapter 9 looks in more detail at the fractality of rivers in an effort to better describe quantitatively their tortuosity. This chapter shows that the geometrical structure of rivers has self-affine properties. The Slope-Area model is used to study the connection between the self-affinity of rivers and the scaling parameter between slopes and areas used in the driving mechanism of the model.

As hydrologists are interested not only in the geometrical form of rivers and their scaling properties but also in the spatial distribution of important hydrologic variables, chapter 10 uses tools from the multifractal formalism to study such distributions. This analysis goes one step beyond what is done in chapter 4, where no consideration is given to the spatial organization of the variables studied and only the lumped distribution is observed. In chapter 10 the similarities in the multifractal spectrum of the spatial distribution of contributing area, slope and energy across different basins in the U.S. are shown.

Most of the data analysis up to this point in the present work look at the entire landscape. However, for hydrologic applications it is very important to understand the difference between channels and hillslopes and their spatial organization. In practical applications of DEMs it is necessary to identify channel pixels because of the different way in which they respond hydrologically. Chapter 11 examines a threshold criteria proposed by Willgoose et al. (1991a) to differentiate between channels and hillslopes. The behavior of mean slope versus contributing area is used to infer the dominance of different processes at various scales. A modified version of the SIBERIA model developed by Willgoose et al. (1991a) is presented and the simulated landscapes are shown to reproduce the observed slope-area scaling behavior.

In chapter 12 the break in the power-law behavior of the cumulative distribution of areas observed in chapter 4 and one of the threshold criteria described in chapter 11 are used to guide a modification of the landscape evolution model presented in chapter 11. The objective is to show that the break in the distribution of areas is caused by a change in the spatial organization of drainage flow in the basin at the hillslope scale and at the channel scale. While channels are aggregating structures that collect water, hillslopes can be either divergent or convergent.

Finally, chapter 13 presents some concluding remarks and proposes some questions not addressed in the present work as possible avenues of future research.

Chapter 2

Literature Review

2.1. The Early Years

The extensive literature on the area of fluvial geomorphology eludes a complete and exhaustive review. Rather than trying to present everything that has been written, we will try to focus on those pieces of research that have been most influential in the development of the ideas to be presented in later chapters.

This work will concentrate on the analysis of the river basin as the geomorphic unit of interest, with its channel network and the surrounding hillslopes:

> "Every river appears to consist of a main trunk, fed from a variety of branches, each running in a valley proportioned to its size, and all of them together forming a system of valleys, communicating with one another..." Illustrations of the Huttonian Theory of the Earth by John Playfair. (Tinkler, 1985, p.59).

This work will not only concentrate on new characterizations of the river basin but it will also try to present evolution models to infer the processes behind our observations. We should probably go back to the work of W.M. Davis (1850-1934) and his scheme of landscape evolution called the "geographical cycle," which became the predominant paradigm in the geomorphology of the first half of the twentieth century.

Davis' ideal cycle of erosion begins with a rapid uplift of mass which is wasted by erosion as the basin passes through stages of youth, maturity and old age. The river basin goes from a stage with an imperfect channel network and many lakes, to a final stage called the peneplain where all the mass has been consumed. The key idea of the cycle is that by looking at the current properties of the landscape, it would be possible to infer its age (at least qualitatively) and its future evolution. The concept was analogous to Darwin's biological evolution which was very much in vogue at that time (Ritter, 1988).

Contemporary to Davis but working outside the paradigm of the geographical cycle we find G.K. Gilbert (1843-1918). His emphasis in studying landscapes was directed more towards how processes create the observed features rather than the placement of landforms in a certain historical sequence. Gilbert considered the observed features as the result of an equilibrium between erosive and resistive forces. Decades later his approach was praised by those who started the quantitative analysis of landscapes (Sack, 1992).

2.2. The Quantification of Geomorphology

One of the most influential papers in the quantification of geomorphology was the paper "Erosional development of streams and their drainage basins; hydrophysical approach to quantitative morphology" by R.E. Horton, published in 1945. In this paper Horton, a hydrologist, brought an entirely new

set of tools, from hydraulics to statistics, to the study of quantitative geomorphology (Morisawa, 1985). The emphasis in this paper was on the study of infiltration, runoff and slope properties as key parameters of channel initiation. Also, Horton presented a complete statistical analysis of the network structure (Ritter, 1988).

The paper by Horton inspired A.N. Strahler and his group of students at Columbia University, as well as L.G. Leopold and coworkers at the U.S. Geologic Survey, to develop a quantitative study of geomorphic forms. Strahler announced his programme in a controversial paper (Strahler, 1950) where the ideas of Gilbert and Horton were exalted against the denudation cycle of Davis (Kennedy, 1992). The group of students at Columbia included names like Chorley, Schumm, Melton, Morisawa and Woldenberg whose work will be reviewed later in this chapter. An interesting review of these years is presented in Strahler (1992).

Horton (1945) introduced a way to classify and order the various streams of channel networks. Strahler (1952) later revised the scheme in a footnote making it purely topological. The network is seen as a rooted tree. Nodes are defined as points where two river segments merge or a river is initiated. In the latter case the node is called a source node. Streams and their corresponding order are defined as follows:

1) Segments initiated at a source are assigned order one.
2) When two streams of order ω join, a stream of order $\omega+1$ is created.
3) When two streams of different order join, the stream with higher order continues down the tree.

This way of classifying streams allows the statistical analysis of mean properties of the families of segments with the same order. Horton (1945) found that mean properties of streams (for example number, length, areas and slopes), grouped by order, behaved approximately in a geometric fashion:

$$\frac{N_{\omega-1}}{N_\omega} = R_b \quad ; \quad \frac{\overline{L_\omega}}{\overline{L_{\omega-1}}} = R_L \quad ; \quad \frac{\overline{A_\omega}}{\overline{A_{\omega-1}}} = R_A \quad ; \quad \frac{\overline{S_\omega}}{\overline{S_{\omega-1}}} = R_S \quad (2.1)$$

where N_w, L_w, A_w and S_w are the number, mean length, mean area and mean slope of the streams of order ω. R_b, R_L, R_A and R_S are called Horton's bifurcation, length, area and slope ratio and their values in actual basins are usually around 4, 2, 4 and 2 respectively. The law of areas was more precisely formulated by Schumm (1956). Although Horton's laws have been criticized, especially because of the large amount of averaging implied by the ordering scheme, they remain one of the key descriptors of network topology.

Another important property of the catchment defined by Horton (1945) is the drainage density:

$$D = \frac{L_T}{A_\Omega} \quad (2.2)$$

29

where L_T is the total length of channels within a basin of order Ω and total area A_Ω. The drainage density is one of the fundamental scales of drainage basins because it determines the limit of the extension of the drainage network.

Horton (1945) also proposed a law for the angle θ at which a tributary enters a main stream (see Figure 2.1):

$$\cos \theta = S_M / S_T \qquad (2.3)$$

where S_M and S_T are the slopes of the main channel and the tributary. Howard (1971a) posed a different criteria which appears to work better for streams of similar size that join at an angle θ. If θ_1 and θ_2 are the angles between the incoming and the outgoing streams (i.e. $\theta=\theta_1+\theta_2$, see Figure 2.1) then Howard proposed:

$$\cos \theta_1 = S_3/S_1 \qquad\qquad \cos \theta_2 = S_3/S_2 \qquad (2.4)$$

where S_1 and S_2 are the slopes of the incoming streams and S_3 the slope of the outgoing stream. Relationship (2.4) was related to minimum power loss at the stream intersection (Howard, 1971b).

In 1948 J.H. Mackin introduced the idea of a graded river where the slopes and other channel characteristics are adjusted to give the river precisely the velocity necessary to carry the sediment out of the basin, i.e. it is a system in equilibrium (Mackin, 1948). Although qualitative (Morisawa, 1988), Mackin's paper presented a number of ideas
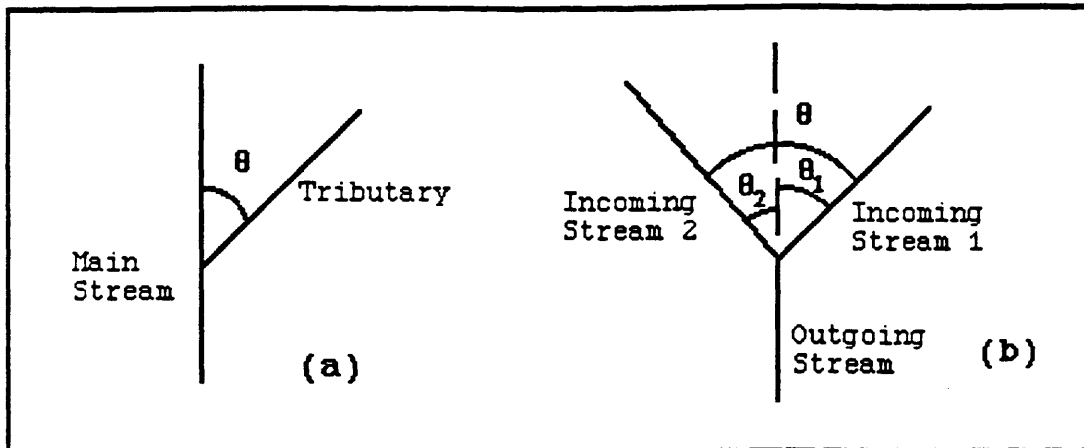
Figure 2.1: Angles in (a) Horton's and (b) Howard's junction models (adapted from Abrahams, 1984).

later analyzed with much greater rigor by Leopold and Maddock (1953) and Leopold and Miller (1956). In these papers, the hydraulic geometry of channels was thoroughly investigated and many experimental relationships were measured in the field, for example:

$$w \sim Q^b \qquad d \sim Q^f \qquad v \sim Q^m \qquad S \sim Q^{-\theta} \qquad (2.5)$$

where w, d, v, S and Q are channel width, depth, velocity, slope and discharge respectively and the measurements are taken at discharges of the same frequency at different points in the network. The mean values of the exponents b,f,m and θ were found to be around 0.5, 0.5, 0.1 (i.e. velocity is approximately constant in the network) and 0.5 respectively. Tarboton et al. (1989a) found a value of θ of 0.5 in the analysis of drainage networks obtained from digital elevation maps using contributing area as a surrogate for flow. Flint

(1974) related the slope-flow scaling relationship to
Horton's slope and area laws.

In 1947 Langbein et al. introduced the non-dimensional
hypsometric curve. This curve shows the proportion of area
above a certain percent elevation, where the percent
elevation is equal to the elevation above the outlet divided
by total relief. This curve is a combination of both the
slope-area relationship $(S{\sim}A^{-\theta})$ and the network structure
which aggregates contributing area. The hypsometric curve has
been used as a tool to examine age of river basins as shown
in Figure 2.2 (Schumm, 1956). However, the hypsometric curve
may also reflect the degree of tectonic activity in the basin
(Scheidegger, 1977, Willgoose et al., 1989).
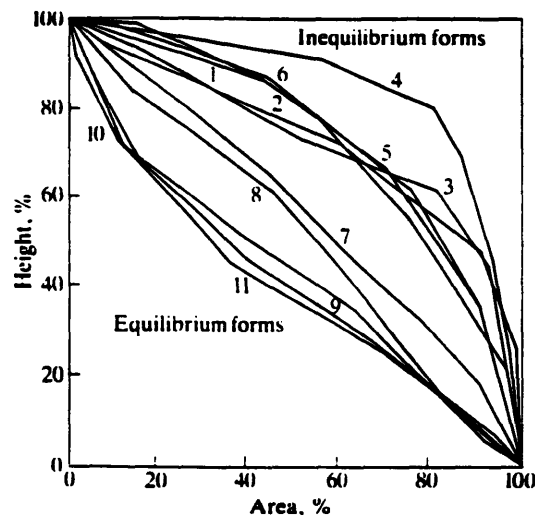
Figure 2.2: Hypsometric curves from sub-
basins in the Perth Amboy Badlands, New
Jersey. Numbers increase from youthful to
mature basins (from Schumm, 1956).

32

In 1957 Hack studied the relationship between the length L of the main channel and the area A of the basin and found a scaling behavior of the form $L \sim A^{\alpha}$ with $\alpha = 0.6$. Grey (1961) confirmed the result with $\alpha = 0.568$. Hack explained the value of α greater than 0.5 as a result of the elongation of basins with larger area.

2.3. The Topological Random Model

In 1966 Shreve introduced the concept of link as the section of channel between two forks (points of confluence of two channels) or between a source (point furthest upstream of a channel network) and a fork. The former segments were called interior links and the latter exterior links. The magnitude of the network was defined as the number of exterior links. Shreve (1966) used the concept of link as the basic unit of the channel network instead of using the stream and introduced the random topology model. The main idea was to consider all topologically distinct channel networks (TDCN) with the same number of links to be equally likely and to use combinatorial graph theory to study average properties of such a family of networks. Notice that link-based analysis of channel networks is much more disaggregate than stream-based analysis.

The most probable set of stream numbers in a TDCN family (in which its members have the same number of links) follows approximately Horton's law of stream numbers. Shreve (1967,

1969) and Smart and Werner (1976) added a second postulate which assumed that interior and exterior links had separate distributions of length and area which are independent of location. These distributions have usually been assumed to be exponential or gamma. With the second postulate, Horton's length and area laws can be obtained as the most probable behavior in a TDCN family. Other properties that do not depend on orientation are well described by the random topology model as either the most probable or the average behavior of a TDCN family.

Numerous tests have been devised to check the postulates of the random topology model. The tests that this model has not been able to pass when compared to actual networks are usually related to orientation. A classical example is the distribution of cis and trans links, defined by James and Krumbein (1969) analogously to the definition in organic chemistry. The idea is to look at which side the tributaries that bound a certain link in the channel under study are coming from. If both tributaries come from the same side, the link is called cis. If the tributaries come from opposite sides the link is defined as trans. A bias was found in the distribution against short cis links but not against short trans links. Also there were many more trans links than cis links. Other more complicated link classifications proposed by Mock (1971) also showed divergence from the random topology model. Most of the differences appear to be related

to space-filling constraints and network development dynamics. An excellent review is presented in Abrahams(1984).

2.4. The Hydrologic Response of the Basin and Geomorphology

Hydrologists have recently been using a different approach in an effort to establish a link between the geomorphological characteristics of a basin and its hydrologic response. This approach consists of using a linear transport assumption and the random topology model to find the mean ensemble response.

The first attempt in this direction was the geomorphologic instantaneous unit hydrograph (GIUH) introduced by Rodriguez-Iturbe and Valdes (1979) and restated by Gupta et al. (1980). The GIUH was seen as the probabilistic distribution that a raindrop that fell in the basin would reach the outlet at a certain time. The network was divided into states corresponding to streams of different orders. The movement of drops between streams was defined in terms of transition probabilities between states. The drop would fall in a state with certain probability (measured according to area) and follow a Markov chain through higher states until reaching the outlet. Using Horton's laws, expressions can be found for the GIUH and simplified regressions for peak discharge and time to peak have been performed (Rodriguez-Iturbe and Valdes, 1979).

Gupta and Waymire (1983) argue that the Strahler ordering is a coarse characterization and propose to use links instead of streams for the geomorphologic study of the basin response. The basic tool is the width function (Surkan (1968), Calver et al. (1972), Kirkby (1976)). This function measures the number of links $N(x)$ at a topological distance x from the outlet. If the velocity in the network is constant, the width function, when rescaled appropriately, is precisely the instantaneous unit hydrograph. The idea is to find the average width function for a family of random networks that share certain property. In order to do that, it is useful to see the second postulate of the topological random model from a different point of view. Gupta and Waymire (1983) showed the second postulate to be equivalent to having sources and forks occurring independently of one another and with an equal probability of one-half. Therefore, the topologically different networks can be seen as the graph of a birth and death Markov process, growing from the outlet upward with exponential lifetimes for the individuals of the population (links in this case). Mesa (1986) and Troutman and Karlinger (1984, 1985, 1986) studied the ensemble average of the width function given magnitude and diameter for a birth and death process.

Mesa (1986) also analyzed the vertical dimension of the network which is important when considering energy in the basin. He defined the link concentration function (lcf) in an analogous way to the width function. The lcf $N(h)$ counts the

number of links crossing the elevation contour h. Mesa (1986) showed that a homogeneous birth and death process was not a good representation of N(h), due to the concavity of rivers. Gupta and Waymire (1989) suggested a self-similar model for link drops that was based on the slope-area relationship $S \sim A^{-\theta}$. This model implied that the moments of the slope distribution would scale as $-k\theta$ where k is the order of the moment. Tarboton et al. (1989a) argued for a different type of scaling based on DEM analysis.

2.5. Modeling of Networks, Hillslopes and Landscapes

Another active area of research in geomorphology has been the modeling of networks, hillslopes and landscapes. Random models tied to space (i.e. not topological) have been formulated by various authors. Most of them belong to the random walk class. The first model was developed by Leopold and Langbein (1962) where source points are selected at random and the walker wanders randomly until it reaches another stream or the boundary. Scheidegger (1967) restricted the walker's possible directions to only two in order to study tributaries to a main stream. A different approach was formulated by Howard (1971a) where the network develops by headward growth and branching. The model was improved by including stream capture and the law of angles between tributaries shown in Equation (2.4) (Howard, 1990).

The evolution and recession of slopes have also been modeled by numerous authors (see Scheidegger (1970) for a

review). Ahnert (1976) developed a slope model that included many transport processes (splash, wash, soil creep, etc.) as well as modes of weathering (mechanical, chemical or combined). His main interest was to model not only the form of the slope but also the waste cover. Kirkby (1971) proposed a sediment continuity equation of the form $\partial z/\partial t = \partial Q_s/\partial x$ where Q_s is a sediment transport law, z elevation and x the location along the hillslope. The form suggested for the sediment transport was $Q_s \sim Q^m S^n$ where Q is discharge, S slope and m and n are coefficients dependent on the governing process (e.g. 0.0 and 1.0 for soil creep, 1.3.-1.7 and 1.3-2.0 for soil wash, 2.0-3.0 and 3.0 for channels, respectively). If tectonic uplift T is included, then equilibrium forms can be found using:

$$\frac{\partial z}{\partial t} = 0 = T - \beta Q^m S^n \qquad (2.6)$$

where $Q=Rx$, $S=\partial z/\partial x$ and R is excess rainfall. The solution to the equation is:

$$z = z(0) - \left[\frac{T}{\beta R^m}\right]^{1/n} \left[\frac{n}{n-m+1}\right] x^{-(n-m+1)/n} \qquad (2.7)$$

and therefore:

$$S = \frac{\partial z}{\partial x} = - \left[\frac{T}{\beta R^m}\right]^{1/n} x^{(1-m)/n} \qquad (2.8)$$

Figure 2.3 from Kirkby (1971) shows the equilibrium profiles for different values of m and n. If one notices that x corresponds to the contributing area, then Equation (2.8)
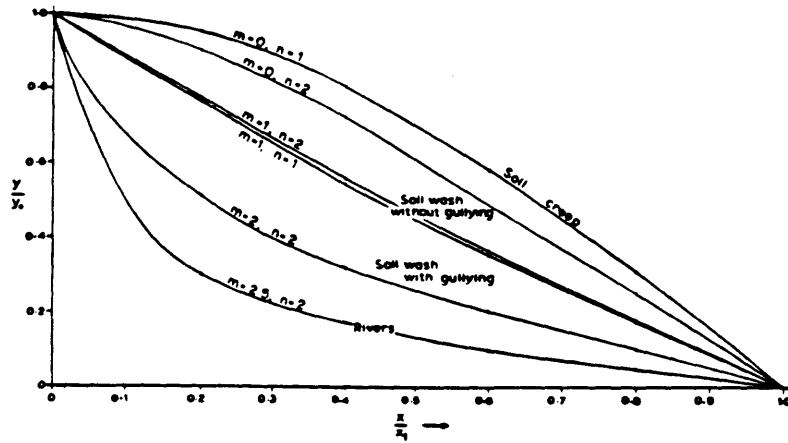
Figure 2.3: One-dimensional equilibrium profiles for sediment transport of the form $\beta Q^m S^n$ (from Carson and Kirkby, 1972).

is the slope-area relationship observed in rivers with $\theta=(1-m)/n$. Also, if $m>1$, the equilibrium profile is concave and if $m<1$ it is convex.

The natural extension of hillslope models is the analysis of the entire three-dimensional catchment. Smith and Bretherton (1972) studied the stability of landscapes using an equation of sediment transport of the form:

$$\frac{\partial z}{\partial t} = -\nabla . \mathbf{n} \, Q_s \qquad (2.9)$$

where

$$\mathbf{n} = -\frac{\nabla z}{|\nabla z|} \qquad (2.10)$$

and Q_s, the function that represents sediment transport, depends on slope $S=|\nabla z|$ and discharge Q, which can also be

39

parameterized as r*A where r is a measure of mean excess rainfall and A is contributing area defined as:

$$\nabla \cdot \underline{n}\, A = 1 \qquad\qquad (2.11)$$

Using a linear stability analysis, it can be shown (Smith and Bretherton (1972), Tarboton et al. (1989b, 1992), Loewenherz (1991)) that the landscape is unstable when:

$$Q_s - a\,\frac{\partial Q_s}{\partial a} < 0 \qquad\qquad (2.12)$$

If Q_s is assumed to have the form $\beta Q^m S^n$, then condition in Equation (2.12) is equivalent to have m>1, which as we saw in Equation (2.7) is equivalent to a concave profile. A different model is presented in Luke (1974).

The criteria implied by Equation (2.12) (a change in profile from convex to concave with increasing area) was used by Tarboton et al. (1989a) to determine the location of channel heads. In a log-log diagram of link slopes versus areas, the change from stable slopes to unstable rills and channels would manifest itself in a break of the slope-area relationship. Dunne and Aubry (1986) and Loewenherz (1991) argue for a stabilizing effect of sheetwash flow that would move the head of channels downhill from the observed slope-area break. The latter author presents a more detailed and rigorous stability analysis of the original Smith and Bretherton (1971) formulation.

Models of landscape evolution have been developed by Cordova, Rodriguez-Iturbe and Vaca (1982) and Roth et al. (1989) using fluvial transport equations. Willgoose, Bras and Rodriguez-Iturbe (1990 a,b,c,d) present a model where hillslopes and channels are explicitly differentiated through a channel initiation function. The evolution of the model is driven by:

$$\frac{\partial z_i}{\partial t} = T + \sum_j Q_j^m S_j^n f(Y_i) + D_z \frac{\partial^2 z_j}{\partial x_j^2} \qquad (2.13)$$

where Y is an indicator function that moves from a value of zero (at hillslopes) to a value of one (at channels) whenever the channel initiation function (a measure of processes that tend to promote channelization parameterized as $\beta_2 Q^{m_2} S^{n_2}$) exceeds a certain threshold. The function $f(Y)$ is used to represent the different sediment transport coefficients for hillslopes and channels ($f(Y)=\beta$ for channels and $f(Y)=O_t\beta$ for hillslopes with $O_t<1$). The third term represents diffusive processes like rainsplash, rock slides, etc. Other details of this model will be reviewed in later chapters of this report. This model by Willgoose et al. (1990a) is able to simulate natural looking channel and reproduce the values observed in nature of the most common geomorphological statistics. The effect of a subsurface saturation mechanism instead of the original Hortonian runoff production was investigated in Ijjasz-Vasquez et al. (1992).

In the experimental side of basin evolution research it is important to mention the work that began in 1969 at Colorado State University where a series of studies of drainage basin evolution in their rainfall-erosion facility was initiated. This facility of 9m wide, 15 m long and 1.8m deep was used to analyze the evolution of drainage systems, to study the influence of slope and relief on the developing network and to understand the effect of baselevel lowering among other effects. A complete review of the results can be found in Parker (1977) and Schumm et al. (1987).

2.6. Scaling in Networks

Recently, new characterizations of the channel network and the landscape based on ideas of scaling and fractals (Mandelbrot, 1977, 1983) have been developed. Mark and Aronson (1984) and Culling and Datko (1987) looked at the fractal dimension of the landscape and found different values at large and small scales.

Tarboton et al. (1988) and La Barbera and Rosso (1989) examined the fractal dimension D of the network in terms of Horton's numbers and the fractality of individual channels expressed as:

$$D = D_l \frac{\log R_b}{\log R_l} \tag{2.14}$$

where the value of D_l (the fractal dimension of individual river courses), calculated with the box counting algorithm,

was found to be around 1.1. This value was used to explain Hack's law of elongation. We will examine this issue in more detail in Chapter 8.

Finally, as mentioned in Section 2.3, scaling in the third dimension of river basins has been investigated by both Gupta and Waymire (1989) where a self-similar model of slope scaling versus area was proposed and by Tarboton et al. (1989) where a multi-scaling model was proposed. The difference resides in the way different moments of the distribution of slopes scale with contributing area.

The present work will develop many of the issues introduced in this chapter and try to develop new characterizations of the river basin using the data now available with digital elevation maps. The goal is to move into more disaggregate measures away from streams and links and looking at the entire landscape at a small resolution.

Chapter 3

Digital Elevation Maps

The analysis of basin landscapes and channel networks in this work will use elevation data from Digital Elevation Maps (DEM). In this chapter we will present a small review of current methodologies for analyzing DEM data, the data structure and programs developed by Tarboton et al. (1989b) used in this work, and the basic characteristics of the river basins analyzed in later chapters.

Digital Elevation Maps provide elevation data over a rectangular grid usually 30 m to a side. Each rectangular component of the grid is termed a pixel. Numerous methods have been proposed to recognize the location of valleys, their extension and the location of drainage lines.

One of the first methods was proposed by Peucker and Douglas (1975). They identified valley pixels using the elevation of neighboring pixels to check for 'v-' shaped profiles. An efficient way to identify these pixels is by passing a 2x2 window and flag the highest pixel of the four. The unflagged cells are defined as the valley lines. Unfortunately, the method does not assure a continuous network nor single-pixel channels. Band (1986) presents some rules for connecting the network. Tribe (1991, 1992) proposes

a related method using wider windows and a threshold slope
for accepting 'v-' shape profiles.

Another method, and probably the most commonly used, was
proposed by Mark (1984) and O'Callaghan and Mark (1984). The
method consists in assigning to each pixel a drainage
direction based on the steepest direction. Using these
directions, a cumulative area is assigned to each pixel by
counting the number of pixels that would flow through it
following the drainage lines. The calculation of areas is
done recursively in the algorithm of Tarboton et al. (1989b)
rather than iteratively as originally proposed. Finally, the
drainage network is defined as the set of pixels with
contributing area above a certain threshold value. This
criteria assures a connected network. This method has been
used by numerous researchers (Band (1986, 1989), Jenson and
Domingue (1988), Morris and Heerdegen (1988) and Tribe
(1991)). Tarboton et al. (1989a) present a criteria for
finding the threshold value based on a break on the scaling
behavior between slopes and contributing areas in the basin.

There are two other problems with the method of
O'Callaghan and Mark (1984). First, digital elevation maps
have many pixels (and sets of adjacent pixels) surrounded by
neighbor pixels with higher elevations. These lower pixels
are termed pits. The drainage network cannot flow out of them
and spurious "lakes" are formed. The most common method to
remove pits is by finding the pit's outflow point and then

increase the height of the pit to overflow it (Tarboton et al, 1989b). The second problem is to determine the flow direction of pixels in flat areas. The resolution of the DEM is in meters making it impossible to find the proper drainage direction in areas with small slopes like floodplains. Different researchers use different rules usually not clearly explained. Tarboton et al. (1989b) use a rule to handle floodplains where directions are assigned iteratively towards neighbors whose direction has already been defined. In this way the pixels in the flat areas point toward the outflow pixel of the region without creating loops. However, this method creates parallel flow lines in a few cases around the main channels in some of the basins as are shown later in Figure 3.1. This is unrealistic and prevents the use of the DEMs analyzed in this work for the study of features like meandering. We believe these two problems are minimal in the regions studied in this work because the basins chosen have enough relief to be detected in the DEM without much uncertainty. The appropriateness of this method in mountainous regions has been discussed by Tribe (1992).

The grid structure of DEMs is not the only form in which elevation maps are provided. Two other possibilities include triangular irregular networks (TIN) (Palacios-Velez and Cuevas-Renaud, 1986) or contour based DEMs (Moore et al., 1988). Some authors claim that the presence of pits is the result of an incorrect data structure like grid DEMs (Tribe,

1992). However, most of the data available comes in the rectangular matrix structure.

The elevation data used in this work was provided by the U.S. Geological Survey at either of two resolutions: 7.5. minute quadrangle in a 30 m grid or 1 degree quadrangle on a 3 sec arc grid. The accuracy of the first set is quoted to be 7 m of root mean square error. This is the difference between the true elevation and the linearly interpolated elevation from the DEM for benchmark points. The second set has a quoted absolute vertical accuracy of ±30 m relative to mean sea level. However, since the analysis of this work is entirely based on relative elevation within the basin, we are interested in the relative accuracy and not the absolute. The U.S.G.S. claims that the relative vertical accuracy conforms to the actual hypsographic effects. Tarboton et al. (1989b, 1992) and Lee et al. (1992) study the effect of accuracy on certain aspects of the analysis of basin landscapes with DEMs.

The basins used in this work have been processed from the raw DEM data into a usable data set by Tarboton et al. (1989b). Table 3.1. shows the properties of the ten river basins located across the US which will be used in the present work. Figure 3.1. shows the boundaries and channel networks of these basins.

Beaver Creek $A_t=150$

Brushy Creek $A_t=250$
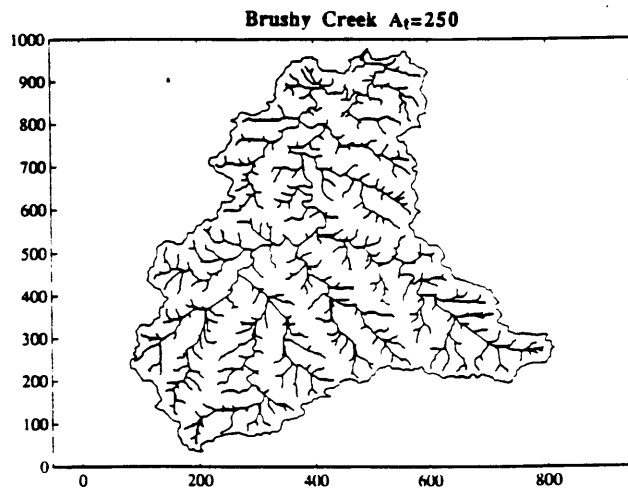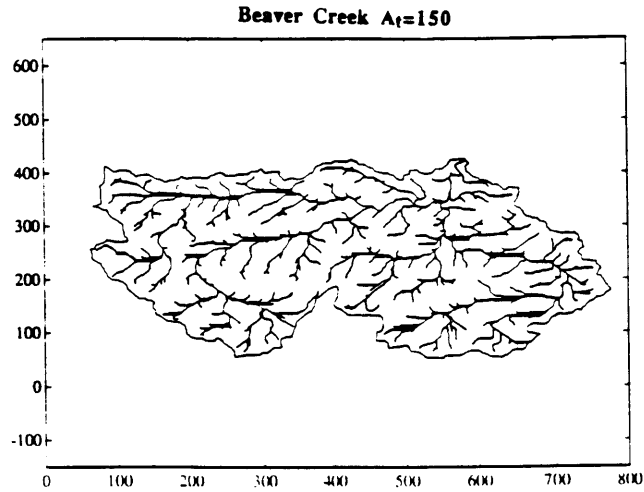
Figure 3.1: Boundaries and channel networks (defined using a threshold value of contributing area) for the DEMS used in this work (continues).

Big Creek A_t=200

Schoharie Creek Headwaters A_t=100

East Delaware River A_t=200

Figure 3.1: (contd.)

North Fork Cour d'Alene River $A_t=100$

Buck Creek $A_t=500$

Racoon Creek $A_t=500$

Figure 3.1: (contd.)

Schoharie Creek $A_t=400$

St. Joe River $A_t=350$
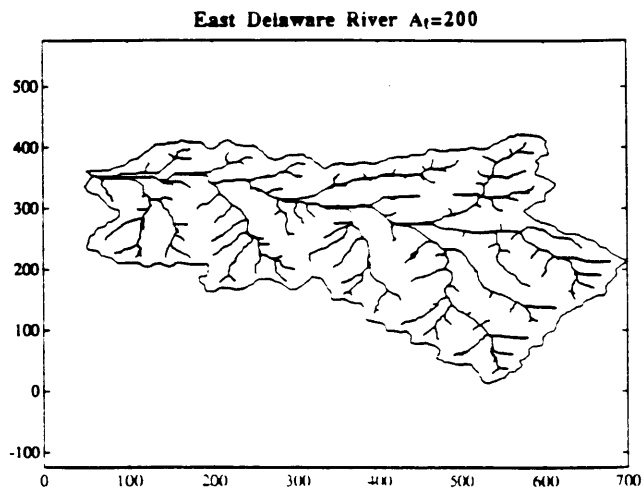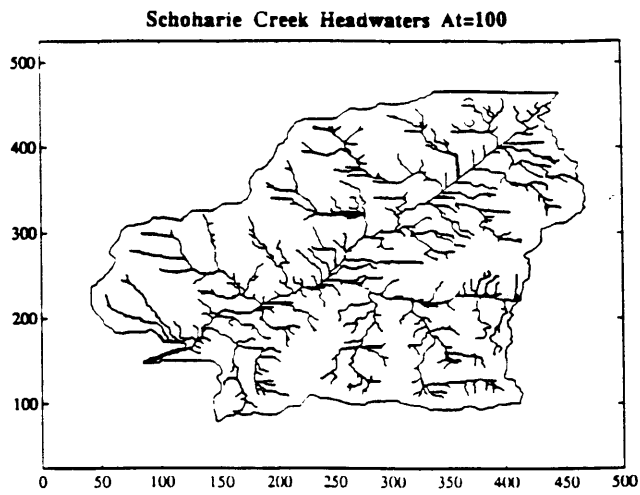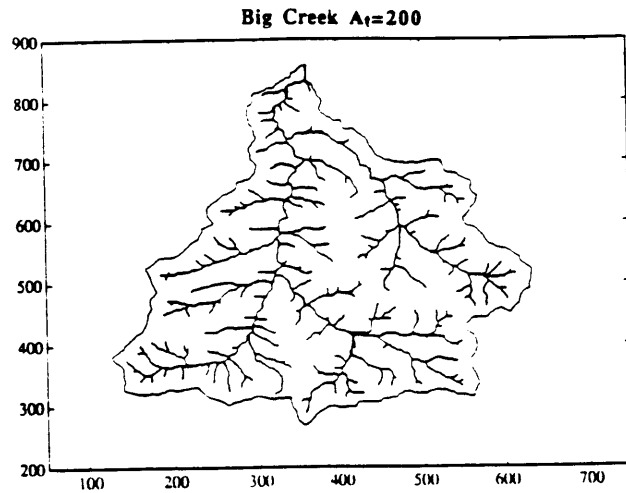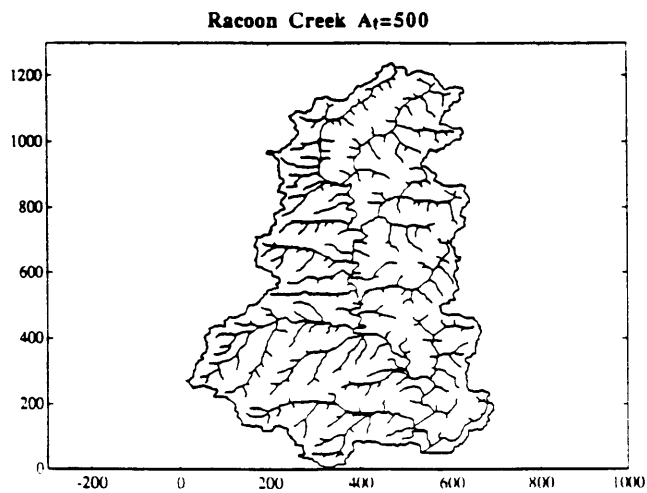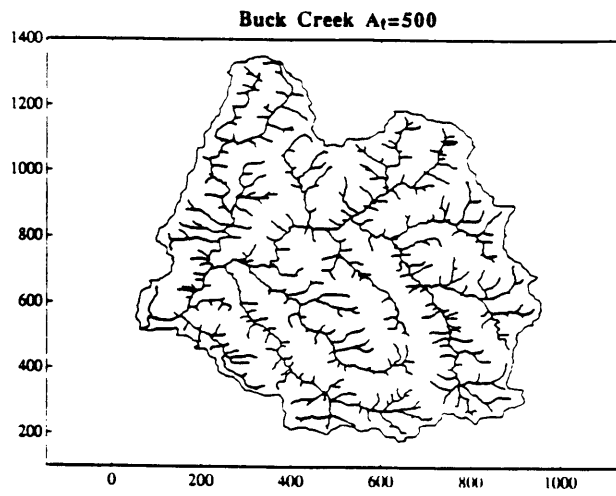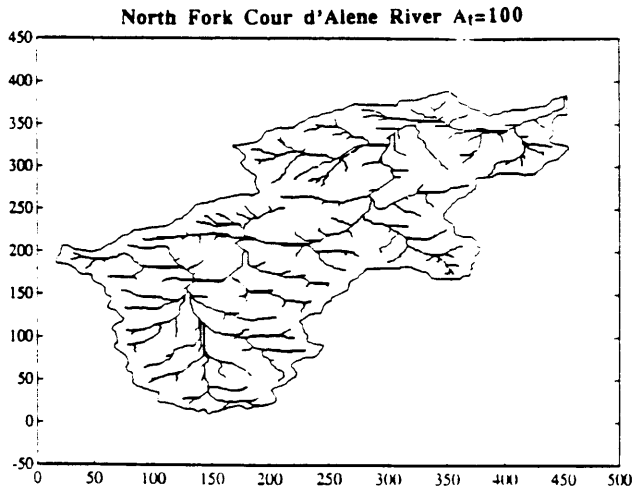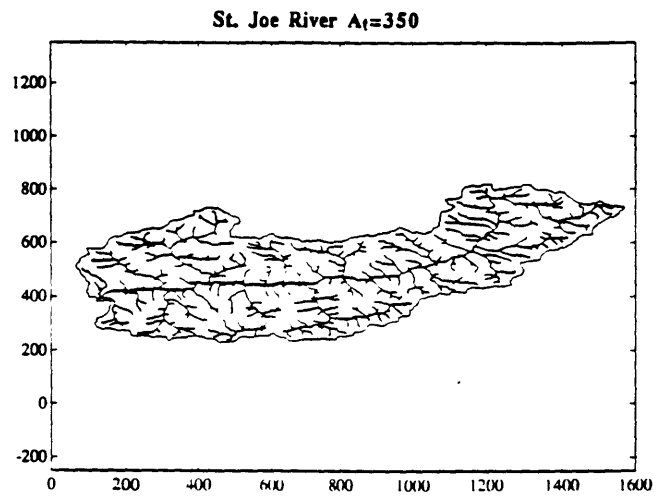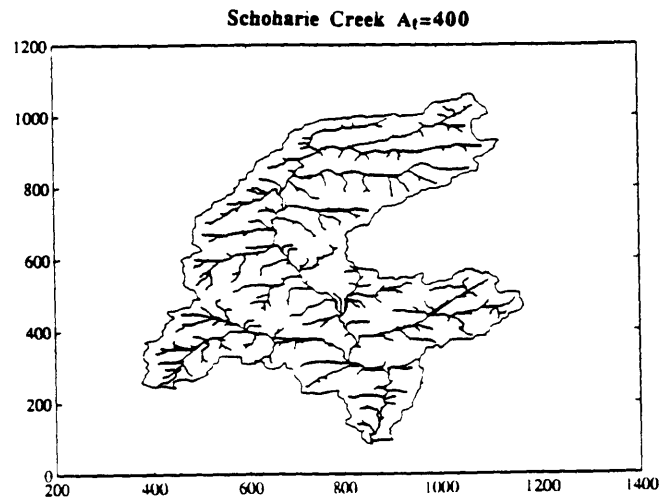
Figure 3.1: (contd.)

Basin	Map Quadrangles Used	Location	Area (km^2)	Pixel Size (mxm)
Beaver Creek	Canton E	PA,OH	1223	70.5x92.67
Brushy Creek	Upshaw, Houston, Graytson, Massey, Moulton, Addison	AL	322	30x30
Buck Creek	Gasquet SW and SE Ship Mtn NW, NE SW and SE, Dillon Mtn. NW and SW, Preston Peak SW	CA	606	30x30
Big Creek	Calder NW, NE, SW and SE	ID	147	30x30
East Delaware River	Binghampton	NY	933	68.3x92.67
Schoharie Creek Headwaters	Hunter, Kaaterskill	NY	98	30x30
North Fork Cour d'Alene River	Spokane	ID	440	62.6x92.67
Racoon Creek	Hookstown, Midway Burgettstown, Clinton Alquippa, Avella	PA	448	30x30
Schoharie Creek	Binghampton	NY	2408	68.3x92.67
St. Joe River	Spokane E Hamilton W,Wallace W	MO,ID	2834	62.2x92.67

Table 3.1: Characteristics of river basins analyzed in this work.

Chapter 4

Power-law Distributions of Contributing Area

and Energy in River Basins

4.1. Power-law Distributions in Spatially Extended Systems

It has been shown recently (Bak et al, 1987, 1988) that many spatially extended dynamical systems evolve naturally towards a critical state with no characteristic time or length scale. These systems have been called self-organized critical systems. The system at the critical state presents a scale-invariant (fractal) structure which manifests itself into power-law distributions.

One of the first models that motivated the study of power-law distributions in spatially extended systems and the relationship to the dynamics of the system is a very simple sandbox model developed by Bak et al. (1987, 1988). In this model avalanches of sand are modeled using a threshold rule. Whenever the slope at a point exceeds a threshold value, grains of sand are distributed to neighbor pixels. This movement could make the slopes of neighbor pixels exceed the slope threshold and could cause an avalanche. Many of the avalanches are small but a few are as big as the entire domain. The distribution of these sizes follows a power-law indicating that there is no characteristic scale in the

avalanche process between the grid size and the entire domain.

Another system that shows power-law distributions, at least in space, is Scheidegger's (1967) stochastic model of river networks, as shown in Takayasu et al. (1988). In Scheidegger's model, every point in a triangular grid is connected with its left or right neighbor downstream with equal probability of one-half. In this way a network is constructed (see Figure 4.1). Takayasu et al. (1988) examined the distribution of sizes of sub-basins draining to the lower boundary (like the one highlighted in Figure 4.1) and found a power-law behavior of the form:

$$P[A>a] \sim a^{-\beta} \qquad (4.1)$$

with $\beta=1/3$. Dhar and Ramaswany (1989) proved that the value of β was precisely 1/3 and this model, along with some
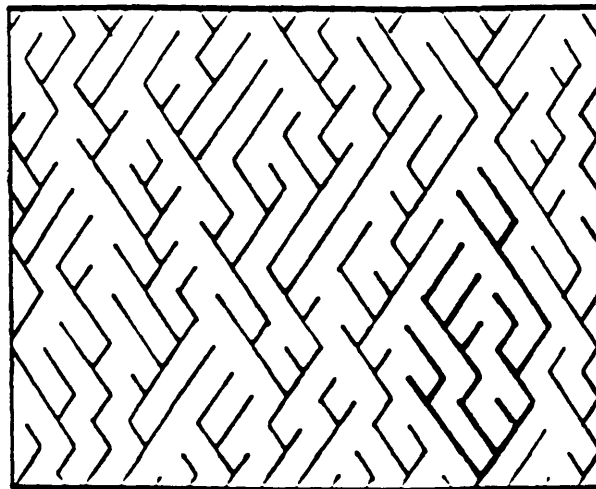
Figure 4.1: Dendritic structure formed by Scheidegger's (1967) stochastic river model (from Takayasu et al, 1988).

Abelian group models, is one of the very few self-organized critical systems where a theoretical proof of the power-law nature of the distribution exists and the value of the scaling exponent can be derived.

4.2. Power-law Distribution of Contributing Areas in River Basins

The behavior of Scheidegger's model motivated us to examine what is the distribution of sub-basin sizes in actual basins. Using DEM data, river networks were identified for different catchments. The cumulative distribution of contributing areas to each link of the networks (which is a measure of the size of the sub-basin draining through that link) is presented in Figure 4.2 (Rodriguez-Iturbe et al, 1992a) for the basins in our data set. The distribution follows a power-law of the form (4.1) but with a value of β around 0.43 for the basins in our data set. Table 4.1 shows the values of β for various basins. The break in the power-law at large areas appears to be a finite size effect and it is also observed in models like Bak's sandbox. The power-law character of the distribution of contributing area and its scaling exponent serves then as a test of networks generated by simulation models when they are compared to actual networks. For example, although Scheidegger's model presents a power-law distribution of areas, the scaling exponent β is much smaller than the value found for natural basins.
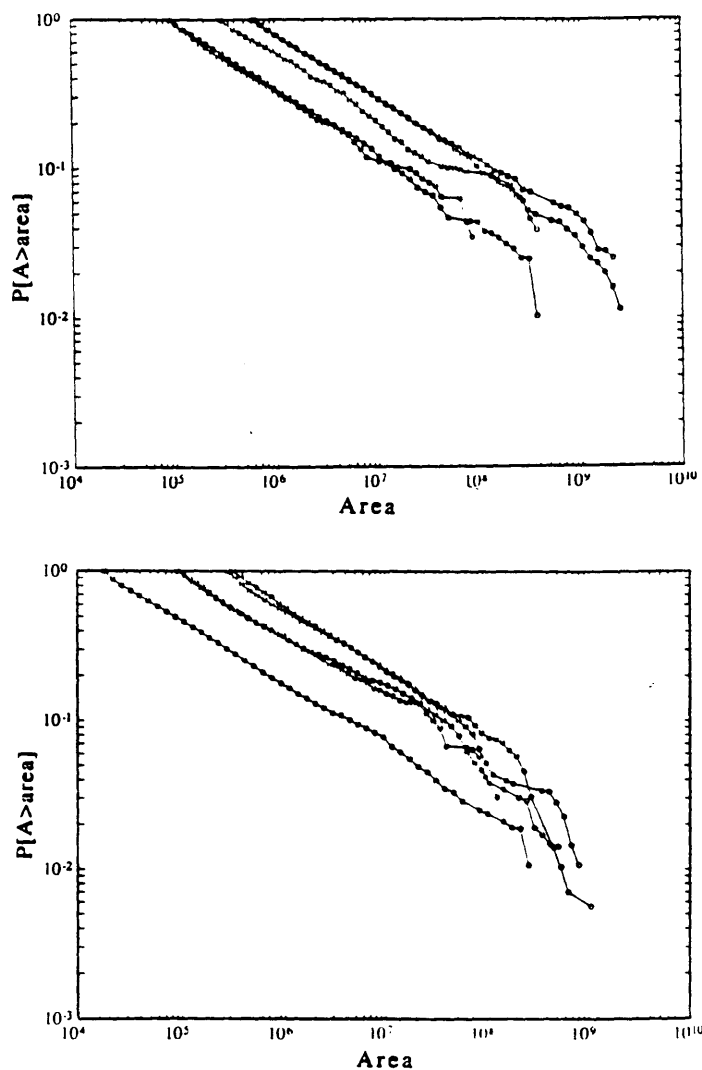
Figure 4.2: Cumulative distribution of link contributing areas for different basins across the U.S. (after Rodriguez-Iturbe 1992a) Top figure (left to right): Schoharie Creek Headwaters (NY), Racoon Creek (PA), North Fork Cour d'Alene River (ID), St. Joe River (MO,ID), Schoharie Creek (NY). Bottom Figure (left to right): Brushy Creek (AL), Big Creek (ID), Buck Creek (CA), East Delaware River (NY), Beaver Creek (PA,OH).

Basin	Scaling slope link-based distribution of areas	Scaling slope link-based distribution of energy.
Beaver Creek	0.44	0.72
Brushy Creek	0.42	0.87
Buck Creek	0.36	0.74
Big Creek	0.40	0.90
East Delaware River	0.41	0.95
Schoharie Creek Headwaters	0.45	0.98
North Fork Cour d'Alene River	0.45	0.97
Racoon Creek	0.46	0.99
Schoharie Creek	0.41	0.83
St. Joe River	0.44	0.98

Table 4.1: Scaling slopes of power-law behavior of cumulative distributions of link-based area and energy for different basins.

We have examined whether the threshold value used to determine the network could influence the distribution of areas. Figure 4.3 (Rodriguez-Iturbe et al, 1992a) shows the cumulative distributions for networks identified in the St. Joe River basin using different threshold areas to find the network. As the threshold area is decreased, the distribution moves to the left because the minimum value of area considered is smaller. Also, the range over which the distribution follows a power-law increases. The scaling exponent β remains approximately constant.

4.3. Power-law Distribution of Energy in River Basins

Besides contributing area, another variable of interest in river basins and which will be analyzed in great detail in Chapter 6 is energy expenditure $E=Q*S$ (or equivalently $A*S$)
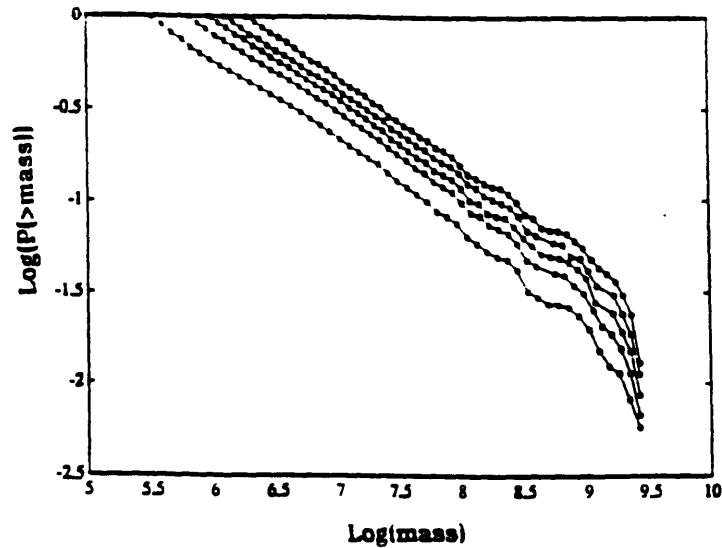
Figure 4.3: Cumulative distribution of link areas for St. Joe river basin using different threshold values of contributing area to identify the network, (after Rodriguez-Iturbe 1992a).

where Q is discharge, S slope and A contributing area. One of the areas where the concept of self-organized criticality is being studied in detail is earthquakes. The classical Gutenberg-Richter law shows that the cumulative distribution of earthquake magnitudes (a measure of energy release) follows a power-law indicating the possibility of a self-organized critical state at play (Bak and Tang, 1989).

Using DEM data we examined the cumulative distribution of energies at the link level using contributing area as a surrogate for discharge Q. Figure 4.4 (Rodriguez-Iturbe et al, 1992a) shows the distribution of energy for five different basins. Again a power-law is observed with scaling exponent around 0.9. Table 4.1 shows the value of the scaling exponent for different basins. The flattening of the
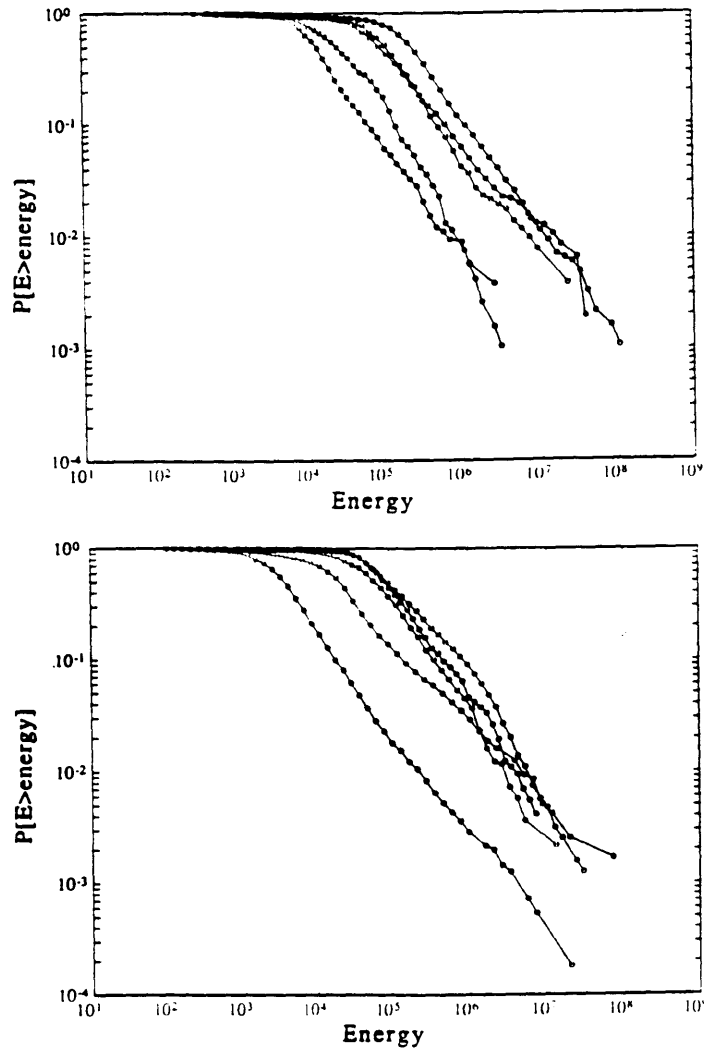
Figure 4.4: Cumulative distribution of link energy expenditure for different basins across the U.S. (after Rodriguez-Iturbe 1992a) Top figure (left to right): Racoon Creek (PA), Schoharie Creek Headwaters (NY), North Fork Cour d'Alene River (ID), Schoharie Creek (NY), St. Joe River (MO,ID). Bottom Figure (left to right): Brushy Creek (AL), Beaver Creek (PA,OH), East Delaware River (NY), Big Creek (ID), Buck Creek (CA).

distribution for small energy values is similar to that observed in earthquakes (Bak and Chen, 1991) and it is probably due to problems of resolution for small slopes given the integer values of elevation in DEMs.

The existence of a power-law distribution of link energy expenditure is not surprising if one realizes that slope and areas in rivers are related through a scaling relationship of the form $S\sim A^{-\theta}$ with $\theta=0.5$ (Tarboton et al., 1989). Then, using (4.1):

$$P[E>x] = P[AS>x] \sim P[A^{1-\theta}>x] \sim \int_{x^{1/(1-\theta)}}^{\infty} a^{-1-\beta}da \sim x^{-\beta/(1-\theta)} \quad (4.2)$$

With $\beta\approx0.43$ and $\theta=0.5$, the predicted scaling exponent for energy is approximately 0.86 not far from the measured value.

4.4. Distribution of Contributing Area at the Pixel Scale.

Clearly in Figure 4.3, there is a value of the threshold area below which the analysis would include hillslopes in the distribution. Therefore, instead of defining and using links as the basic unit for the distribution we will also investigate the behavior of the distribution of areas moving down to the pixel level. This implies that the contributing areas for all the pixels in the basin are included in the distribution.

Figure 4.5 shows the entire distribution for the St. Joe
River basin. The behavior shown in this figure is
characteristic of all the basins examined. There appears to
be a certain value of contributing area (at approximately 20
pixels for the case shown in Figure 4.5) where the power-law
behavior breaks. To the right of this break, the distribution
follows a power-law with an exponent β which is approximately
equal to 0.47 for all basins. Table 4.2 shows the values of
the slope β in the region to the right of the break for the
basins analyzed.
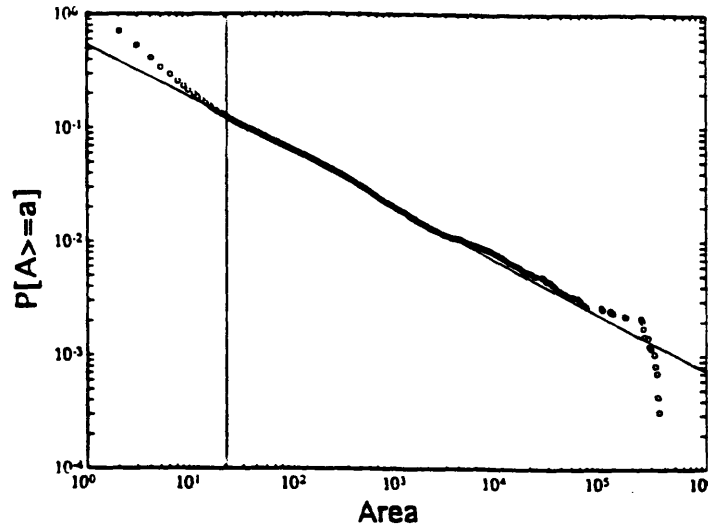
Figure 4.5: Cumulative distribution of
pixel-based contributing areas for Brushy
Creek basin. The vertical line corresponds to
the value of area for which a break in the
power-law behavior is observed.

To the left of the break, the distribution increases its
slope but it does not necessarily follows a straight line in
all basins. This behavior appears to be an indication of a
change in the character of the spatial organization of flow
directions in the basin. We will use this break as one of the
criteria for differentiating channel and hillslope pixels in

Chapter 11 as well as a motivation for an improvement in the modeling of landscape evolution at the hillslope scale in Chapter 12.

Basin	Scaling slope pixel-based distribution of areas
Beaver Creek	0.49
Brushy Creek	0.46
Buck Creek	0.45
Big Creek	0.45
East Delaware River	0.45
Schoharie Creek Headwaters	0.53
North Fork Cour d'Alene River	0.50
Racoon Creek	0.47
Schoharie Creek	0.48
St. Joe River	0.48

Table 4.2: Scaling slopes of power-law behavior of cumulative distribution of pixel-based contributing area after the break.

4.5. Summary

Motivated by the lack of characteristic spatial scales in self-organized critical systems like Scheidegger's stochastic river model, we examined the cumulative distribution of mass and energy in actual basins. It was found that these distributions followed a power-law with common scaling exponents 0.43 and 0.9, respectively, across different basins. The value of 0.43 is different from the 1/3 for Scheidegger's model which illustrates the possibility of using the characteristics of the distribution as a test for simulated networks.

Finally, when the cumulative distribution of areas is examined at the pixel scale instead of the link level, a break is found in the power-law behavior. This break is an indication of different flow organizations at the hillslope and channel scales and will be used later to distinguish between these two scales and to guide modeling efforts of landscape evolution at the hillslope scale.

Chapter 5

A Simple Basin Landscape and

Channel Network Growth Model

5.1. Motivation

The existence of spatial power-law distributions in river basins hints to the possibility of a self-organized critical system at work in the evolution of landscapes. The results shown in Chapter 4 are only one part of the story because they show only the spatial aspects of the system but not the temporal properties.

In order to study the temporal aspects of landscape evolution, it is necessary to have a model able to simulate landscapes in a domain large enough to allow the study of temporal as well as spatial distributions of the process over various orders of magnitude. At the same time, the model should have enough realism included in its formulation to be able to reproduce at least some basic geomorphological properties observed in actual basins.

The landscape evolution model could be used then to check whether the dynamical system shaping the catchment organization shares some of the properties usually observed in self-organized critical systems, namely: (1) power-law distribution in space (in Bak's sandbox it is the

distribution of spatial sizes of the avalanches), (2) power-law distribution in time (in Bak's sandbox it is the distribution of lifetimes of the avalanches), and (3) power-law growth of perturbations. This last property means that the system evolves "at the border of chaos" (Bak and Tang, 1991).

5.2. The Slope-Area Model

One of the most detailed models of catchment evolution and channel network growth is the SIBERIA model developed by Willgoose et al. (1991 a-d). In this model the landscape evolution is simulated by a sediment transport continuity equation. The simulated catchments and river networks look realistic and reproduce topological and metric properties observed in actual basins. However, the non-linearity of the sediment transport equation and the spatial coupling of the process makes the numerical solution of the system's evolution a difficult task.

The purpose of developing a different model in the present work was to have a simpler description of the evolution of the landscape that would allow simulations in a large domain in reasonable computer time. The key mechanism by which a channel network grows and extends to cover the basin is a reinforcing feedback occurring at the tip of the channels (Willgoose et al, 1989). The headtip of the channel is a point that has lower elevation and is therefore able to capture more flow (or equivalently more contributing area)

than its neighbors. This larger area gives the tip higher erosive power allowing the channel to move uphill thereby lowering the elevation of the point at the tip by evacuation of sediment. This feedback process will be the main driving mechanism of the landscape evolution in the model to be presented in this chapter.

A scaling relationship between slopes S and contributing areas A (as a surrogate for flow Q) of the form:

$$S \sim A^{-\theta} \qquad (5.1)$$

has been observed in rivers with the value of the scaling exponent usually around 0.5 (Tarboton et al, 1989a). What Relationship (5.1) represents is the concavity of river profiles. Among others, Leopold et al. (1964) report a mean observed value of θ in streams of the U.S. of 0.49 using flow measured in the field (although for ephemeral streams in semiarid regions a value of 1.0 is quoted). Flint (1974) relates (5.1) to Horton's slope and Schumm's area laws. The value of contributing area at which Relationship (5.1) breaks down has been used by Tarboton et al. (1989a) as a criteria to identify channels.

Theoretically, Relationship (5.1) has been the object of numerous studies. It can be obtained formally in 1-D profiles subject to uplift and erosion with a sediment transport function of the form $Q^m S^n$. In this case the equilibrium profile has slopes that scale as in (5.1) with $\theta = (m-1)/n$

(Carson and Kirkby (1972), Kirkby (1971), Smith and Bretherton (1972), Willgoose et al. (1991c), Tarboton et al. (1992)). Another way of looking at Relationship (5.1) is as the result of the minimization of energy expenditure (Yang (1971), Yang and Song (1979), Rodriguez-Iturbe et al. (1992b)) as we will examine in Chapter 6. In general, Relationship (5.1) is at the heart of every study of the three-dimensional structure of river basins.

The relaxation of slopes to follow the slope-area scaling relationship will be used as the driving mechanism of our simple model. The Slope-Area model simulates the elevation field over a gridded domain. At every iteration the model assigns flow directions along the steepest slope downhill. Following these flow directions, the model calculates the drainage area A_i of each pixel i. Then, the slope at pixel i at the next iteration is set to $S_i = k\, A_i^{-\theta}$ where k is a constant and θ the scaling parameter. The model keeps the elevation of the outlets (and any lakes) constant and uses them to recursively calculate the elevations of all pixels draining to the outlet using the assigned slopes. The more area a pixel is able to capture, the smaller its slope and consequently, its elevation at the next iteration. In this way the model simulates the reinforcing feedback necessary for the growth of the drainage network. The process is iterated until an equilibrium landscape is reached (Ijjasz-Vasquez et al, 1993a).

Boundary and initial conditions are similar to those of Willgoose et al. (1991a). The initial condition is usually a flat plateau with the same mean elevation but very small random perturbations in order to properly define drainage directions. The elevation of the outlet (or outlets) is kept at a lower level. Boundaries are closed except for the outlet. Figure 5.1 shows an example of how a landscape and its network develop in a square basin draining through one of its corners. This simulation uses $\theta=0.5$. The drainage network is presented by defining pixels that have a contributing area of at least five pixels as channels. This threshold concept is commonly used to infer networks from DEMs. Figure 5.1.e is the equilibrium landscape. At this point the entire area is drained by the network, the landscape is at equilibrium, and the slope of each pixel is equal to $kA_i^{-0.5}$.

Figure 5.2 presents simulations of the Slope-Area model in large domains (500x500) with different outlet locations: lower left-hand corner (Case a), center (Case b) and lower edge (Case c).

5.3. Signatures of Self-Organized Criticality

At this point there is not yet a clear and definite consensus on what a self-organized critical (SOC) system is. However, there are certain properties common to all these systems which make them interesting to study. Going back to the sandbox model of Bak and others (1987, 1988, 1989), there are two distributions of interest which correspond to the
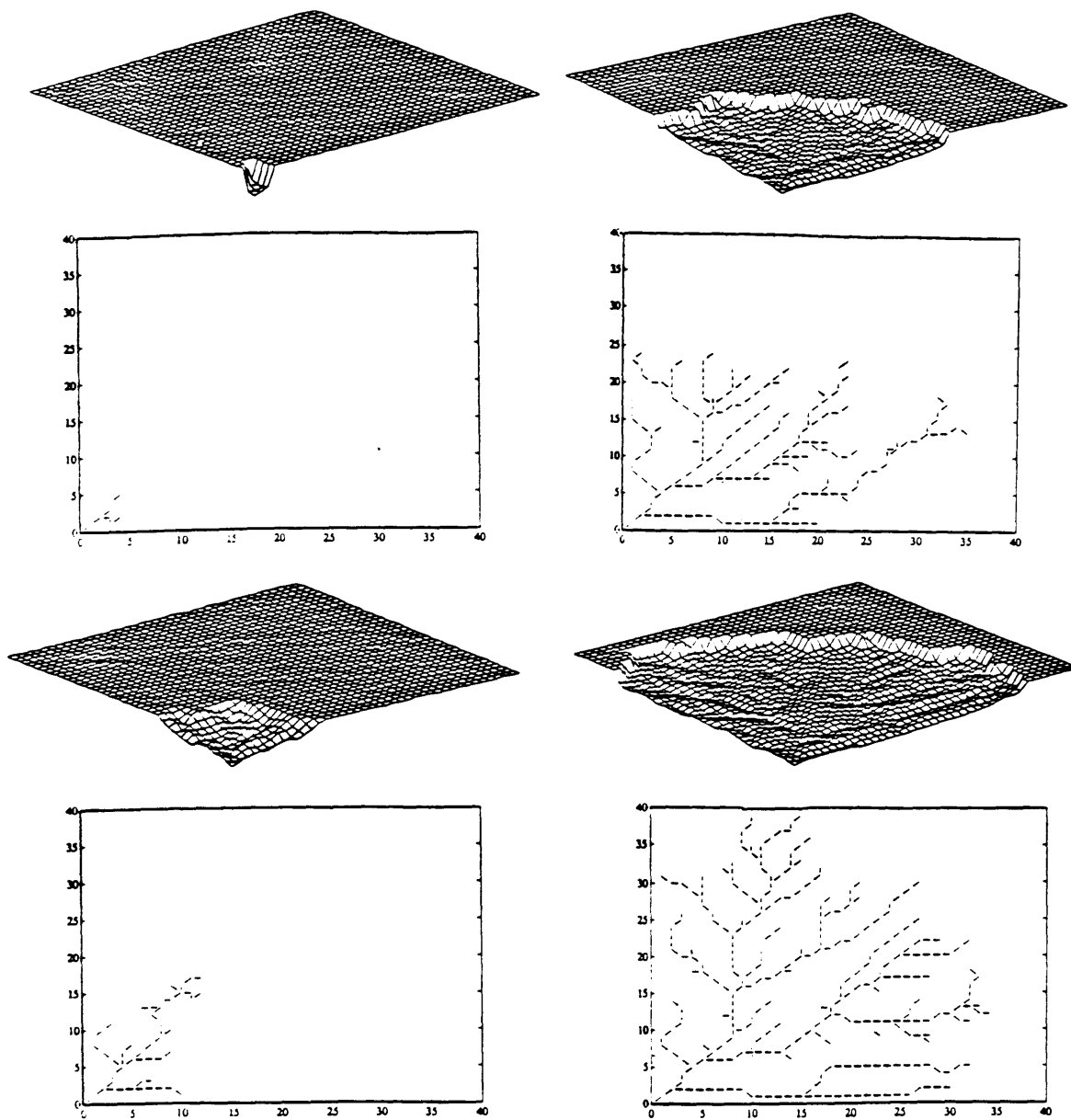
Figure 5.1: Isometric view and drainage network (identified with a threshold contributing area of five pixels) at different iterations of a simulation with the slope-area model (continues).
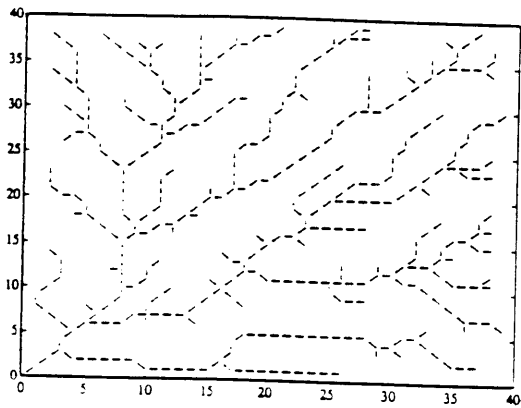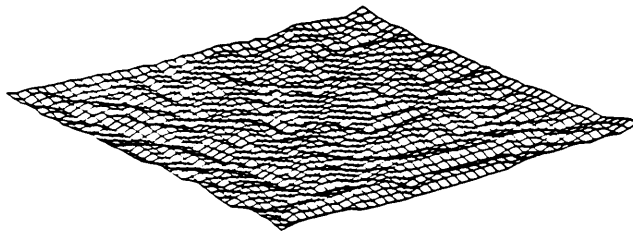
Figure 5.1: (contd.)
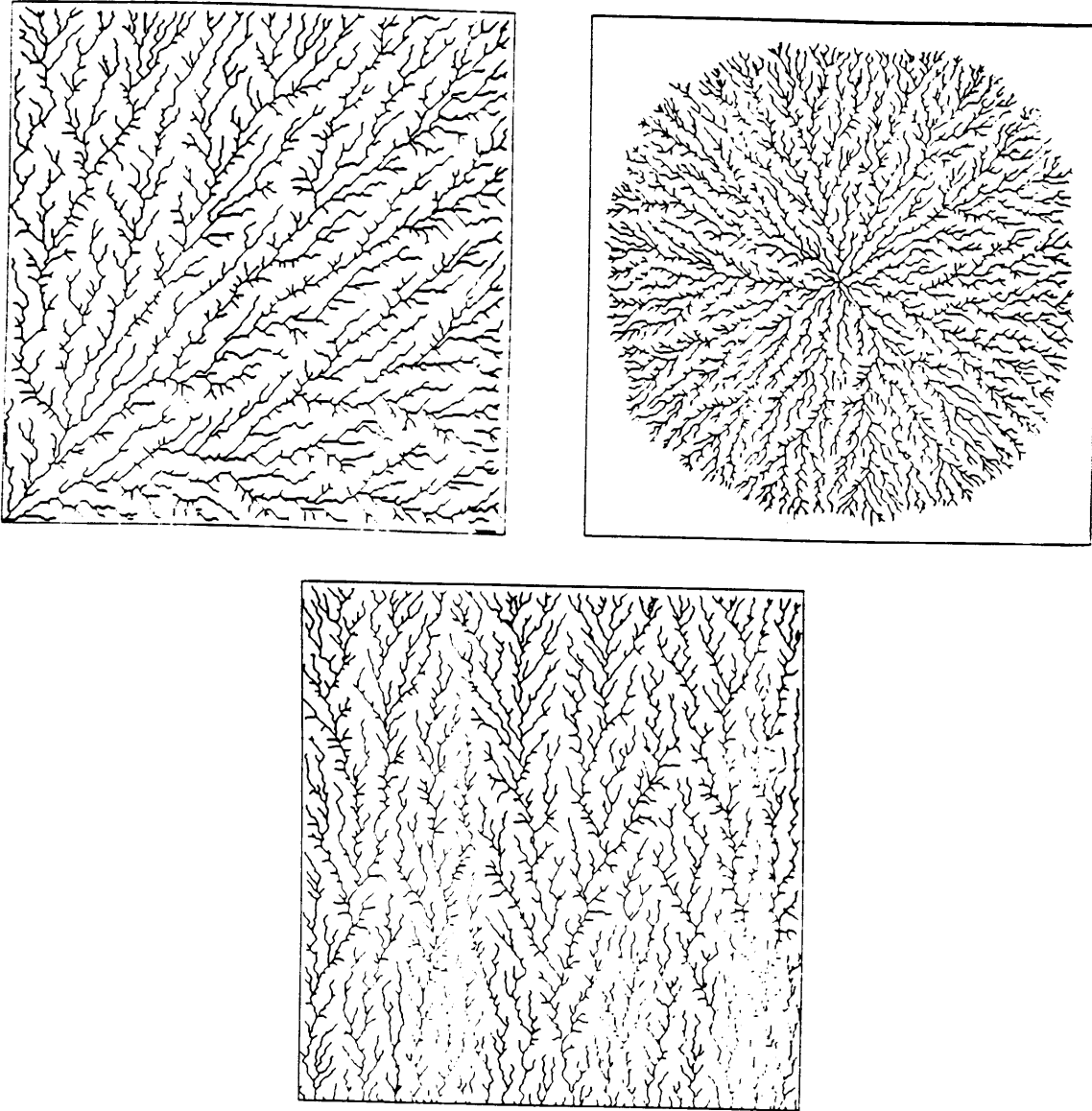
Figure 5.2: Drainage network for landscapes simulated with the slope-area model in large domains (500x500 pixels) with different outlet locations: (a) lower left-hand corner, (b) center and (c) lower edge.

size of the avalanches and their duration or lifetime. The power-law character of these distributions shows the spatial and temporal fractal signatures of the dynamics. It is the dynamics itself and not a tuning parameter that is responsible for the lack of spatial and temporal scales. A third property of the sandbox model, and one which is not frequently analyzed in SOC systems, is the power-law growth of perturbations (Bak, 1991). In chaotic dynamical systems, the growth of perturbations is exponential (Berge et al. (1984), Holden (1986)). SOC systems evolve "at the border of chaos" as P. Bak has called this behavior.

Another model that has been studied in the context of self-organized criticality is the Diffusion Limited Aggregate (DLA). This is a structure formed by random walkers that stick to a structure grown around a central seed (Feder (1988), Vicsek (1989)). Figure 5.3 presents an example of a DLA. Alstrom (1990) and Alstrom et al. (1990) make an analogy between the sub-trees of the structure and the avalanches of the sandbox model. They study the distributions of sizes and lifetimes of the sub-trees. The lifetime corresponds to the amount of time it takes for each sub-tree to grow. In the case of the Slope-Area model we will examine the distribution of sizes of sub-basins (a spatial signature) and their lifetimes (a temporal signature). Figures 5.4 and 5.5 (Ijjasz-Vasquez et al, 1991) are diagrams in log scale of these distributions. They follow a power-law as in SOC systems.
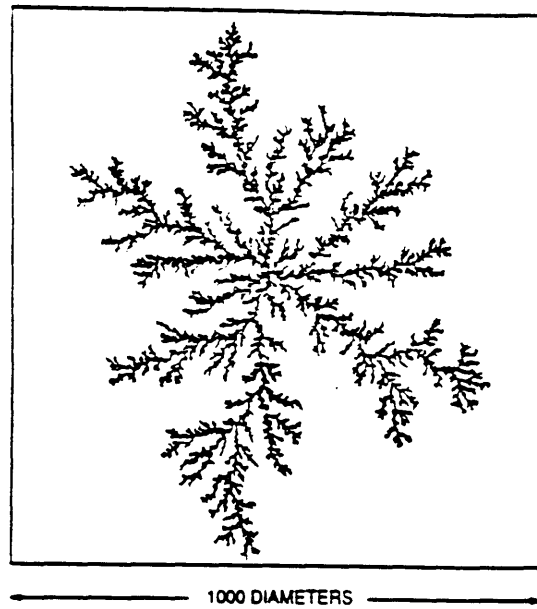
Figure 5.3: A typical Diffusion Limited Aggregate (from Vicsek, 1989).
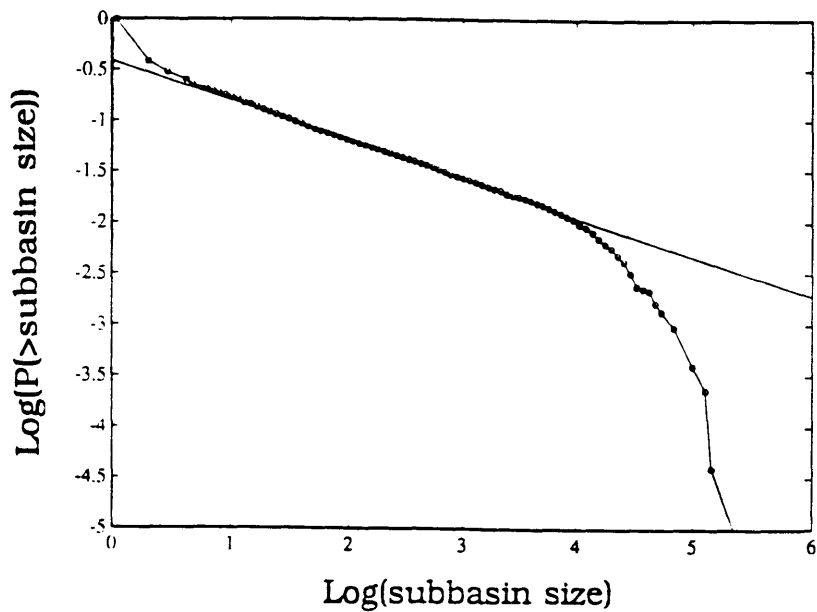
Figure 5.4: Cumulative distribution of contributing areas (i.e. sub-basin sizes) for a network simulated with the slope-area model.

73
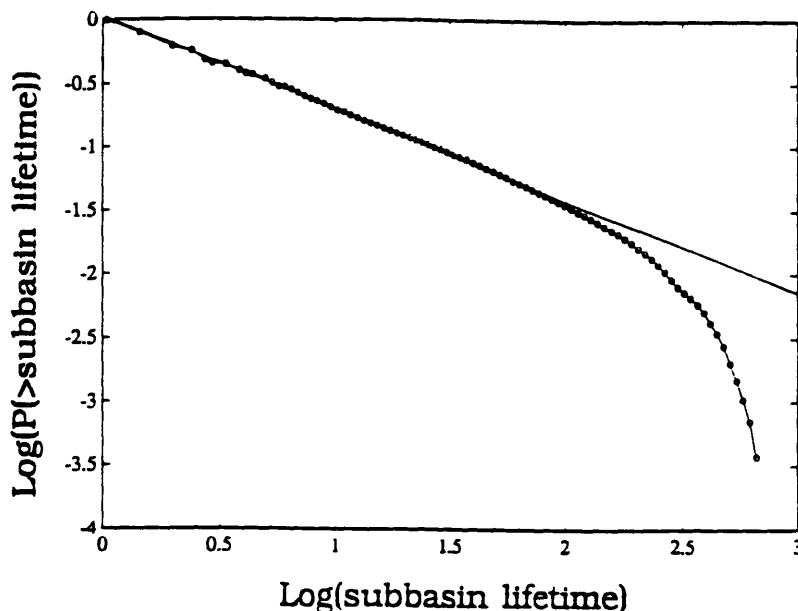
Figure 5.5: Cumulative distribution of sub-basin lifetimes for a network simulated with the Slope-Area model.

To examine the way in which perturbations grow we ran two experiments with identical parameters but minute differences in the perturbations of the initial elevation field. The landscapes were simulated to equilibrium and the difference between the two evolutions was measured in phase-space using (Ijjasz-Vasquez et al, 1992b):

$$d_{12}(t) = |z_1(t) - z_2(t)| = \sum_i |z_{1i}^{(t)} - z_{2i}^{(t)}| \qquad (5.2)$$

where $z_{ji}^{(t)}$ is the elevation of node i at time t in simulation j (j=1,2). Other measures could be used as well. For example, the square root of the sum of squares of the elevation difference at grid nodes. Figure 5.6 (Ijjasz-Vasquez et al, 1991) shows the behavior of d_{12} with time. The growth of the perturbations was found to be geometric and not exponential as in chaotic systems.
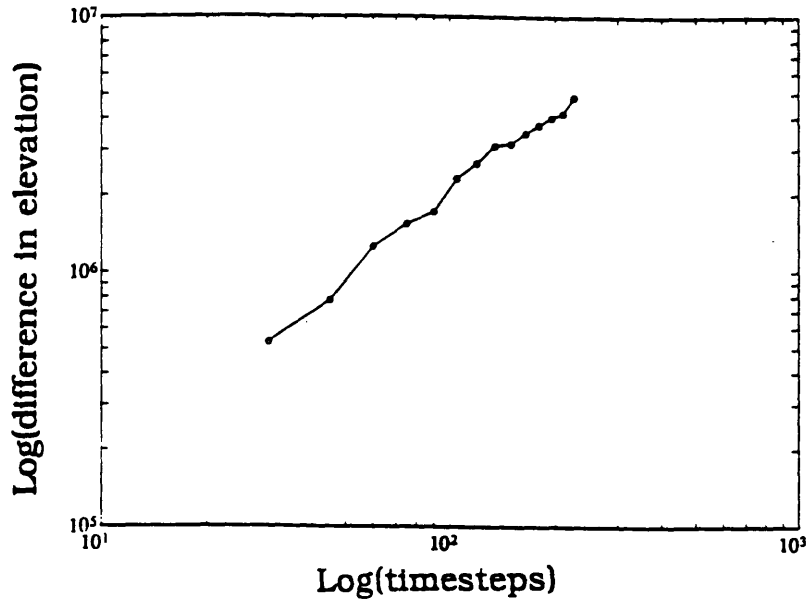
Figure 5.6: Growth of perturbations measured between two simulations of the Slope-Area model started with very similar initial elevation fields.

Although the analogy between avalanches and sub-basins shows that power-law distributions in space and time are generated by the dynamics of the Slope-Area model without the need of tuning a parameter, there is still a difference between models like the Slope-Area model or DLA and models like Bak's sandbox. In most SOC systems the evolution reaches a metastable state where avalanches continuously occur in time. In river basins, the system goes to an equilibrium and the structure is frozen in time with respect to small perturbations. The fractal signature of the dynamics is the lack of characteristic scale in the distribution of sub-units at equilibrium.

Recently, other models of channel network have been shown to have power-law distributions in space, for example Rinaldo et al. (1993), Takayasu and Inaoka (1992).

Finally, it is worth making an observation regarding Figure 5.4. The cumulative distribution of areas shown in this figure was calculated using all the pixels in the simulation. However, a break in the power-law behavior is not apparent as was the case in the actual basin presented in Figure 4.4. This indicates that the Slope-Area model is properly reproducing the aggregating features of the landscape at the channel level but a different flow organization occurs at the hillslope scale. This is related to a different slope-area scaling in hillslopes as will be shown in Section 7.3.

5.4. Summary

A simple landscape simulation and channel network growth model based on the scaling relationship between slopes and areas observed in actual basins was presented. The simplicity of the formulation of the dynamics allows large simulation domains. These large simulations permit the analysis over various log scales of the spatial and temporal signatures of the system. It was shown that not only the cumulative distribution of areas, a spatial feature, follows a power-law as is the case in actual basins, but also the lifetimes of the sub-basins and the growth of perturbations, which are temporal features, follow power-laws. These three properties are common to self-organized critical systems.

The Slope-Area model will be used later for comparison with actual basins in the framework of energy expenditure in

Chapter 8. Also, a configuration like the one shows in Figure 5.2.b. will be used in Chapter 7 to study the way river networks allocate space to their sub-units. The influence of the parameter θ of the scaling Relationship (5.1) on the structure of the network will be examined in Chapter 9.

Chapter 6

The Three-Dimensional Structure of Networks and its Relation to Energy Expenditure

6.1. Three Principles of Energy Expenditure in River Basins

Chapter 5 showed a way to study basin landscapes by examining the evolution of the dynamical system on its way to equilibrium. An equally valid approach could be to study the structure of river networks from an energy optimization point of view. The idea is not new: Woldenberg (1969) argues for honeycomb-like organization of sub-basins based on arguments of least-work shapes; Howard (1971b), Roy (1983) and Woldenberg and Horsfield (1986) use principles of minimum energy dissipation to explain the observed behavior of angles of incoming tributaries; Yang (1971) uses energy concepts in his study of river profiles; Stevens (1974) talks about different patterns of connectivity and some optimality criteria; and Howard (1990) applies the local minimization of energy at junctions to drive a network organization model. However, all these studies concentrated on a single aspect of the river network and did not look at the entire network as a unit.

Rodriguez-Iturbe et al. (1992b) have postulated three principles of energy expenditure in river basins. The goal is

to derive from these three principles the average behavior of the most commonly observed relationships of the river network structure. The three principles are:

(1) Minimum energy expenditure in each individual link of the network given the flow it has been assigned to carry.

(2) Equal energy expenditure per unit area of channel in every link of the network.

(3) Minimum total energy expenditure in the network given the area it has been assigned to drain.

The first two principles are related to local conditions at the link level and from them relationships between the width, depth, slope, velocity and flow at the link level can be derived. The third principle is of global character and is related to the way in which the network structure is organized to deliver water and sediment out of the assigned area. It is this organization of the network that will determine how much flow each of the individual links has to carry.

Maybe as important as the minimum energy conditions themselves are the constraints imposed in principles (1) and (3). Without them, the minimization of energy would imply unrealistic conclusions as will be examined later in this chapter.

The first principle is similar to Murray's (1926) law in physiological vascular systems. The observation that the sum

of the cubes of the radii of incoming vessels is equal to the cube of the radius of the large parent vessel was explained in terms of energy minimization. The second principle was conceptually suggested by Leopold and Langbein (1962).

We will now proceed to examine the implications of the three principles of energy expenditure on the three-dimensional structure of river basins at the local link level and the global network scale.

6.2. Implications of the Energy Expenditure Principles at the Link Level

In this section we will use principles (1) and (2) to derive relationships between the physical characteristics of the channel and the flow carried, following Rodriguez-Iturbe et al. (1992b). Let us consider a channel of length L, slope S, assigned flow Q and rectangular section of width w and flow depth d.

The flow to be assumed throughout the analysis is the mean annual flow as a representative value of the work done by the link. Although it is also possible to think of the bankful discharge as a key value of the flow, most of the work performed by the flow through time occurs at discharges smaller than the bankful capacity.

The force responsible for the flow is the downslope component of weight $F_1 = \rho g A_w L S$ where A_w is the cross-sectional flow area $w_* d$. The force resisting is $F_2 = \tau P_w L$ where τ is the

stress per unit area and P_w is the wetted perimeter $2d+w$. Under no acceleration conditions $F_1=F_2$ and then $\tau=\rho gRS$ where R is the hydraulic radius A_w/P_w. Assuming turbulent incompressible flow, the boundary shear stress is also $\tau=C_f\rho v^2$ where C_f is a dimensionless resistance coefficient. Taking together the last two expressions we obtain $S=C_f v^2/(Rg)$. Now, the rate of energy expenditure in a segment of length L can be written as:

$$E_1 = \rho gQSL = C_f\rho v^2 QL/R = C_f\rho v^3 P_w L \qquad (6.1)$$

According to the second principle, the energy expenditure per unit area of channel $(E_u=E_1/(P_w L))$ is constant throughout the network, i.e.

$$E_u = C_f\rho v^3 = constant \qquad (6.2)$$

which implies that the velocity tends to be constant throughout the network if the coefficient C_f is constant. Leopold and Maddock (1953), Wolman (1955) and Brush (1961) have found that the increase of velocity downstream in the network is not significant $(v{\sim}Q^{0.1})$.

In order to find a relationship between d and Q, let us substitute $R=(wd)/(2d+w)$ in Equation (6.1):

$$
\begin{aligned}
E_1 &= C_f\rho v^2 QL(2d+w)/(wd) = \\
&= QLC_f\rho v^2(2/w) + QLC_f\rho v^2(1/d) = \\
&= QLC_f\rho v^2(2d/A_w) + QLC_f\rho v^2/d = \\
&= dL[2C_f\rho v^3] + (QL/d)[C_f\rho v^2] \qquad (6.3)
\end{aligned}
$$

Notice that the terms in brackets are constant. If the value of Q is given, then the first principle of minimum energy expenditure implies:

$$dE_1/d(d) = 0 = L\ [2C_f\rho v^3] - (QL/d^2)\ [C_f\rho v^2] \qquad (6.4)$$

and therefore:

$$Q = 2vd^2 \qquad (6.5)$$

then:

$$d \sim Q^{0.5} \qquad (6.6)$$

The above result has been observed in the field by Leopold et al. (1964) who found a scaling exponent of 0.4 for the dependence between depth and flow in the downstream direction.

Given that d=Q/(vw), then:

$$Q=(v/2)w^2 \qquad (6.7)$$

and:

$$w \sim Q^{0.5} \qquad (6.8)$$

A similar relation between width and flow was found in the field by Leopold et al. (1964).

Equations (6.5) and (6.7) imply that w=2d. This result is a direct consequence of the assumption of a rectangular section. Other sections can be used and the same scaling relationships (6.6) and (6.8), which are the ones we are interested in, are obtained but with different proportionality coefficients.

From (6.6) and (6.8) we have $R=wd/(2d+w)\sim Q^{0.5}$. Given that $S=C_f v^2/(Rg)$ then:

$$S \sim Q^{-0.5} \tag{6.9}$$

which is the slope-area relationship observed in the field by Leopold et al. (1964) and in DEMs by Tarboton et al. (1989) among others.

Notice that Equation (6.1) is only accounting for energy expenditure in the "operation" of the channel. It is also possible to represent the energy expenditure related to the "maintenance" of the channel as $F(soil,Q)P_wL$ where $F(.)$ is a function representing the work per unit time and unit area involved in the removal and transportation of sediment (Rodriguez-Iturbe et al, 1992b). A reasonable form for F is $F=K\tau^m$ where K depends only on the properties of the soil and water and m is a constant. Equation (6.1) would then change to:

$$E_1 = C_f\rho v^2QL/R + K\tau^m P_wL \tag{6.10}$$

The derivation of all the relationships in this section using (6.10) is analogous and none of the results change (see Rodriguez-Iturbe et al, 1992b for details). It is foreseeable that a third term may be required, related to the "construction" of the channel network, to measure the work done in removing material to build the network structure.

Summarizing, the local energy principles (1) and (2) imply the average behavior of the well-known empirical relationships $d \sim Q^{0.5}$, $w \sim Q^{0.5}$, $S \sim Q^{-0.5}$ and v constant throughout the network at a certain time when measured at flows with the same recurrence.

6.3. Minimum Total Energy Expenditure and the Spatial Organization of the River Network

Principle (3) states that the different regions in the basin should be connected in such a way that water and sediment are taken out of the basin most efficiently, i.e. minimizing total energy expenditure. Replacing (6.5) in (6.3) we can obtain the energy expenditure at each link:

$$E_l = k \, Q^{0.5} L \qquad (6.11)$$

where the proportionality factor k is a function of C_f, ρ and v and therefore is constant across the network. The total energy expenditure is the sum of the energy expenditure for all the links:

$$E_T = \Sigma_i \, k \, Q_i^{0.5} L_i \qquad (6.12)$$

The configuration with the lowest value of E_T is the one chosen by the third principle. The comparison across networks in the same domain requires the assumption that k has the same value across them (and not only inside each of the networks).

The third principle, nevertheless, has an important constraint: the network has a certain area to drain. If one were to use, for example, all the different TDCN configurations, which are not tied to a metric space, the results would not be reasonable. Assuming a unit area for each node of the TDCNs and comparing the values of E_T, the optimal network would have $R_b=2$ which is unrealistic but not surprising. Included in the family of TDCNs with the same number of links are networks with both a wide-fan structure and a narrow-strip structure depending on the value of R_b (see Figure 6.1) It is clear that in terms of energy expenditure a network with all its nodes near the outlet (in the fan case) would be more economical than one with most of the nodes far away (in the strip case). This comparison is
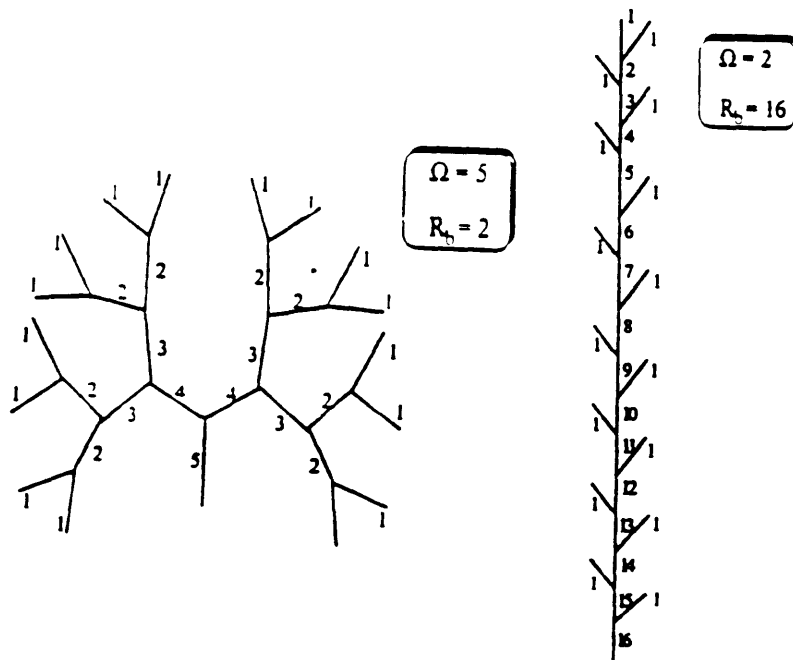
Figure 6.1: Two extreme examples in the family of TDCNs with 16 external links. The comparison between networks that do not drain the same basin domain gives unrealistic results (from Rodriguez-Iturbe et al, 1992b).

not fair. The optimization criteria cannot be used in a topological space but should be tied instead to a real space by fixing the area to be drained, before the comparison of E_T between networks is made.

Suppose an area of 100x100 pixels with closed boundaries except for an outlet at a corner is to be drained in an optimal way (i.e. with minimum E_T). Three examples of networks draining such an are shown in Figure 6.2, the third one being a random network. Assuming unit grid size and area as a surrogate for flow, the values of the total energy expenditure E_T of these three networks are 72,862, 60,410 and 58,786 respectively.

The combinatorial problem of finding the optimal configuration in a domain of this size is NP-hard and is not possible to solve due to the enormous number of combinations. Similar Operations Research problems use heuristic methods to find near-optimal solutions. One strategy that can be adapted to our network optimization problem is the one developed by Lin (1965) for the traveling salesman problem. The idea is to iteratively change at random the flow direction of a randomly chosen node.

Beginning with a network like the ones shown in Figure 6.2, the search proceeds, looking for an optimal network. The changes in flow direction should be such that no lakes are formed and the entire area is still drained by the network. The value of E_T is calculated for the new network and the
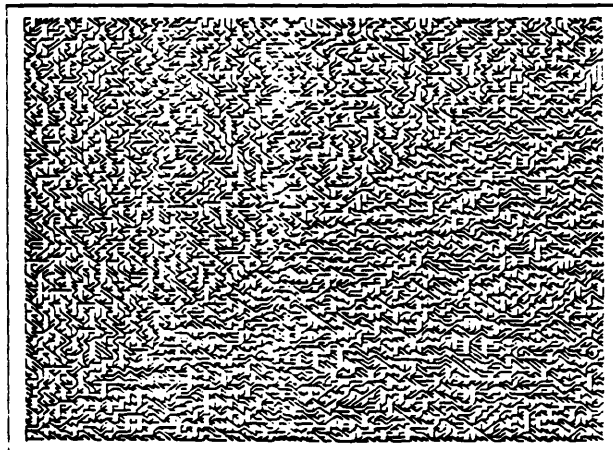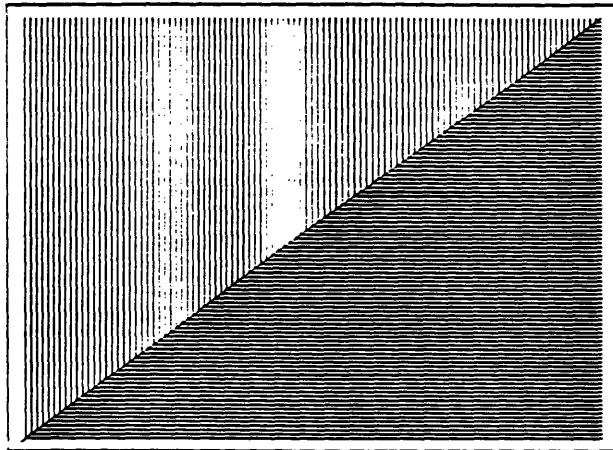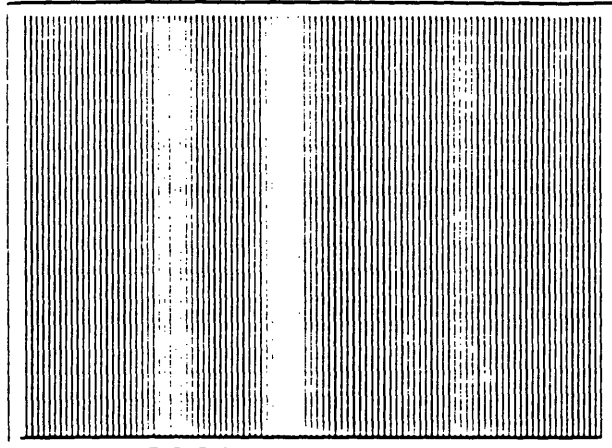
Figure 6.2: Three networks given as initial condition to the random search algorithm used to find OCNs. The total pixel-based energyexpenditure for each of these cases is 72862, 60410 and 58786 respectively.

configuration is accepted if E_T for the new network is smaller than the value for the old network. The procedure is repeated until no further improvement on E_T is obtained after a large number of iterations.

Although there is no assurance that the solution represents a global minimum, we have seen that the final values of E_T fall very near each other and probably near the absolute minimum. Figure 6.3 shows the final network obtained after the optimization procedure. The value of E_T is 39,816 which is much lower than the value for the original networks in Figure 6.2.

Other heuristic optimization strategies can be implemented, like simulated annealing. In this method new configurations with higher values of E_T are accepted with certain probability instead of always being rejected as in the method previously described. This allows the system to escape from local minima with small trapping boundaries (Johnson (1987), Wejchert(1989)). The methods give very similar answers (Rinaldo et al, 1992).

Networks with minimum values of E_T are called Optimal Channel Networks (OCN). These networks not only reproduce Horton's laws with appropriate values of R_b, R_l and R_A (Rinaldo et al, 1992) but also exhibit a power-law cumulative distribution of areas with scaling exponent very near the

value of 0.43 encountered in actual basins (Rodriguez-Iturbe et al, 1992c), as shown in Figure 6.4.
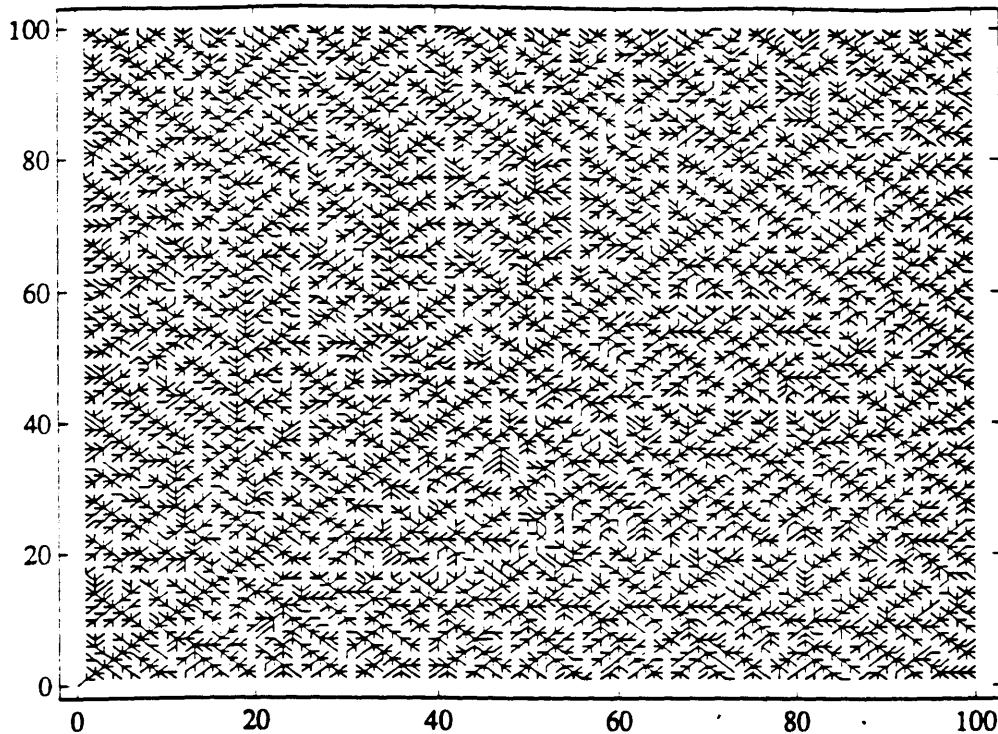
Figure 6.3: An Optimal Channel Network constructed in a 100x100 domain. The total pixel-based energy expenditure for this OCN is 39550.
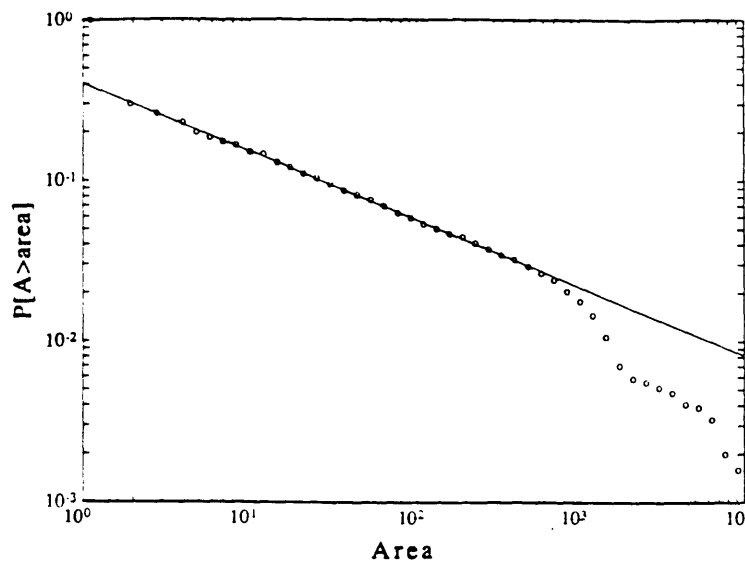
Figure 6.4: Cumulative distribution of areas for the optimal network shown in Figure 6.3. The scaling slope is -0.42

It is important to mention two issues regarding the way OCNs reproduce Horton's scaling laws and the power-law cumulative distribution of areas observed in actual channel networks. First, there is a difference between the "explanation" of Horton's laws from the TDCNs and the implications derived from OCNs. In TDCNs the observation of Horton's laws in nature is seen as the result of the presence of this behavior in a large proportion of the family of random networks. On the other hand, the OCN formalism implies that Horton's laws are a direct consequence of the search for organization with minimum energy expenditure. Networks that do not obey Horton's laws would be too expensive in terms of energy. Nevertheless, we have found an enormous variety of near-optimal networks that differ in the small scale details but whose levels of energy expenditure are very similar. This is in consonance with the enormous variety of networks without geologic controls observed in nature in which Horton's laws hold remarkably well.

The second issue is the interesting fact that the network structure in its search for low energy states does not choose any preferential spatial scale but chooses a fractal scaling behavior, opening up the question of whether other fractal structures may be seen as states of minimum energy expenditure. Studies on other aggregating structures hint towards this possibility (Feuerecker et al. (1987), Merte et al. (1988))

90

Recently, many other properties of OCNs have been examined, confirming the ability of this formalism to reproduce the most common geomorphological and scaling properties of actual river networks (Rinaldo et al. (1992), Rigon et al. (1993)).

Finally, notice that although the analysis in this section concentrated on the planar organization of the network, the three-dimensional structure was embedded through the scaling relationship $S \sim Q^{-0.5}$ derived from the first two principles. The third principle sets the flows that each link has to carry so the network minimizes total energy expenditure, and then each individual link adjusts its slope, configuring in this way the three-dimensional structure of the basin.

6.4. Summary

Three principles of energy expenditure proposed by Rodriguez-Iturbe et al. (1992b) and their implications on the structure of river networks have been studied in this chapter. The first two principles, which work at the link level, imply that, given the flow Q carried by the link, the geometry of the link is adjusted so that width and flow depth scale as $Q^{0.5}$, slope scales as $Q^{-0.5}$ and velocity is constant across the network. The third principle is in charge of organizing the network structure to minimize total energy expenditure as well as connecting all the nodes in the area given to drain. Using tools from Operations Research it was

found that Optimal Channel Networks reproduce common geomorphological measures like Horton's laws (Rinaldo et al, 1992) and the power-law distribution of areas observed in actual basins.

As mentioned at the beginning of the chapter, the OCN approach is a different way of studying networks from that of models of landscape evolution like the SIBERIA model (Willgoose et al, 1991 a,b) or the Slope-Area model described in Chapter 5. The OCN formalism presents postulates regarding the equilibrium organization of the network without taking into consideration the evolution process that brought the network to its optimum state. The relationship between OCNs and evolution models will be studied in Chapter 7, in order to understand the physical mechanism used by the network to minimize energy expenditure.

The OCN formalism was used in this chapter to study the preferred internal structure of the best network to drain a given area. Later on, in Chapter 8, we will combine issues of minimum energy expenditure with competition to study how the basin areas are distributed among competing units and what implications this process has on the shape of river basins.

Chapter 7

Optimal Channel Networks, Slope-Area Networks and Digital Elevation Maps

7.1. Motivation

The evidence presented in Chapter 6 and other related papers (Rodriguez-Iturbe et al. (1992b,c), Rinaldo et al. (1992), Rigon et al. (1993)) shows that OCNs are able to reproduce the most important statistics of actual channel networks. Another comparison test might be made to determine how similar the total energy expenditure in actual basins is to the value predicted by an OCN constructed within the same domain. However, the random search strategies used in OCNs are computer intensive procedures, and only domains of up to 10^4 pixels have been analyzed. This size is about two orders of magnitude smaller than the typical size of basins in DEMs at the scale of resolution available.

One way in which OCNs and DEMs can be compared is by using, as an intermediate step, networks generated with the Slope-Area model. This model is able to simulate networks at the scale of DEMs, given its simple dynamics. We will show that Slope-Area networks and OCNs have very similar values of total energy expenditure E_T when compared with each other in the small domains where the random search methods of OCNs

work. We will then use the Slope-Area model to study whether the value of E_T in DEMs is near the optimal level.

Next, by relating total energy expenditure to potential energy we will present a clue to the mechanism through which networks grow, evolve and organize in order to minimize E_T. Finally, the role of perturbations in the search for configurations having low energy will be examined, as well as the existence of unstable equilibrium landscapes with high levels of energy expenditure.

7.2. Total Energy Expenditure in OCNs and Slope-Area Networks

The first step in the analysis will be to compare the values of E_T for OCNs and for Slope-Area networks in domains that can be handled by the random search algorithm. If both the Slope-Area model and the random search algorithm of OCNs produce networks of similar total energy, then the efficient Slope-Area model can be used to test whether real basins obtained from DEMs actually optimize total energy expenditure. In order to make a fair comparison, 100 repetitions of the search procedure of OCNs in a 24x24 domain were performed. The experiments started from different random initial networks that drain the domain under study. An example of such random initial networks is presented in Figure 7.1. The search procedure rearranges the elements of the network into configurations with smaller total energy dissipation:

$$E_T = k\Sigma_i \ Q_i^{0.5}L_i \qquad\qquad (7.1)$$

Figure 7.2 presents the configuration with the lowest value of E_T obtained from among the networks. Figure 7.3 shows the histogram of the final values of total energy expenditure E_T. Even though there is some variation in these values (between 1620 and 1680, where k=1, Q_i=A_i and A_i=1 in Equation (7.1)), it is very small compared to the amount by which E_T has been reduced from its initial value (from a mean value of 2250 to a mean value of 1640).

Now, using the same 24x24 domain and, as initial landscape, a plateau with the same mean elevation but different random perturbations, 100 repetitions of the Slope-Area model were carried out in a manner similar to the simulation shown in Figure 5.1. The histogram of final total energies is presented in Figure 7.4. In order to demonstrate how similar the energies for OCNs and Slope-Area networks are, Figure 7.5 presents together three histograms of energies: that for the initial random networks used in the OCN procedure (at the right-hand side), that for the final OCNs and that for the networks simulated with the Slope-Area model (the latter two at the left-hand side). The overlap between the histogram of OCNs and that of Slope-Area networks and the small difference between these two histograms, compared to the distance between them and the histogram for random networks, supports the idea of using the Slope-Area model to generate networks with near-optimal energy
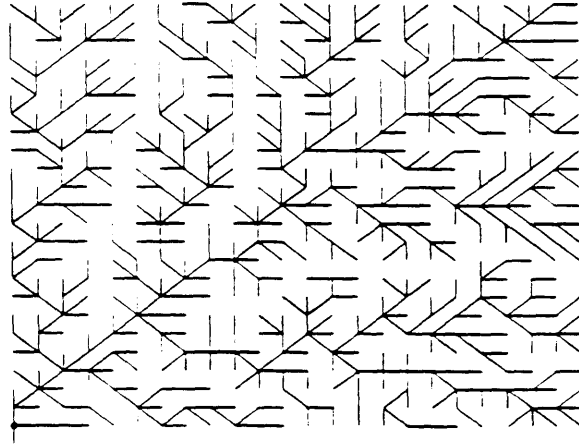
Figure 7.1: Example of a random network used as initial condition in the random search algorithm for an optimal configuration.
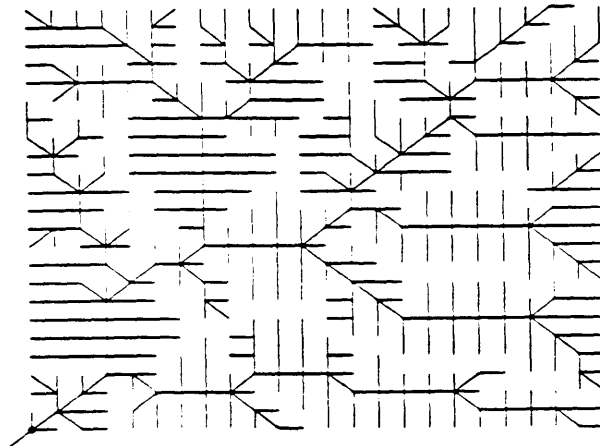
Figure 7.2: OCN with the lowest value of E_T among 100 repetitions of the random search procedure.
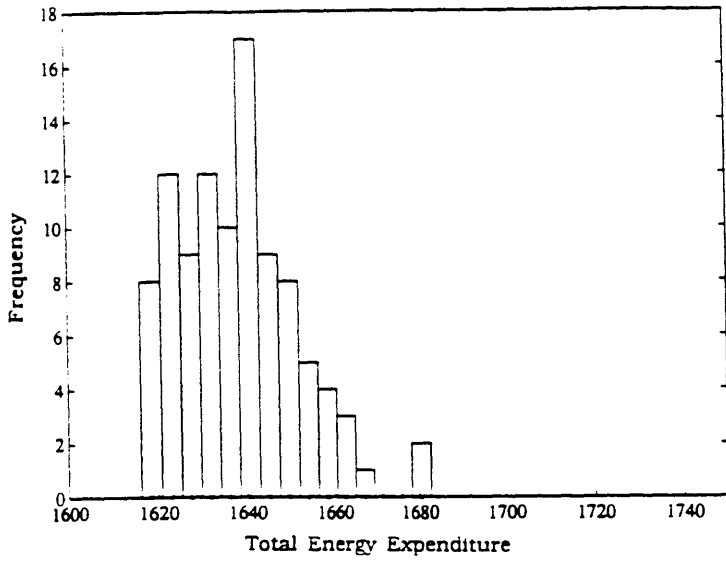
Figure 7.3: Histogram of values of total energy expenditure E_T for the 100 repetitions of the OCN procedure.
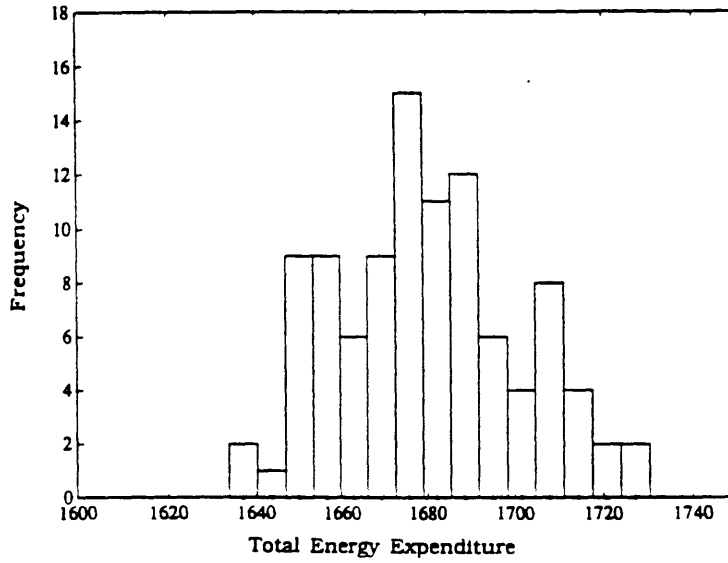
Figure 7.4: Histogram of values of total energy expenditure for 100 networks simulated with the slope-area model.
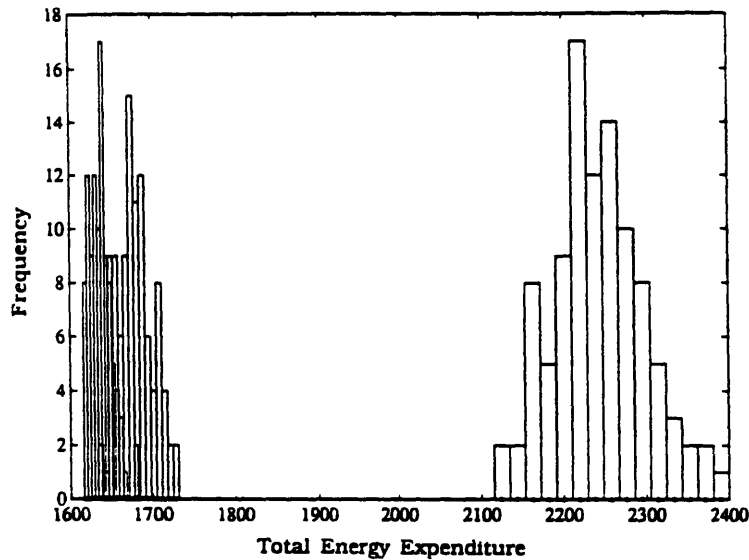
Figure 7.5: Histogram of total energy expenditure for 100 random networks (right-hand side), OCNs and networks simulated with the Slope-Area model (left-hand side).

expenditures. The computational demands of the random search procedure of OCNs prevent the construction of histograms with enough data points for large domains. However, a few OCNs were constructed in a 64x64 domain (each of which required approximately 20 hours of CPU time) and were compared against networks of the Slope-Area model. The difference in total energy between was in all cases less than 5%.

In the search for optimality, the river network may find itself trapped in local minima. The perturbations found by the growing network may have forced it to develop in less than optimal configurations. It is therefore of interest to examine the role of perturbations as a mechanism to move the system out of these minima. Physically, these perturbations may represent the local inhomogeneities encountered by the landscape during its evolution.

For this purpose, the elevation field of an equilibrium landscape obtained with the Slope-Area model was perturbed by adding small random values to the grid point elevations, disrupting in this way the local structure. The landscape was then given back to the model as initial condition and run to equilibrium, eliminating in this process expensive defects in terms of energy. Figure 7.6 presents an example of the final network of the equilibrium landscape before the perturbations. The total energy expenditure E_T was measured each time a new equilibrium was reached. Then, a new perturbation was applied. Figure 7.7 presents the behavior of E_T resulting from this process. The value of E_T decreases as the network cleans its small-scale defects, upon reaching a low energy state. Figure 7.8 shows the final network after the perturbation process has concluded, when the lower energy state has been reached. Even though the changes between the networks in Figures 7.6 and 7.8 are small, they are noticeable. However, the reduction in E_T is not large. Figure 7.9 presents the histogram of total energy expenditure of 100 different networks obtained with the Slope-Area model after perturbations were applied and a new stable equilibrium with lower energy was found. The histogram shifts to the left from its position in Figure 7.4 (which corresponds to the equilibrium networks before the perturbations) and the overlap with the histogram of OCNs is even larger.

Nevertheless, the change is small and the perturbation process requires repeated runs of the model making it very
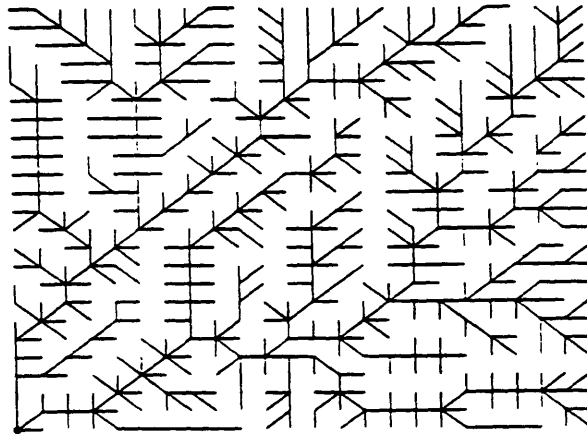
Figure 7.6: Example of a network in an equilibrium landscape generated with the slope-area model before perturbations.
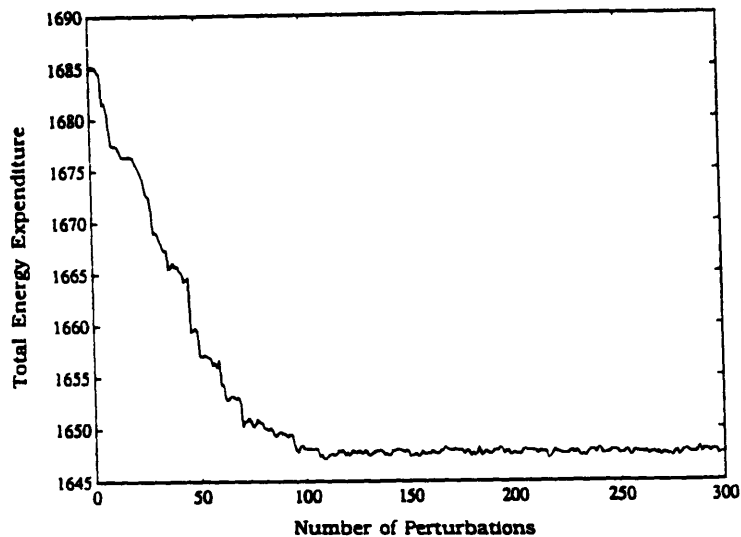
Figure 7.7: Evolution of the total energy expenditure E_T under repeated perturbations. E_T is measured whenever the landscape reaches a new equilibrium after each perturbation. The value of E_T decreases as the network takes care of the small-scale defects in its structure.
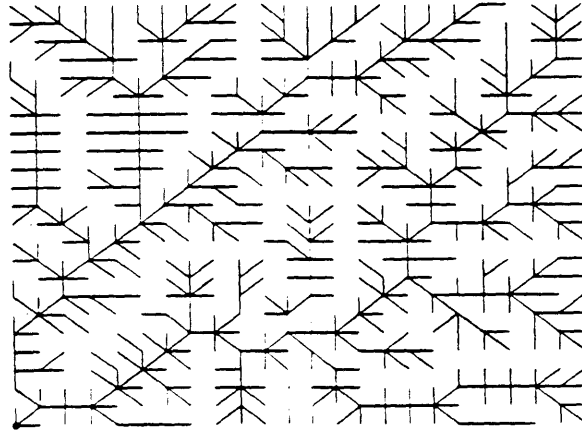
Figure 7.8: Network obtained by repeated perturbations of the landscape corresponding to the network shown in Figure 7.6.
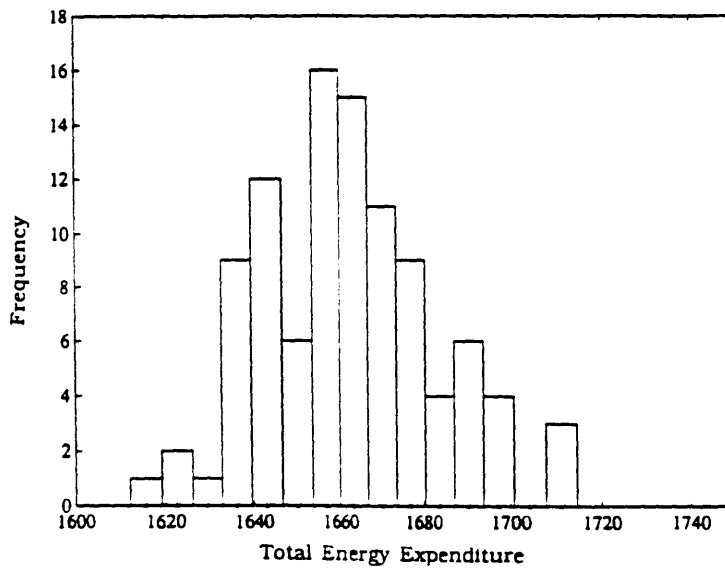
Figure 7.9: Histogram of total energy expenditure for 100 networks simulated with the slope-area model after reaching a lower value of E_T through repeated perturbations.

difficult to be implemented in large domains. Therefore, it
seems reasonable to use the results of the model without
perturbations to compare the energy expenditure level of DEMs
and the value for OCNs.

7.3. Total Energy Expenditure in DEMs and Networks Generated by the Slope-Area Model

The next step is to use actual basins identified from
digital elevation maps and take their boundaries and outlet
location as boundary conditions for the Slope-Area model.
Table 7.1 (Ijjasz-Vasquez et al, 1993a) compares the total
energy expenditure of Slope-Area networks simulated using the
actual domains of four different basins across the US. and
the total energy expenditure of the actual basins calculated
using pixels. In every case, the difference between the total
energy dissipation E_T (measured using equation (7.1)) in the
simulated and the real basin is less than 5%.

Basin	Pixel-based Energy from DEM	Pixel-based Energy of slope-area network
Brushy Creek	2 224 524	2 115 340
Big Creek	914 069	904 377
Schoharie Creek Headwaters	589 091	558 937
North Fork Cour d'Alene River	418 034	404 866

Table 7.1: Comparison of the total energy
expenditure of four actual basins and
corresponding slope-area networks simulated
using the actual domain of the basins.

As an example, Figure 7.10 presents three networks in the same domain taken from North Fork Cour d'Alene river basin in Idaho, US. Figure 7.10.a is the network extracted from the DEM using a threshold contributing area of 50 pixels. Figure 7.10.b shows a network simulated with the Slope-Area model. Figure 7.10.c shows a random network of the kind used as initial condition for OCNs in Chapter 6. All three networks are presented using the same threshold. While the values of E_T in the first and second cases are 4.2×10^5 and 4.0×10^5 (in pixel units), E_T for the third network has the much larger value of 6.1×10^5. The similarity of values of energy expenditure between the real and the simulated network suggest that river networks tend indeed towards a state of minimum energy expenditure.

It has been found, for some basins, that the scaling relationship $S \sim A^{-\theta}$ between slopes and contributing areas does not hold for all the values of areas but instead, there are two scaling regimes (Tarboton et al, 1989a). Figure 7.11 illustrates such behavior in one of the basins studied (Big Creek, Idaho, US). In this figure, the slopes of the pixels in the basin are grouped into bins according to their contributing area. The circles represent the mean value of the slopes for the pixels in each bin. The break observed in scaling has been used by Tarboton et al. (1989) to identify the threshold value of contributing area that separates hillslopes from channels.
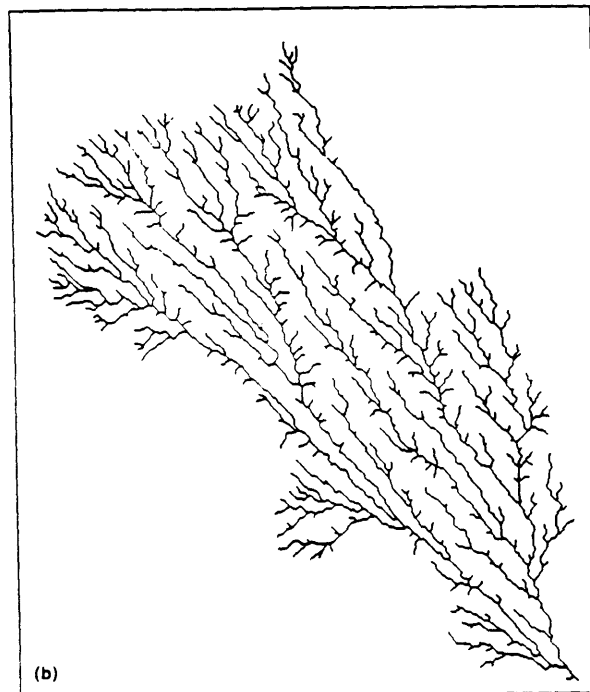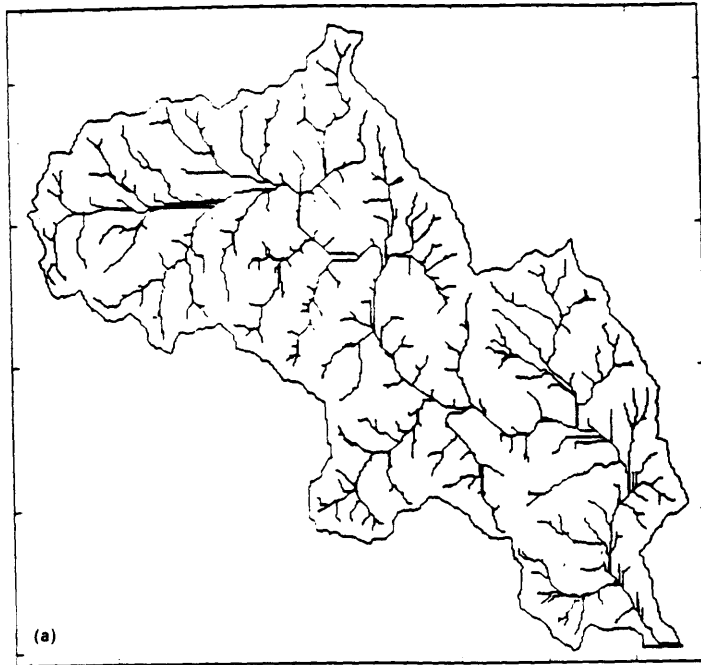
Figure 7.10: Three different networks draining the same boundary domain in the North Folk Cour d'Alene river basin. (a) Drainage network identified from DEM, (b) Drainage network simulated with Slope-Area model, (c) Random drainage network (continues).

104
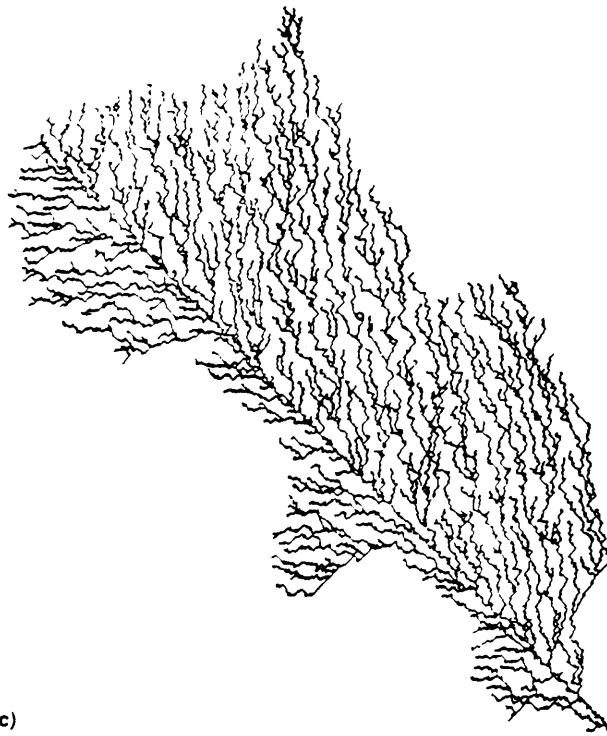
(c)

Figure 7.10: (contd.)
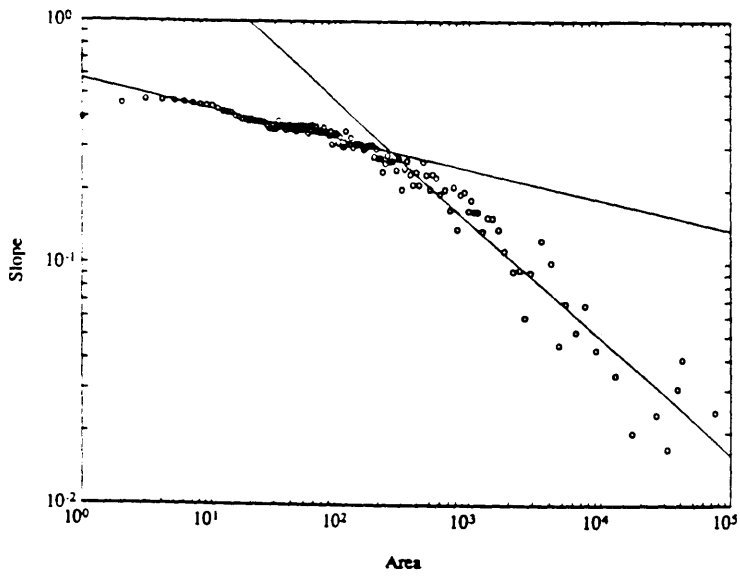
Figure 7.11: Slope-area scaling relationship in Big Creek basin. Two scaling regimes at the hillslope and channel scale can be observed.

A slope-area scaling relationship with two different scaling regimes can be used in the Slope-Area model. We have found that this change affects the flow pattern below the areas at which the break occurs. To illustrate this behavior, Figure 7.12 shows the network of a basin grown with the break in scaling. While the basin in Figure 7.6 was simulated with $S\sim A^{-0.5}$ for every value of A, the basin in Figure 7.12 has $S\sim A^{-0.5}$ if A is larger than 20 pixels and $S\sim A^{-0.0}$ (i.e. S constant) otherwise. In the original model the pattern is aggregated at all scales while in the modified version of the model it tends to be parallel below the threshold value. Actually, this is the behavior observed in DEMs at the hillslope scale.

Using the values of the two scaling regimes between slopes and areas observed in Figure 7.11 ($S\sim A^{-0.12}$ if A<210 pixels and $S\sim A^{-0.5}$ otherwise, values that correspond to the
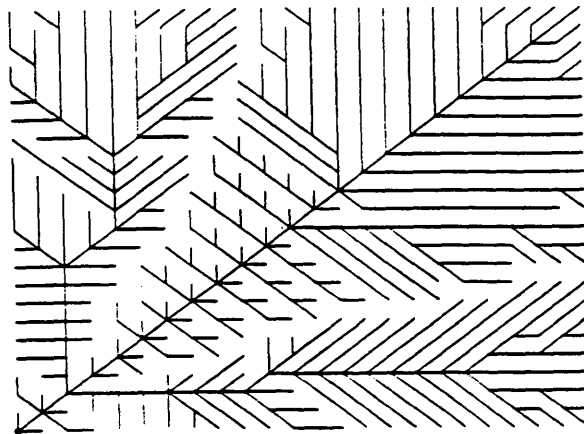
Figure 7.12: Networks simulated with the Slope-Area model using the two mean scaling relationships shown in Figure 7.11.

actual slope-area scaling) and the real boundary of the Big
Creek basin, the Slope-Area model was used to simulate the
drainage network. The total energy expenditure E_T (calculated
using those pixels identified as channels above the threshold
area) is 4.54×10^5 (in pixel units) for the real basin and
4.51×10^5 for the simulated network.

Summarizing, this section has shown that the difference
in total energy expenditure of networks simulated with the
Slope-Area model using actual basin boundaries from DEMs and
the total energy expenditure of the actual river network is
small. This suggests, along with the evidence shown in
Section 6.2, that drainage networks tend to organize
themselves so as to minimize energy dissipation while
delivering water and sediment out of the basin.

7.4. Potential Energy and Total Energy Expenditure

The original expression for $E_T = k\Sigma_i \ Q_i^{0.5}L_i$ is difficult
to manipulate analytically and visualize its minimization is
not an easy task. In this section we will show that the
minimization of E_T is equivalent to the minimization of the
total sum of elevations, constrained by the slope-area
relationship implied by the first two energy principles. This
new interpretation will help in the understanding of the
process through which networks grow and organize to minimize
total energy expenditure and visualize the role of
perturbations in this process.

Using the first two principles of optimal energy expenditure (Rodriguez-Iturbe et al, 1992b) and the scaling relationship that can be derived from them:

$$S_i = k \; A_i^{-0.5} \qquad (7.2)$$

it is possible to show that minimizing the total energy expenditure E is equivalent to the minimization of the sum of elevations:

$$Ep = \Sigma_i \; z_i \qquad (7.3)$$

where z_i is the elevation of pixel i above the outlet. Notice that z_i can be partitioned as the sum of drops from pixel to pixel along the flowing path between pixel i and the outlet, i.e.

$$Ep = \Sigma_i \; \Sigma_{j(i)} \; h_{j(i)} \qquad (7.4)$$

where $h_{j(i)}$ is the drop from pixel j(i) to its neighbor downstream and j(i) indexes the pixels along the flowing path from pixel i to the outlet. The summation in (7.4) can be reorganized by counting how many times a certain drop h_n appears. This number is equal to the number of times a flowing path goes through pixel n, and this is equal to the number A_n of pixels draining through n. Therefore:

$$Ep = \Sigma_n \; A_n \; h_n \qquad (7.5)$$

Now,

$$h_n = S_n \; L_n = k \; A_n^{-0.5} \; L_n \qquad (7.6)$$

108

where S_n is the slope of pixel n and L_n is the length from pixel n to its neighbor downstream. The second equality comes from equation (7.2). Substitution of (7.6) into (7.5) gives:

$$Ep = k \sum_n A_n^{0.5} L_n \qquad (7.7)$$

which is the same expression (7.1) for the total energy expenditure E_T. Another way of looking at this result is by saying that all the potential energy available is spent by the water in its movement downhill and therefore E_p and E_T are the same (Tarboton and Veneziano, personal communications).

By minimizing E_T, the network is also minimizing the sum of elevations Ep (which can be seen as a measure of the total potential energy of the basin). It is important to notice that the state of minimum potential energy for the basin is not the flat plane because of the constraint (7.2) on the slopes. With a flat plane, the network is not able to deliver water and sediment out of the basin. In the Slope-Area model and other landscape evolution models, each pixel is set to drain into the steepest direction downhill. Given that the slope of each pixel comes from the preceding iteration, by choosing the lowest neighbor the pixel is setting its elevation to the lowest possible value. As the network connects all the points in the basin, information is transmitted across the entire domain. On one hand, a change in a pixel's elevation affects the elevation of all the pixels uphill. On the other, the capture of additional area

by pixels uphill changes the contributing area and elevation of pixels downhill. This interaction and communication may be the mechanism through which the principle of global optimality is embedded in the network growth process. The network in its evolution always tends towards states with lower elevation.

7.5. Minimum Total Energy Expenditure, the Stability of Landscapes and the Role of Perturbations

There are landscapes that, if used as initial condition for the Slope-Area model, would not be modified by the algorithm because the slope-area relationship holds at every node. One such landscape is the classic equilibrium form used by Smith and Bretherton (1972) and later by Loewenherz (1991) in their analysis of stability and channelization of surfaces. Figure 7.13.a shows the landscape and Figure 7.13.b the parallel flow directions of the configuration. At every point the slope S is exactly equal to $A^{-0.5}$ and therefore the landscape is at equilibrium and remains unaltered when given as initial condition for the Slope-Area model. However, if a small random perturbation in elevation is applied as was done in Section 7.2, then the configuration changes radically. Figure 7.13.c shows the equilibrium after only one perturbation and Figure 7.13.d after ten perturbations. Figure 7.14 shows the dramatic drop in the value of the total energy expenditure even after a single perturbation. The

110
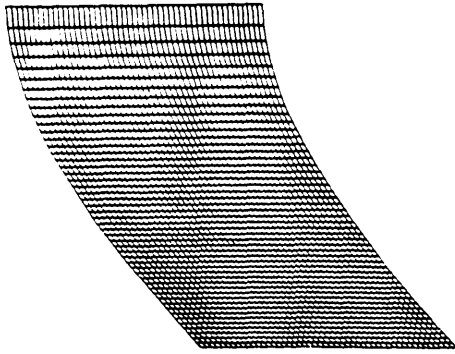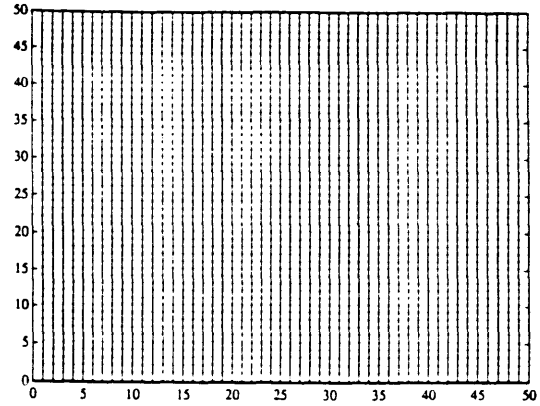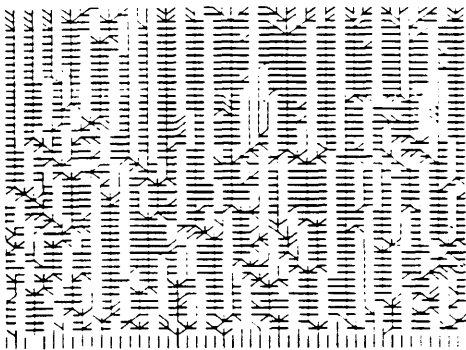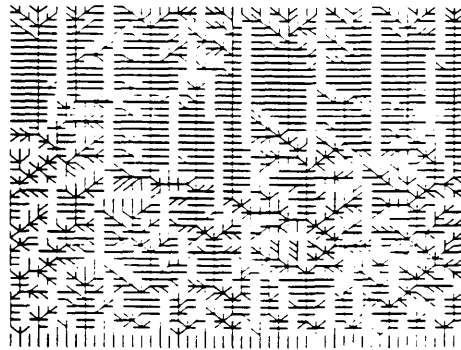
Figure 7.13: Unstable equilibrium landscape
form used by Smith and Bretherton (1972). (a)
Isometric view, (b) Original flow direction,
(c) Equilibrium network after one
perturbation, (d) Equilibrium network after
ten perturbations.
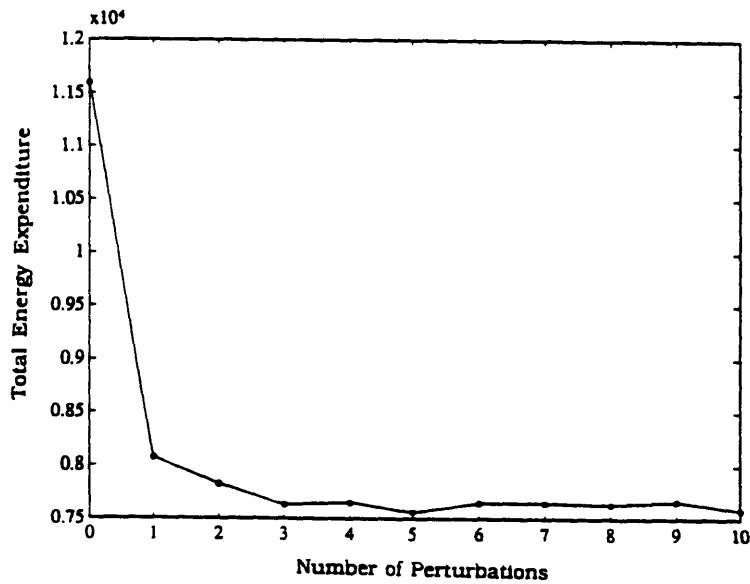
Figure 7.14: Decrease of total energy expenditure for the equilibrium landscape shown in Figure 7.13 affected by repeated perturbations.

system quickly reaches a state of low E_T after three or four perturbations are applied and then remains at that level.

This experiment illustrates the nature of the search for an optimal network configuration. As presented schematically in Figure 7.15, this is a problem with many local minima and the system is able to move between them if its elevation field is perturbed. Each of these local minima (which have very similar values of total energy expenditure) is a different configuration and their large number is consistent with the enormous variety of channel networks found in nature. Even though the details of their structures are different, these configurations have common statistical properties and near-optimal values of E. Furthermore, there are also unstable equilibrium states with high values of E which, when perturbed, move quickly to configurations with

112

low total energy expenditure. An example of these unstable equilibrium landscapes is the one shown in Figure 7.13.a.
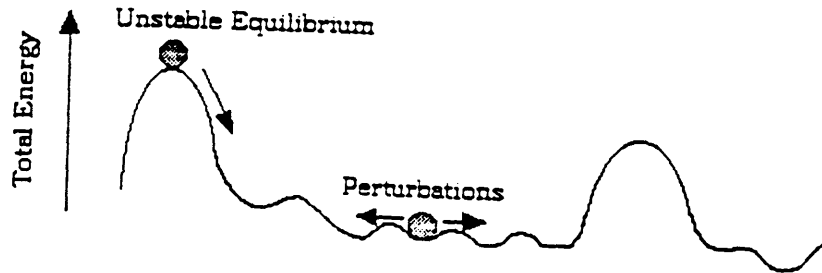
Figure 7.15: Schematic representation of the multiple local minima and unstable equilibrium landscapes in the energy minimization problem of drainage networks.

7.6. Summary

The comparison between levels of total energy expenditure predicted by optimal channel networks and those measured in actual basins identified with digital elevation maps was performed using as an intermediate tool networks generated with the Slope-Area model. First, it was shown that in small domains, that could be handled by the random search algorithm used to find optimal networks in Chapter 6, OCNs and Slope-Area networks have very similar values of total energy expenditure. Then, using the actual boundaries and outlet location of river basins, the Slope-Area model was used to grow networks in these domains. The actual network and the simulated one had very similar values of energy for various basins studied.

By showing the equivalence between total energy expenditure and the sum of elevations in the basin (a measure

of available potential energy), a possible mechanism by which the network evolves to states of low energy was presented. Finally, unstable landscapes in the sense of Smith and Bretherton (1972) were shown to be states of very high energy expenditure which are unsustainable under perturbations.

In the next chapter we will examine the implications of minimum energy expenditure on the shape of river basins. The question is what is the best way to share the space among competing basins from a minimum energy expenditure point of view. The answer will have implications on issues like space allocation and basin elongation.

Chapter 8

Implications of Minimal Energy Expenditure on the Shape of River Basins: Hack's Law and Optimal Allocation of Space

8.1. Hack's Relation

Hack (1957) measured quantitatively his observation that river basins change their shape as their size increases becoming longer and narrower. For the rivers he examined a scaling relationship between the length L of the main channel from the outlet to the divide and the area A of the basin was found:

$$L \sim A^\alpha \qquad (8.1)$$

with α=0.6. Grey (1961) using his own data and those from Taylor and Schwarz (1952) showed the same scaling with α=0.568. Eagleson (1970, p.379) shows that data from different sources fit Hack's relation well.

Mandelbrot (1982) suggested that river courses can be approximated by wiggly fractal lines of dimension D>1. This behavior has been observed using box-counting analysis in DEMs by Tarboton et al. (1988) and La Barbera and Rosso (1989) among others. They have found that the box-counting fractal dimension is on the average 1.1, very near

Mandelbrot's prediction of $2\alpha=1.2$ based on the scaling exponent in equation (8.1).

However, the fractal argument assumes that the shape of the basin does not change as the area increases and that the entire scaling behavior comes from the fractal character of the channels. This does not fit with the original idea of elongation proposed by Hack (1957). Such arguments have been raised by different authors, among them Feder (1988, p.208). The issue of elongation and fractality of rivers has also been studied by Robert and Roy (1990).

We will examine in this section the possibility that the observed elongation of river basins can be regarded as the consequence of the optimum allocation of area in a minimum energy sense. In order to examine such possibility, let us consider the following experiment. Given an area of width L and length h, we will drain it using OCNs constructed in sub-basins of width w and length h, as shown in Figure 8.1. This configuration can be considered as an idealization of tributaries to a main channel.
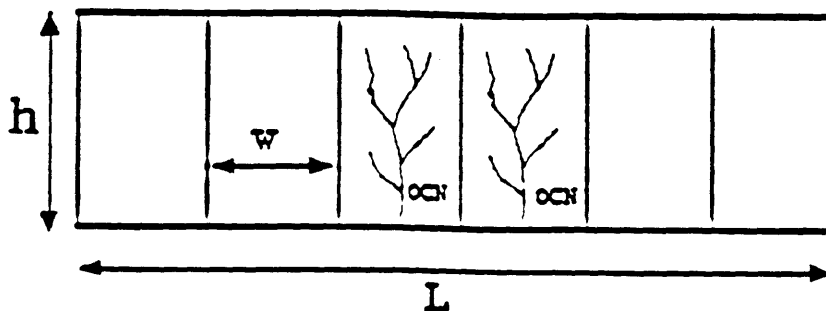
Figure 8.1: Optimization domain of width L and length h. This domain is drained by OCNs of width w and length h.

The total energy expenditure for the entire area is $E_T=(L/w)E_s$ where E_s is the energy of the network in the sub-basin of size $w*h$. In order to find the minimum E_T given L, we should look for the minimum value of E_s/w. To do this, the values of total energy expenditure in OCNs constructed in areas of size $w*h$ with different values of w are calculated. The OCN with the smallest value of E_s/w will yield the minimum total energy expenditure for the entire basin and will determine the optimal length/width ratio.

Figures 8.2.a and 8.2.b show the values of E_s/w versus width for OCNs with h=15 and h=20 for different values of w. The optimal value of width is the one that gives the lowest value of E_s/w. Figure 8.3 shows OCNs with optimal values of width for h=60, 45, 30 and 15 respectively. Using the optimal width $w^{opt}(h)$ for a given h, we can find the relationship between length h and area $A=h*w^{opt}(h)$. Figure 8.4 shows the scaling relationship: $h \sim A^{\alpha}$ with $\alpha=0.57$ which is very similar to the value of 0.568 observed in actual basins (Taylor and Schwarz, 1952). This relationship indicates that in the search for optimal drainage configurations, basins elongate with size and do so at the rate observed in nature (Grey, 1961, Taylor and Schwarz, 1952).

One important point remains to be analyzed in order to make a meaningful comparison between Hack's result and the relationship obtained from optimality principles. In the case of OCNs, the lengths used were the Euclidean lengths from top
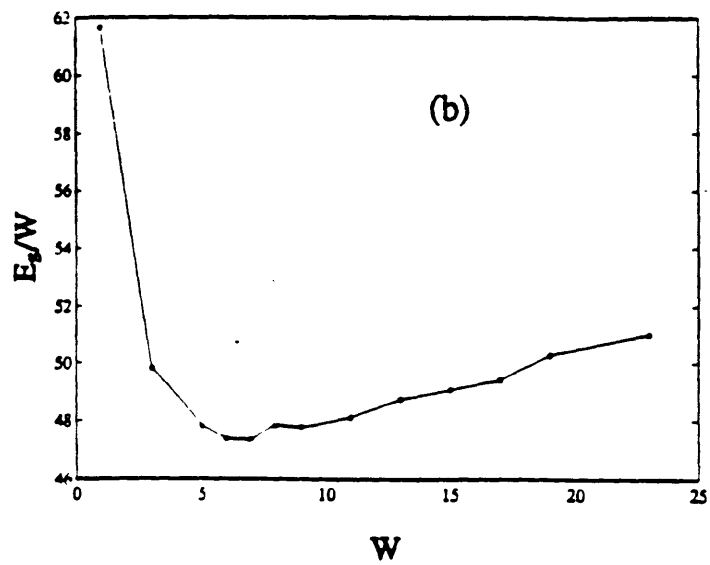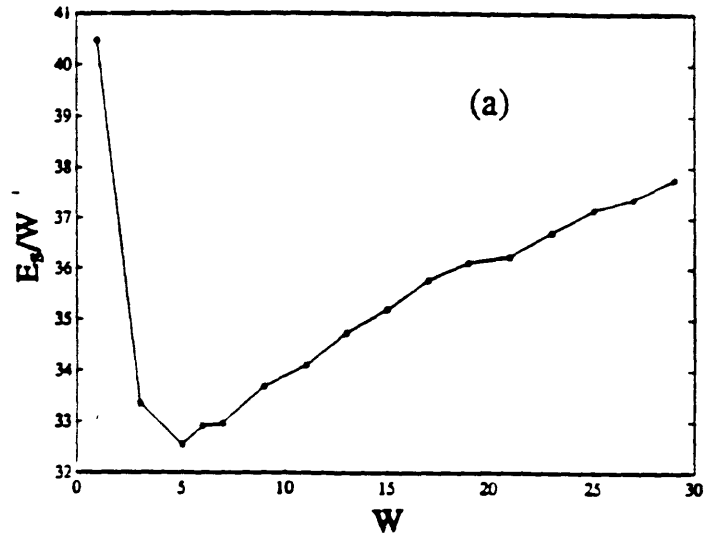
Figure 8.2: Values of E_s/w versus w for OCNs with length (a) h=15 and (b) h=20. E_s is the total energy expenditure of the OCN in the domain of size w*h.
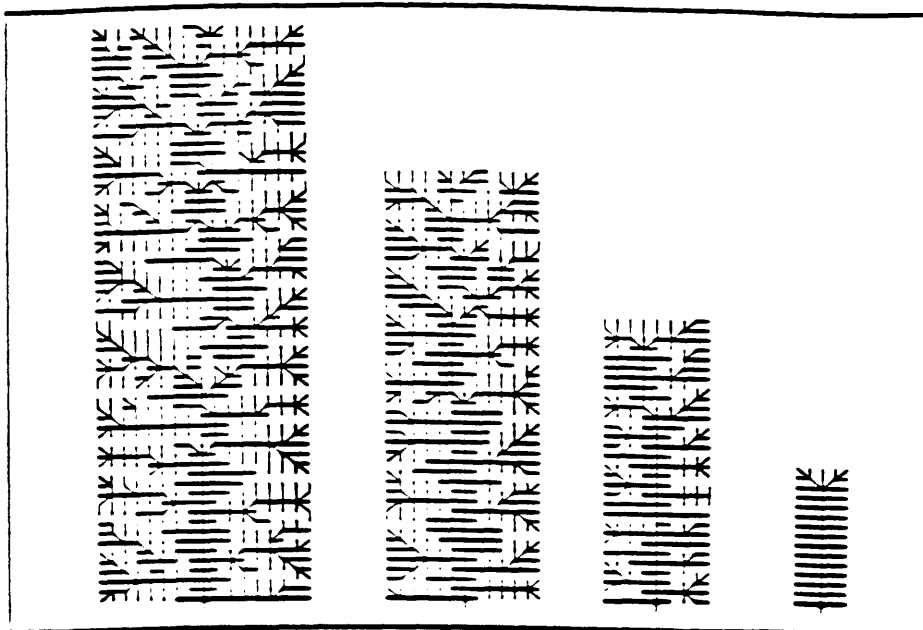
Figure 8.3: OCNs with optimal values of width for h=60, 45, 30 and 15 pixels respectively. The optimal value of w for each h is the one that gives the lowest value of E_s/w.
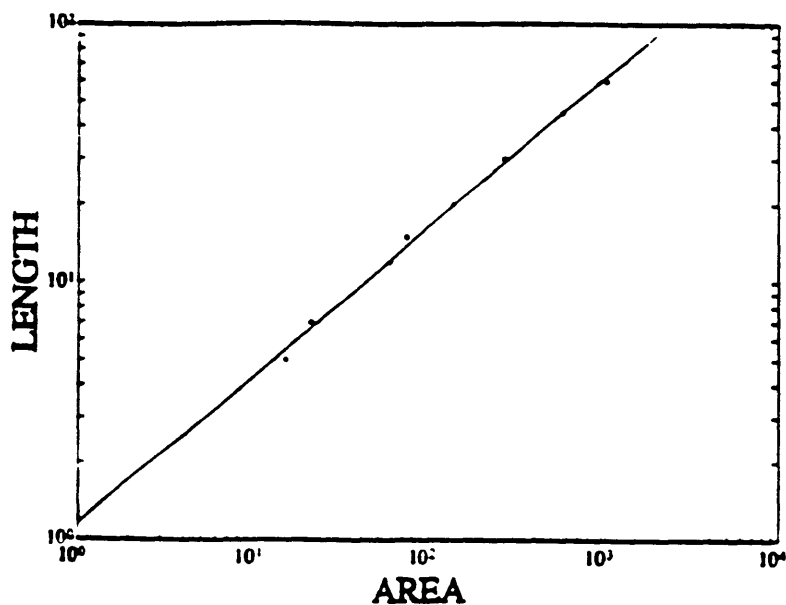
Figure 8.4: Log-log plot of length h versus area $A=h*w^{opt}(h)$. The scaling slope is $\alpha=0.57$.

119

to bottom of the sub-basin and not along the channel as has been the practice in the study of geometrical features of river basins. With the aid of DEMs we can compare the relationship between the Euclidean length (measured with a straight line) and the topological length (measured along the main channel).

Using a threshold value of area, a network can be identified in the DEM (Tarboton et al, 1988). At the intersection of every two links of the network, we defined the outlet of a sub-basin. For each sub-basin we calculated the total topological length measured along the main channel up to the boundary and the Euclidean length from that point in the boundary to the outlet. The two lengths are related by $L_t \sim L_e^{\beta}$. Table 8.1 (Ijjasz-Vasquez et al, 1993b) shows the values of β for different basins located across the US. The average value of β is 1.05. Because of the opportunity the channel has to wander more as the size of the basin increases, a value of $\beta > 1$ is not surprising. We will examine in Chapter 9 the significance of a value of $\beta > 1$ in terms of the self-affine properties of watercourses. Figure 8.5 shows an example of the relationship between Euclidean and topological length for every sub-basin in the case of Brushy Creek basin (AL).

Notice however, that if the boundaries of river basins were geometrically similar, then $L_e \sim A^{0.5}$ and consequently $L_t \sim A^{0.525}$ (using $\beta = 1.05$) which is much lower than the value of

Basin	β
Beaver Creek	1.07
Brushy Creek	1.04
Buck Creek	1.08
Big Creek	1.04
East Delaware River	1.02
Schoharie Creek Headwaters	1.07
North Fork Cour d'Alene River	1.04
Racoon Creek	1.04
Schoharie Creek	1.03
St. Joe River	1.04

Table 8.1: Values of the scaling slope between maximum Euclidean and topological length for every sub-basin in different river basins across the U.S.
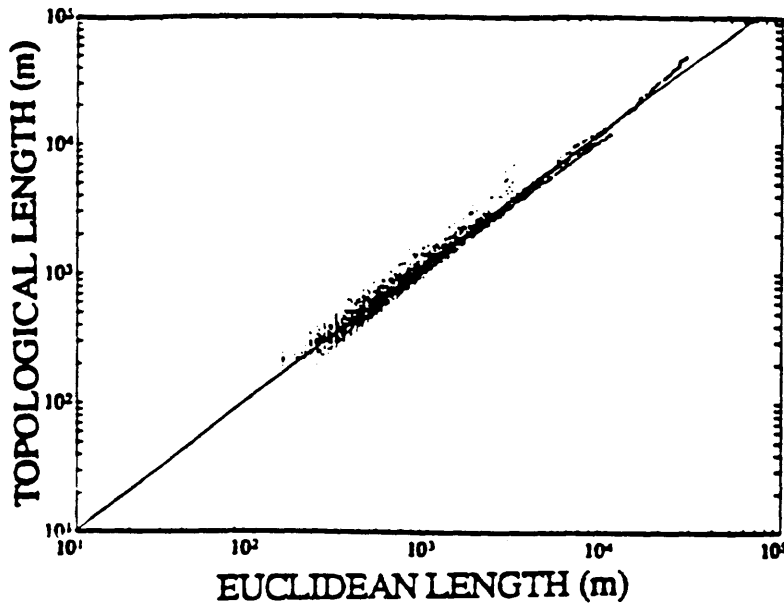
Figure 8.5: Log-log relationship between the maximum Euclidean and topological length for every sub-basin in the Brushy Creek basin. The scaling slope is β=1.04 in this case.

α found in river basins. On the other hand, the measured value of $\alpha=0.6$ along with $\beta=1.05$ would imply that $L_e \sim A^{0.571}$ which is very near what is observed in the elongation derived from OCNs.

Another way of comparing the elongation behavior between OCNs and DEMs is by taking all sub-basins for an OCN grown in a domain as large as possible and using a measure of catchment shape.

There is a large number of measures to describe the shape of catchments using different ratio combinations of area, perimeter and maximum length (Zavoianu, 1985). One of the earliest measures was proposed by Horton (1932) and is called the form factor $R_f = A_b/L^2$ where A_b is the area of the basin and L its maximum length from the mouth to the opposite side. Miller (1953) introduced the circularity ratio $R_c = A_b/A_c$ where A_c is the area of a circle whose circumference is equal to the basin perimeter. Schumm (1956) proposed the elongation ratio $R_e = D/L$ where D is the diameter of a circle of area equal to that of the basin, i.e. $R_e = (2/\pi^{0.5}) A^{0.5}/L$. Also, noting the similarity of an "ideal" basin shape and lemniscate curves, Chorley et al. (1957) defined the lemniscate ratio $R_l = P/P_m$ where P_m is the basin perimeter and P is the perimeter of the ideal lemniscate with parameter k. The value of k is calculated as $\pi L^2/4A$ where L and A are measured in the actual basin. As pointed out by Morisawa (1958), the influence of the irregularity of the divide on

measures based on the perimeter of the basin becomes very high as the size of the basin increases. This is a direct consequence of the fractal character of basin boundaries (Tarboton et al. (1988), Ijjasz-Vasquez et al (1993c)). Therefore, we have preferred to use Schumm's elongation ratio to analyze catchment shapes.

As pointed out by Eagleson (1970), Schumm's elongation ratio cannot be separated from Hack's relation. Schumm's elongation ratio should scale with area as $Re \sim A^{0.5}/L \sim A^{-0.068}$ (Eagleson, 1970, p.379). We will now examine this scaling relationship in DEMs and OCNs.

Figure 8.6 (Ijjasz-Vasquez et al, 1993d) shows, with dots, the scaling relationship between L and A for all sub-basins in the North Fork Cour d'Alene river (ID). The fitted lines gives a scaling relationship $L \sim A^{0.563}$ implying $Re \sim A^{-0.063}$ very near the value presented by Eagleson (1970). Similar scaling values were found for other basins analyzed. Superimposed on Figure 8.6 we have presented, with (+), the values of L and A for all sub-basins from an OCN constructed in a 100x100 domain (shown in Figure 6.3). The results from the OCN fall within the range of variation of the DEM data. The best-fit line to the OCN points gives a slope of 0.573 not very different from the value for the DEM data. In this way we have also shown the elongation of OCN sub-basins when they are free to compete instead of being in a controlled

experiment like the one presented at the beginning of this
section.
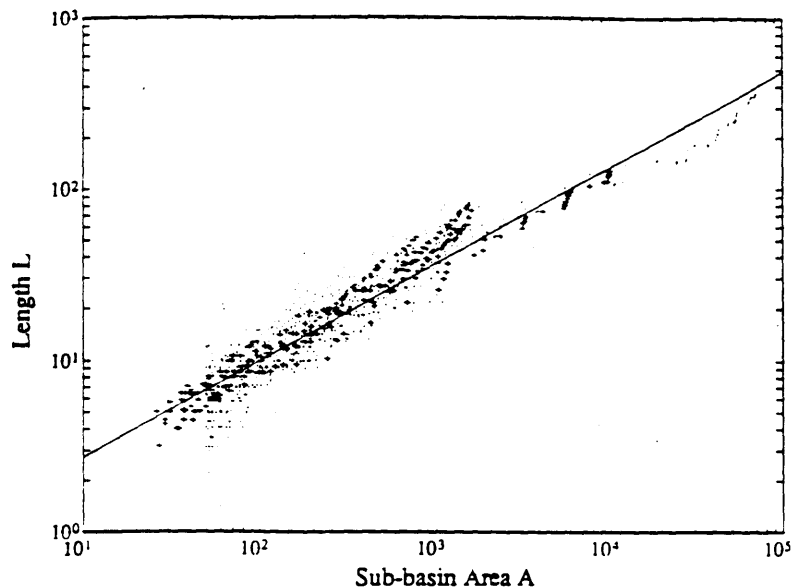
Figure 8.6: Scaling relationship between the
area and maximum Euclidean length for all sub-
basins in the North Fork Cour d'Alene river
basin (.) and for an OCN constructed in a
100x100 domain (+). The fitted line
corresponds to the DEM data.

8.2. Optimal Allocation of Space Around a Central Outlet

8.2.1. Allocation of Space by OCNs

One important geometric characteristic of network
structures and fractal growth patterns is the way in which
their components are organized in space. Such organization
can be studied by examining the set of angles among subtrees.
The understanding of the behavior of these preferred angles
can provide a better picture of the hierarchical ordering of
fractal patterns and the physical dynamics of competition and
screening that generate these structures. Diffusion Limited
Aggregates (DLA) is an example of the kind of structures

124

recently analyzed in this context (Arneodo et al, 1992). The results of such analysis in DLA have been useful in developing hierarchical models to describe the DLA structure (Halsey et al. (1986), Ball (1986), Lee et al. (1990)).

We will study in this section how space is allocated in an optimal way around a central outlet. The results will be compared in the next section against three different models of network organization and a related small-scale erosion experiment. If a drainage network is designed to deliver water and sediment out of a circular domain, a natural question is how many sub-basins (or independent drainage units) are optimal for this work?

Figure 8.7 shows three sectors of a circular domain, with different central angles. Using sectors like these, OCNs were constructed to drain them. The question is whether the entire circular domain is more efficiently drained by 4 sub-basins with a central angle of 90°, 6 of 60°, 12 of 30° or any other angle. The total energy spent in draining the circle is $E_T = (2\pi/\theta)\ E_{c\theta} = n_\theta E_{c\theta}$ where θ is the central angle of the sector of circle used, $E_{c\theta}$ is the total energy expenditure of the OCN constructed within the sector of angle θ and n_θ is the number of sub-units (or sectors) the circle has been divided into for its drainage. Figure 8.8 shows the energy per pixel for the entire circle $(E_T/\pi r^2)$ when drained by OCNs constructed in sectors with different central angles.
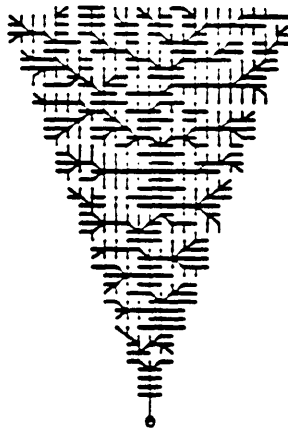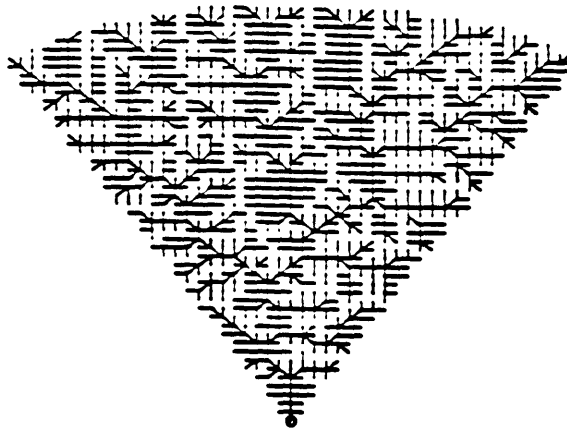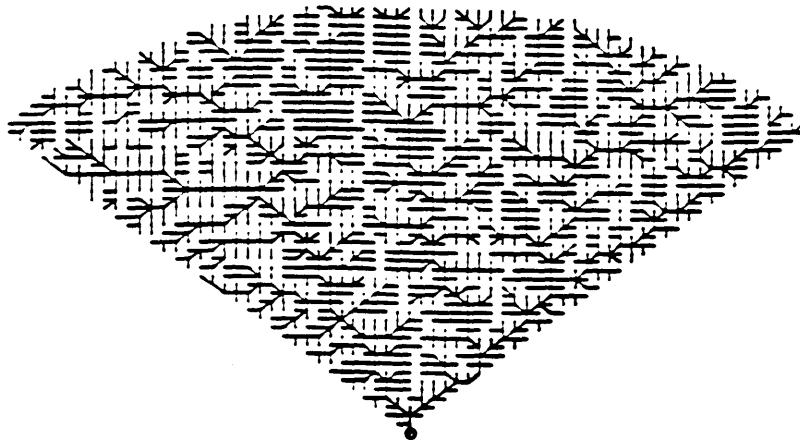
Figure 8.7: OCNs constructed in sectors of a circle with central angles 90˚, 60˚ and 30˚.

There appears to be a minimum of energy at 60° (i.e. 6 sub-basins).

It is interesting to contrast this result with an unconstrained analysis of optimal central angles. In Rigon et al. (1993) triangular domains with different central angles were studied by keeping the area of the basin constant (i.e. changing the base and height of the triangle accordingly). The energy per unit area decreased with larger central angles but no clear minimum was found. The difference with the experiment presented in this section is the division of the same domain using sub-units to minimize the total energy expenditure of the entire domain instead of analyzing domains with different form but equal area.
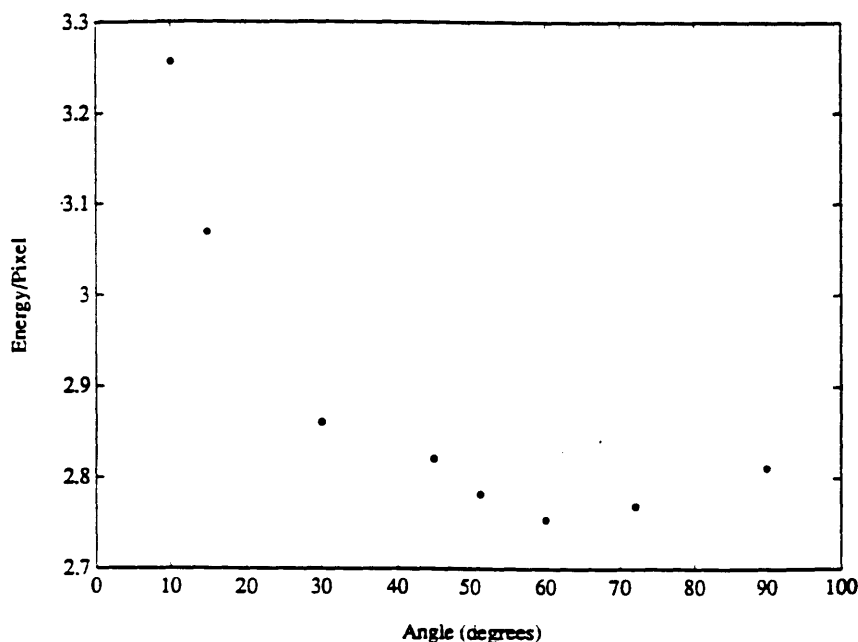
Figure 8.8: Total energy expenditure per unit area for the whole circle when it is drained by OCNs constructed in sectors with different central angles.

8.2.2. Allocation of Space by Other Models

Now we can compare the optimal allocation of areas in six sub-units around a central outlet with the way other network models divide space in a similar domain. We will examine three different models in this section: A DLA-like model, the Slope-Area model and a random network growth model. A method to count major drainage units is developed for the last two models. We will also discuss a related small-scale erosion experiment.

Let us first consider a DLA-like model proposed by Meakin (1991b) In this river network evolution model the elevation field z obeys the Laplace equation and the rate of river growth is proportional to the local gradient of z. The model is equivalent to a diffusion-limited aggregation model. A related invasion percolation model has been presented by Stark (1991) as another possibility of river network growth.

In DLA studies, it has been shown using wavelet transforms (Arneodo et al, 1992) and stability considerations (Procaccia and Zeitak (1988), Derrida and Hakim (1992)) that there exists a preference for a pentagonal symmetry in DLA at the macroscopic level. This means that _five_ major branches are preferred in the organization of the structure around the central seed. Originally, it was this result that motivated our interest in the allocation of space in river networks.
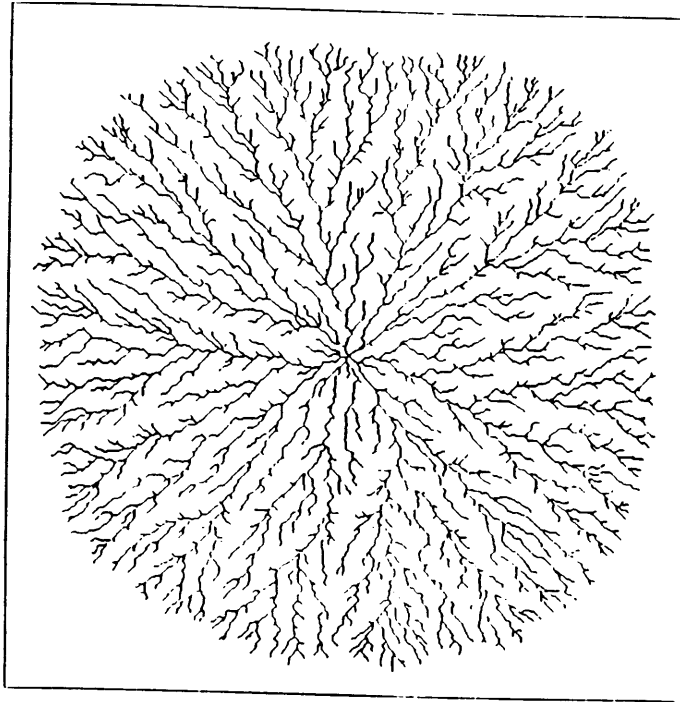
Figure 8.9: Example of a network simulated with the Slope-Area model around a central outlet.

The second model we will consider is the Slope-Area model. Figure 8.9 shows an example of a drainage network grown in a 500x500 domain with the outlet in the center. In order to make a reasonable and unbiased comparison with the results from the previous section, it is necessary to devise a quantitative criterion to count the number of sub-basins around the outlet. There are two extreme cases, illustrated in Figure 8.10: a spiral pattern with a single channel, and an explosion pattern with every node going directly into the outlet without aggregation (Stevens (1974), Rodriguez-Iturbe et al. (1992b)).
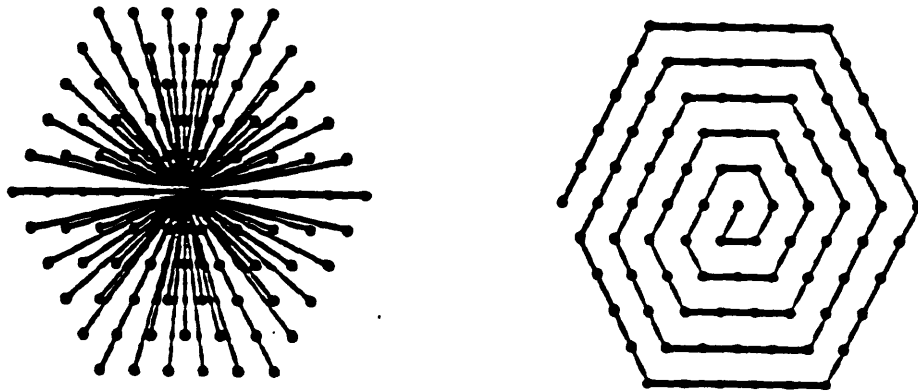
Figure 8.10: Two extreme cases (spiral and explosion patterns) of networks around a central outlet (from Stevens, 1974).

There are two key parameters in the counting procedure to identify structurally different networks: first, the distance from the outlet at which counting should be done and second, the value of contributing area to be used to distinguish the main channels. It is important not to do the counting too near the outlet because of grid effects but not too far away either to avoid counting channels that may merge downstream before entering the outlet. Grid effects occur when the counting is done at a small distance from the outlet because the small number of nodes around the outlet can bias the results. Figure 8.11 shows, for a simulation in a domain with 10^4 pixels, the contributing area of nodes located at different distances from the outlet. At distance 0, there is only one node with area 10^4 (the outlet itself). As we move away from the outlet, some nodes have large areas and some have very small areas (the latter overlap each other on the
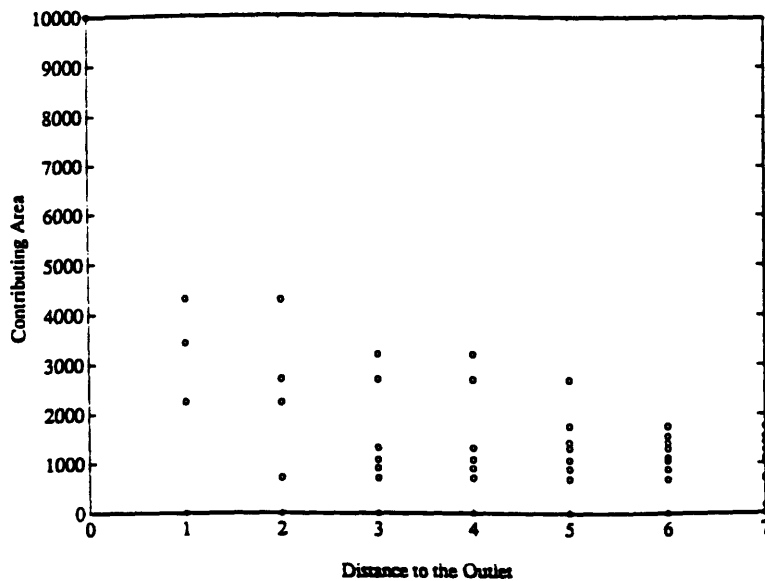
Figure 8.11: Contributing area of nodes located at different distances from the outlet for a network grown in a 10^4-pixel domain with the Slope-Area model. This diagram illustrates the way in which major independent drainage sub-units are counted.

of 4 pixels is a reasonable value for the counting. Nodes at distances 1 or 2 are affected too much by grid effects and at distances 6 or higher it is all too frequent to have major channels which merge downstream before entering the outlet.

The threshold value of contributing area used to identify pixels as channels in this work has been chosen as the ratio between the total area (10^4 pixels in our simulations) and the number of channels that would appear in the explosion case at distance 4 (which in a square grid are $8*4=32$). In this way, we can be sure to count the channels even in the extreme explosion case.

One hundred simulations were performed with the Slope-Area model and the number of branches or major drainage sub-basins were counted using the above procedure. Figure 8.12
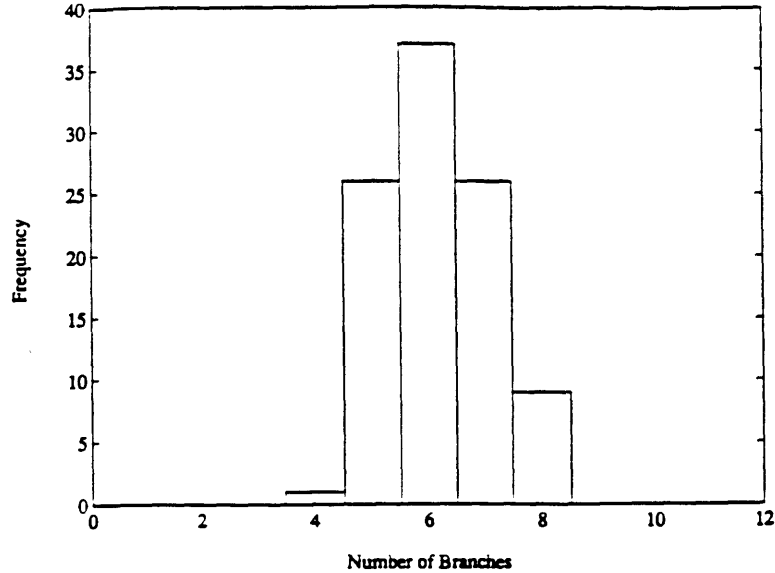
Figure 8.12: Histogram of the number of drainage sub-units for 100 simulations of the Slope-Area model. The histogram shows a peak at a value of six sub-basins.

shows the distribution of the number of drainage sub-units. The histogram shows a peak at _six_ sub-basins which parallels the result obtained from optimality principles. Furthermore, notice that the histogram is concentrated around 6 even though the two extreme cases (spiral and explosion) have 1 and 32 branches. Sensitivity studies on the values of the two parameters of the counting procedure (distance from the outlet and threshold are to identify main branches) show that the peak of the histogram moves at most between five and seven with reasonable values of the parameters.

The third model we will examine is a random network growth model. The structure is grown around a central seed and at each iteration a new layer of nodes surrounding the structure is added. The flow direction at each newly added node is chosen at random as long as it joins another node

already in the structure. The drainage directions allow the calculation of contributing areas and the determination of the network. This random model is similar in spirit to the Eden model (Vicsek (1989), Meakin (1991)) and the classical random network model by Howard (1971). If the counting procedure used for the Slope-Area networks is applied to the random networks, we obtain the histogram of the number of main branches for 100 simulations is shown in Figure 8.13. There is a clear peak at four branches. Varying the parameters of the counting procedure will not move the peak above five branches. It would be interesting to analyze the behavior of the modified version of Howard's model where junction angles are moved to satisfy a minimum-energy expenditure criterion (Howard, 1990) to see the effect of local optimization rules on the allocation of space.
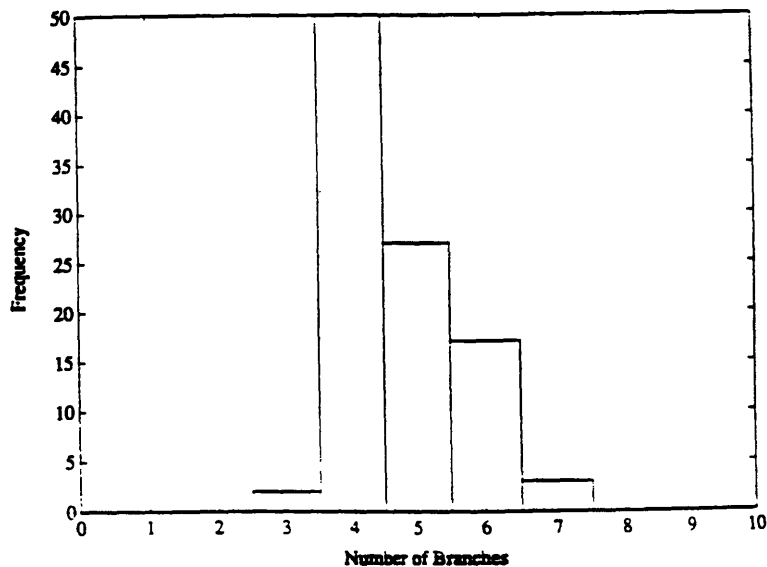
Figure 8.13: Histogram of the number of drainage sub-units for 100 repetitions of the random network growth model .

We have shown in this section the way in which three different models allocate space among independent sub-units to drain a circle area towards a central outlet. A DLA-like model used five major sub-basins, the Slope-Area model used six and a random network growth model used four. These results can be compared to that of Section 8.2.1 where the drainage of a circle by OCNs grown in sectors was optimal when six sub-units were used.

Finally, we would like to include some preliminary results from a related small-scale erosion experiment developed in collaboration with G. Moglen and L. Reingold (unpublished results). The original purpose of this experiment was to study the formation and growth of the drainage structure that develops to do the work of delivering water and sediment out of a sandbox. A similar sanbox experiment was performed by Wittman et al. (1991). Many erosion experiments have been reviewed by Schumm et al. (1987) but they do not have the domain configuration used in this section.

The sandbox in our experiment had an outlet in the center through which water and sand were drained. Water was poured on the outer boundary through a porous tube. The outlet was closed until the sand in the box was saturated. Once the outlet was opened, water and sand began to flow towards the center and a drainage structure formed. We counted the number of sub-basins formed around the center:

out of 5 experiments, 3 of them had 6 independent drainage sub-units, 1 had 5 and 1 had 7. Although there are many differences between this experiment and the formation and growth of actual river basins, including for example the way water comes into the system (from the boundary instead of uniform rainfall), scale issues (slopes, relief, droplet size, etc.) and channel stability differences, it is interesting nevertheless to observe some features of competition and probably optimal energy dissipation on such a small scale sharing the behavior observed in landscape evolution models.

8.3. Summary

We have examined in this chapter the implications of the principles of energy expenditure on the shape of river basins, specifically on the problems of elongation of basins with increasing size and the optimal allocation of space around a center outlet.

The elongation of basins, described by Hack's relationship was reproduced by Optimal Channel Networks with the appropriate scaling exponent. A discussion on the explanation of Hack's law based on the fractal character of rivers was presented.

It was shown also that the optimal way to distribute space around a central outlet is by using six independent drainage units. This behavior was reproduced by the Slope-

Area model but not by a random network model nor a DLA-like model. A related small-scale erosion experiment also showed six branches in its drainage structure.

Despite the fact that Mandelbrot's argument of the fractality of river courses as the cause of Hack's law was not valid because of the lack of geometrical similarity of river shapes, it is clear that watercourses do not follow a straight line. The next chapter uses new tools to better characterize the tortuosity of individual channel and basin boundaries and also to relate it to physical parameters.

Chapter 9

Self-Affinity of River Courses

and Basin Boundaries

9.1. Introduction

The extraordinary geometrical complexity of river systems has been studied with success in numerous papers using the tools of fractal geometry. The concept of fractals was introduced by Mandelbrot (1977) to study irregular shapes with similar geometric characteristics over a range of scales. Fractals are objects in which properly scaled portions are identical (in a deterministic or statistical sense) to the original object. A descriptor of this scaling behavior is the fractal dimension. Common examples of fractals include the shore of continents, the shape of clouds, the profile of mountains and river systems (Peitgen and Saupe (1988), Meakin (1991b)). In river systems the fractal scaling can be observed at two different levels, either at the scale of organization of the river network structure or at the individual wandering watercourse (Nikora, 1991). Fractal properties of river systems at both levels have been analyzed by Tarboton et al. (1988), Hjelmfelt (1988), La Barbera and Rosso (1989), Snow (1989) and Nikora (1991) among others. These studies have described the fractal scaling of the geometrical properties of river systems and

have calculated the corresponding fractal dimensions. All of these studies have considered rivers as self-similar fractals based on the calculation of the box-counting dimension.

There are however, two types of fractal objects: self-similar and self-affine. The difference between them resides in whether the appropriate rescaling of the parts to obtain the original object is isotropic or anisotropic (i.e. the amplification scales are not the same in different directions). Two classical examples of self-similar and self-affine fractals are coastlines and mountains. In coastlines, the small peninsulas and bays at the beach scale are indistinguishable from the peninsulas and gulfs at the continental scale when amplified isotropically, i.e., they are self-similar fractals. Mountains, on the other hand, look very flat when viewed at planetary scale but very rough when viewed at human scale. However, if different scales are used for the horizontal and vertical amplifications, the rescaled mountain profiles look the same, i.e., they are self-affine fractals. So, in order to characterize the scaling invariance of 2-D self-similar fractals, one needs a single number, the fractal dimension, while for self-affine fractals, the anisotropic scaling requires two numbers (Matsushita and Ouchi, 1989).

The purpose of this chapter is to investigate the scaling properties of individual watercourses and basin boundaries and to study whether these objects are self-affine

or self-similar fractals. Similar structures in other fields have shown self-affine scaling, for example directed polymers (Kardar and Zhang (1987), Perlsman and Schwartz (1992)) and the boundary of growing interfaces (Kardar et al. (1986), Meakin (1989)). We will also use the Slope-Area model to analyze the influence of the vertical dimension and the dynamical evolution of the landscape on the scaling behavior of the planar form of channels.

Section 9.2 describes the method used to analyze the scaling of river structures and to discern its self-affine or self-similar character. Section 9.3 presents the scaling analysis of channels extracted from digital elevation maps. Section 9.4 studies the channels of simulated landscapes under different conditions. Section 9.5 looks at the scaling behavior of catchment boundaries and compares it to the results of Section 9.3. Finally, Section 9.6 presents two simple stochastic models of watercourses that graphically illustrate the difference between self-affine and self-similar fractals.

9.2. Self-Affine Scaling of Curves

As explained in the introduction, self-affine objects are invariant under anisotropic rescaling. The most commonly studied self-affine objects are single-valued functions which hold:

$$F(x) = b^{-H}F(bx) \tag{9.1}$$

with H>0 (Vicsek, 1989). If we take the graph of this function and rescale the x-axis by a factor 1/b and the y-axis by a factor $1/b^H$ we obtain the original graph.

A well-known function that behaves in a similar fashion to (9.1) is the trace of a fractional Brownian motion (fBm). This process describes the movement of a particle such that the increments of its position scale with time as:

$$x_H(t) - x_H(0) \sim t^H \tag{9.2}$$

Notice that $x_H(t)$ and $b^{-H}x_H(bt)$ are identical in distribution (Feder, 1988). fBm has been used in hydrology to simulate series that reproduce the Hurst phenomenon (Mandelbrot and Van Ness (1968), Mandelbrot and Wallis (1968)). Extensions to surfaces have been used to simulate mountains and clouds (Peitgen and Saupe, 1988).

The trace of a fBm is a self-affine object because the scaling necessary to obtain the original distribution is different in the horizontal and the vertical axis. Matsushita and Ouchi (1989) have developed an algorithm to study the self-affinity of curves which are not necessarily uni-valued functions as are the examples presented so far.

Let us consider a curve in which the smallest length scale is 1 (defined as unit length). In the case of a digital elevation map, 1 is the pixel size. Now, we can take two arbitrary points P_i and P_{i+N} separated by N units (i.e. by a

distance N1) along the curve, and calculate the variance of the x and y-coordinates of the points between P_i and P_{i+N}:

$$X^2 = \frac{1}{N} \sum_{j=i}^{i+N} \left(x_j - \mu_{i,i+N}(x)\right)^2 \qquad Y^2 = \frac{1}{N} \sum_{j=i}^{i+N} \left(y_j - \mu_{i,i+N}(y)\right)^2 \quad (9.3)$$

where:

$$\mu_{i,i+N}(x) = \frac{1}{N} \sum_{j=i}^{i+N} x_j \qquad \text{and} \qquad \mu_{i,i+N}(y) = \frac{1}{N} \sum_{j=i}^{i+N} y_j \qquad (9.4)$$

By repeating the calculations for many pairs of points at different distances N, we can find the scaling behavior of:

$$X^2 \sim N^{2\upsilon_x} \qquad \text{and} \qquad Y^2 \sim N^{2\upsilon_y} \qquad (9.5)$$

If the scaling exponents υ_x and υ_y in (9.5) are the same, we have a self-similar fractal with fractal dimension $D=1/\upsilon_x =1/\upsilon_y$. If υ_x and υ_y are different, then we have a self-affine fractal because the scaling behavior is anisotropic (Matsushita and Ouchi (1989), Matsushita et al. (1991)). Methods commonly used to measure fractal dimensions, like box counting, are not able to identify this kind of anisotropy.

To illustrate the procedure described, let us use a well-known example of a self-affine object: the trace of a simple Brownian motion (which is a fBm with Hurst coefficient H=0.5). A simplified version was used by Scheidegger (1967) to simulate river courses. In this case, at each timestep the particle moves one unit up or down with equal probability.

Figure 9.1 shows a realization of such motion. Figure 9.2 shows the scaling of X^2 and Y^2 versus N. The slopes of the lines give, from equation (9.5), υ_x =1.0 and υ_y =0.5 as predicted by the theory of fBm (Kondoh et al, 1987). What these exponents indicate is that a rescaling of the horizontal axis by a factor 1/b needs a rescaling of the vertical axis by a factor $1/b^{1/2}$ to leave the distribution invariant in a statistical sense.

9.3. Self-Affine Scaling of Watercourses

In this section we will study the scaling properties of the main channel in a river basin using the procedure of Matsushita and Ouchi (1989) described in Section 9.2. The main channel is identified by beginning with the outlet and travelling upwards. At each bifurcation the path with largest contributing area was followed. Figure 9.3 shows an example of a river basin, its boundary and its main channel.

There are two points to be noticed when analyzing the scaling properties of channels. First, in the case of the Brownian motion shown in Figure 9.1, the preferential axis of the walker's movement was the horizontal. This is not the case in rivers where the overall flow orientation may occur in any direction. Therefore, it is necessary to repeat the analysis of Section 9.2 using different orientations to find the principal axis of anisotropy.
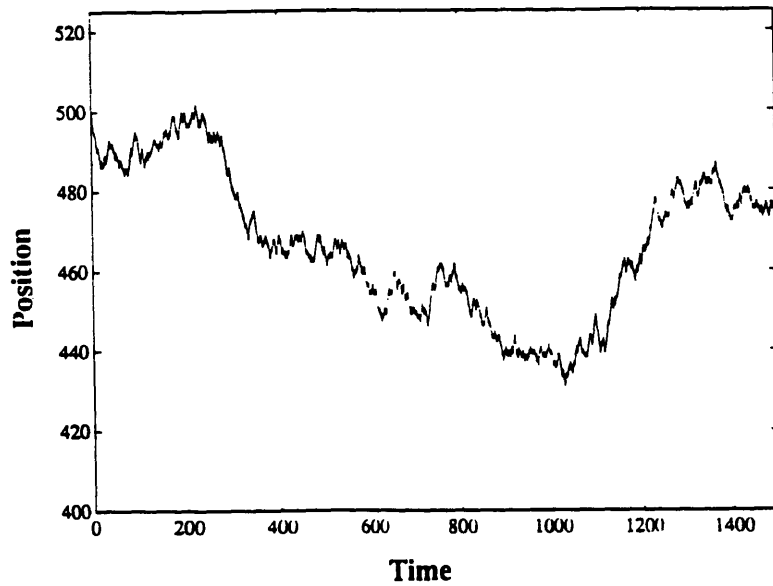
Figure 9.1: Trace of a Brownian motion with unit jumps. The horizontal axis represents time and the vertical axis the position of the particle.
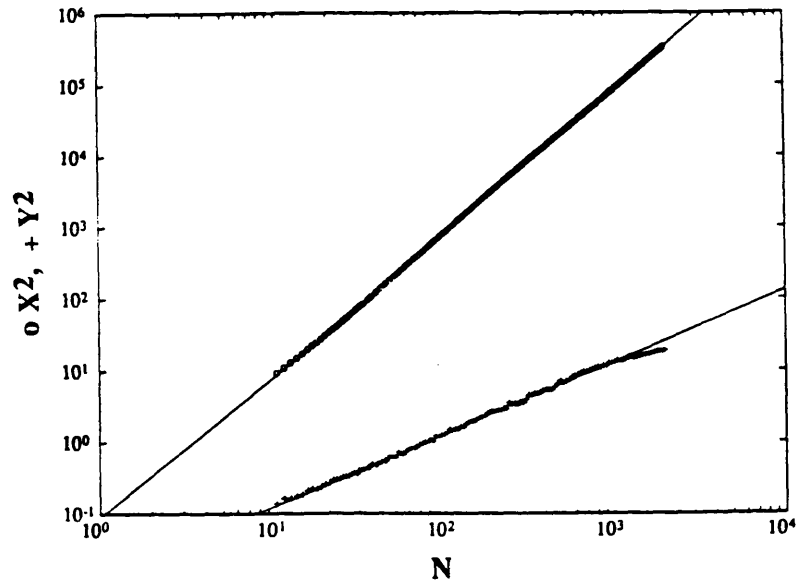
Figure 9.2: Self-affine scaling of the trace of a Brownian motion. (o) represents the scaling of X^2 and (+) the scaling of Y^2, calculated using Equation (9.3). The slopes of the fitted lines give $v_x=1.0$ and $v_y=0.5$.

Second, in order not to over-estimate the scaling and roughness of self-affine curves, linear trends have to be taken away (Malinverno, 1990). The method of Matsushita and Ouchi (1989) handles a linear trend well as long as this trend does not change. It is not uncommon to observe in actual rivers an overall trend but sometimes such a trend shifts near the top of the basin as tributaries of similar size merge to form a larger channel. Figure 9.3 shows with a line across the main channel the point where the shift in direction occurs for that particular basin. In this section of the paper we will do the scaling analysis excluding the small portion at the top. In Section 9.5 we will describe a more elaborate method for detrending the entire river. Both methods give very similar results.
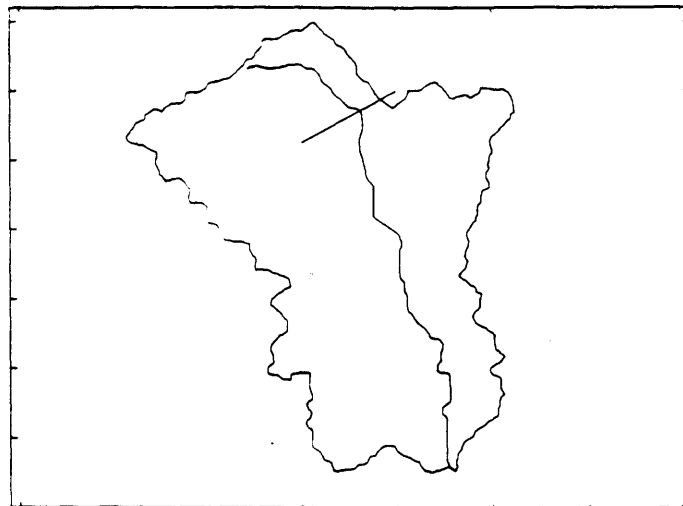
Figure 9.3: Boundary and main channel of the East Delaware river basin. The small line across the main channel indicates the change in trend.

Now we can proceed to find the scaling of X^2 and Y^2 for different axis orientations. Figure 9.4 shows the log-log scaling of Y^2 versus N for different axes oriented at every 15°. If the watercourse were a self-similar object, the slopes would be the same for different orientations. However, this is not the case and Figure 9.5 presents the scaling of X^2 and Y^2 for the principal anisotropy axes. The slopes give $\upsilon_x=1.0$ and $\upsilon_y=0.75$ showing that indeed we have a self-affine object. The principal anisotropy axes are located, not surprisingly, along the overall direction of the channel and perpendicular to it.

Table 9.1 (Ijjasz-Vasquez et al, 1993c) shows the scaling exponents of the main channels of nine different basins located throughout the US. In all cases we have found self-affine scaling with $\upsilon_x\approx1.0$ and $\upsilon_y\approx0.75$. Given that these
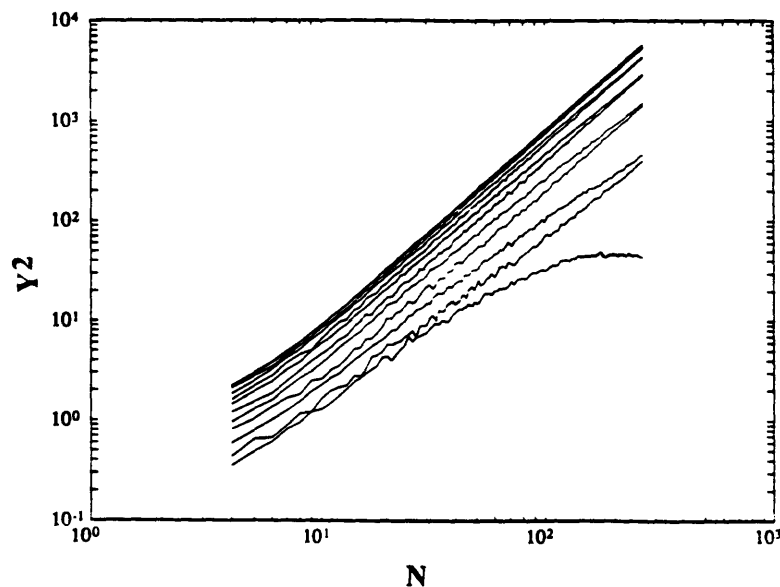
Figure 9.4: Scaling of Y^2 of main channel of the East Delaware river basin for different axis orientations every 15°.

145

rivers are located in regions where the relief can be appropriately measured with DEMs, it is possible that in regions where meandering is a dominant feature of the river, the scaling parameters will change. Related work on fractal dimensions of meandering rivers has been presented by Nikora (1991) and Snow (1989). Different tools to identify the river courses were used in these cases.
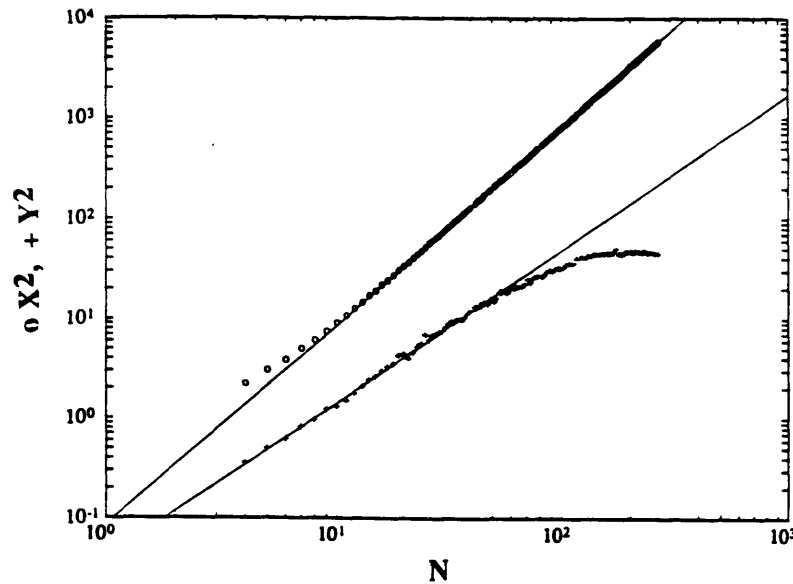
Figure 9.5: Scaling of X^2 (o) and Y^2 (+) along the principal anisotropy axis for the main channel of East Delaware river basin. The slopes of the fitted scaling lines give $\upsilon_x=0.99$ and $\upsilon_y=0.79$ for this basin.

Basin	υ_x	υ_y
Beaver Creek	1.00	0.75
Buck Creek	0.98	0.73
Big Creek	0.99	0.71
East Delaware River	0.99	0.79
Schoharie Creek Headwaters	0.97	0.75
Racoon Creek	1.00	0.76
Schoharie Creek	1.00	0.76
St. Joe River	1.00	0.76

Table 9.1: Self-affine scaling of the main channel for different basins across the U.S.

9.4. Self-Affine Scaling of Channels in Simulated Landscapes

In the Slope-Area model, the driving mechanism is the relaxation of slopes to hold the scaling relationship between slopes and areas:

$$S \sim A^{-\theta} \qquad\qquad (9.6)$$

The scaling exponent θ is a measure of the concavity of rivers. However, θ affects not only the vertical profile of channels in the model but also the overall appearance and tortuosity of the simulated networks. Figure 9.6 shows four simulated networks with $\theta=0.01$, 0.25, 0.5 and 2.0 respectively. The outlet is located at the lower left-hand corner. The tortuosity of the watercourses increases with the value of θ. Notice that θ is the parameter that connects the third dimension of the landscape with the aggregation pattern of the network and the planar form of the watercourse.

It is possible to use the procedure described in Section 9.2 to study the scaling properties of the main channels from the simulated basins with different values of θ. Figure 9.7 shows the values of υ_y versus θ (the value of υ_x is around 1.0 for all cases). The value of υ_y for the simulated basin with $\theta=0.5$ matches well the value of 0.75 found for actual rivers in Section 9.3. This result illustrates the link between the planar form of watercourses and the dynamics of the landscape evolution. The scaling of actual rivers is reproduced only
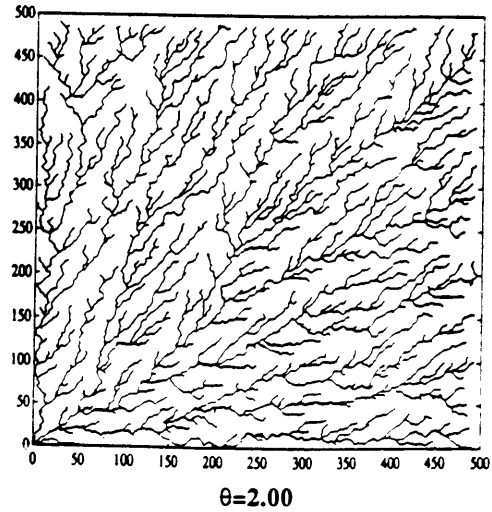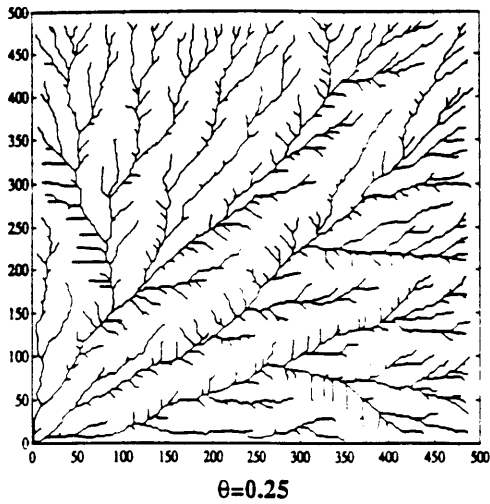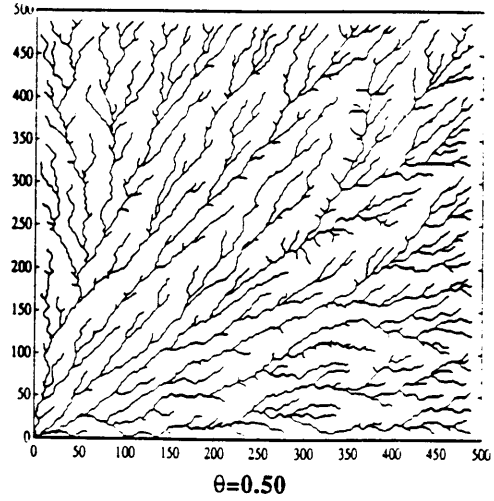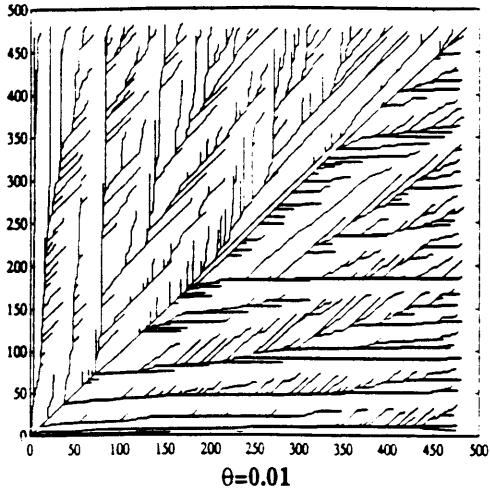
Figure 9.6: Simulated networks with the slope-area model. Values of θ are 0.01, 0.25, 0.50 and 2.00 respectively. The networks are drawn with a threshold value of area of 150 pixels.

when the appropriate exponent θ=0.5 is used in the model. Notice again that this value of θ is the one derived from the OCN principles analyzed in Chapter 6 and is the value observed in actual basins (Tarboton et al, 1989a).
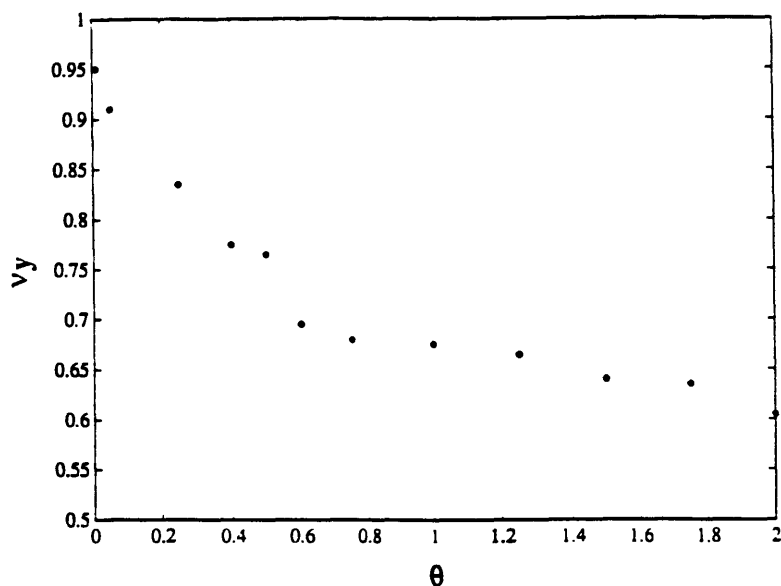
Figure 9.7: Values of v_y for networks simulated with the Slope-Area model using different values of the scaling parameter θ.

9.5. Self-Affine Scaling of Basin Boundaries

It has been suggested that basin boundaries and river courses are in essence mirror images of each other. Also, it has been shown that, under certain general assumptions, the topological characteristics of the channel and ridge networks are identical (Werner, 1991). It is of interest then, to compare the scaling characteristics of basin boundaries and river courses.

Numerous models of growing boundaries have been shown to have self-affine behavior. Examples include the Eden model

(Family and Vicsek, 1985), ballistic deposition models (Meakin, 1989) and even experimental ink fronts on sheets of paper (Buldyrev et al, 1992). In the study of interfaces that grow in the vertical direction starting from a horizontal line as initial condition, the scaling of interest corresponds to the behavior of the height-height correlation function of the "surface width" (where height is the elevation of the surface at each point and the correlation function is defined in a way directly analogous to equation (9.3), for more details see Vicsek (1989)). In all these experiments the scaling studies have been performed in a strip geometry where the boundary has a clear anisotropy axis.

In this section we will study the scaling behavior of the tortuosity of basin boundaries normal to the basin domain. An example of a basin boundary was shown in Figure 9.3. In previous studies of growing interfaces, the direction normal to the boundary is clearly defined. In basin boundaries, on the other hand, in order to perform the analysis we have divided the boundary into sections (of 200 pixels in length for the analysis to follow, although similar results were obtained using sections of different lengths). The individual linear trends were taken out from each of these sections and a single detrended curve was obtained, to which the self-affinity analysis was applied. Figure 9.8 shows, with circles, the scaling behavior of the oscillations normal to the basin domain along the boundary for the basin

shown in Figure 9.3. The slope gives a value of $\upsilon_y=0.75$, showing that indeed the self-affine scaling of boundaries and channels is similar.
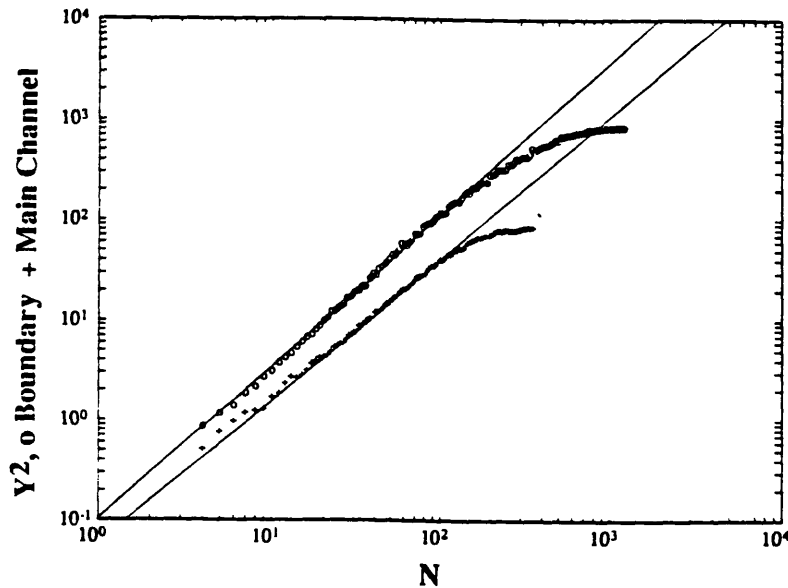
Figure 9.8: (o) Scaling of Y^2 for detrended boundary of the East Delaware river basin $(\upsilon_y=0.75)$. (+) Scaling of Y^2 for detrended main channel of the same basin $(\upsilon_y=0.74)$.

We have also presented in Figure 9.8 the results of the analysis for the entire watercourse of Figure 9.3 after detrending (without taking away the upper portion as in Section 9.3). The resulting slope is similar to what was found in Section 9.3. Table 9.2 (Ijjasz-Vasquez et al, 1993c) presents the values of υ_y for the main channels and the boundaries of the nine basins analyzed.

The results in Table 9.2 indicate that the self-affine scaling of rivers and boundaries is in fact very similar. However, visually, boundaries seem to have larger oscillations than channels and one would tend to say that

Basin	υ_x Boundary	υ_x Main channel
Beaver Creek	0.75	0.77
Buck Creek	0.74	0.77
Big Creek	0.79	0.74
East Delaware River	0.75	0.74
Schoharie Creek Headwaters	0.79	0.72
Racoon Creek	0.74	0.77
Schoharie Creek	0.76	0.75
St. Joe River	0.75	0.79

Table 9.2: Self-affine scaling of detrended main channels and boundaries for different basins.

they look "rougher" (see Figure 9.3). We can indeed appreciate how this effect manifests itself in Figure 9.8. Although the slopes are similar for the boundary and the main channel, notice that the scaling of the latter breaks at a smaller distance N between points along the curve. This behavior is observed for all the basins analyzed. What this means is that even if we take points further and further apart along the channel, the variance does not increase because oscillations of larger magnitude do not appear. On the other hand, such oscillations do appear on the boundary of the basin and the linear portion of the scaling is more extended in this case. Furthermore, the scaling curve for boundaries is located above the curve for channels, indicating that the variance for the same distance between points is larger for boundaries than for channels, even if the self-affine scaling slope is the same.

We have shown that basin boundaries have similar self-affine characteristics to watercourses but the linear log-log scaling is more extended in boundaries as a result of self-affine oscillations of larger magnitude. So, although the scaling properties are similar, boundaries and rivers cannot be considered mirror images of each other in their planar configurations.

9.6. Self-Affine Scaling of Two Random Walker Models of River Courses

If rivers are self-affine fractals, a natural question is how would a self-similar river look? In this section we present two simple Markovian models that try to reproduce river courses with different levels of complexity and as a consequence different levels of success. Let us consider a channel extracted from a digital elevation map as shown in Figure 9.9. We can simulate this curve with a random walker model. Numerous models of this type have been developed to simulate rivers (Leopold and Maddock (1953), Scheidegger (1961), Howard (1971), and Meakin et al. (1991) to mention only a few).

In our model the walking particle chooses at each pixel to continue with its previous flow direction with probability p or change direction with probability (1-p). If the walker decides to change, it will do so in the same direction (right or left) it had turned the last time in the course of its trajectory, with probability q and in the opposite direction
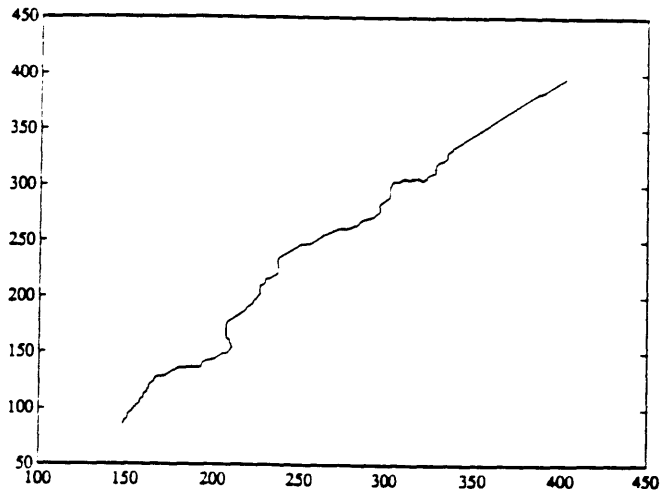
Figure 9.9: Main channel of Schoharie Creek
Headwaters river basin.

with probability (1-q). Figure 9.10 shows a simulation with

parameter values p=0.7 (which means that the channel prefers

to stay in the direction it is already flowing in) and q=0.15

(which indicates that the channel has an overall sense of

direction and if it deviates from such a direction, it has a

tendency to return to it). These parameters were calculated

from the main channel of Schoharie Creek Headwaters shown in

Figure 9.9. We have not included self-avoiding conditions for

the sake of simplicity of the model, but these could be added

without any problem.

We can apply the method used in this chapter to analyze

the scaling behavior of the simulated river. Figure 9.11

shows the scaling in different orientations. In this case we

have found $\upsilon_x = \upsilon_y = 0.885$. According to the theory, $1/D = 0.885$,

i.e. D=1.13. This value of the fractal dimension matches what

has been measured in actual rivers using the box-counting
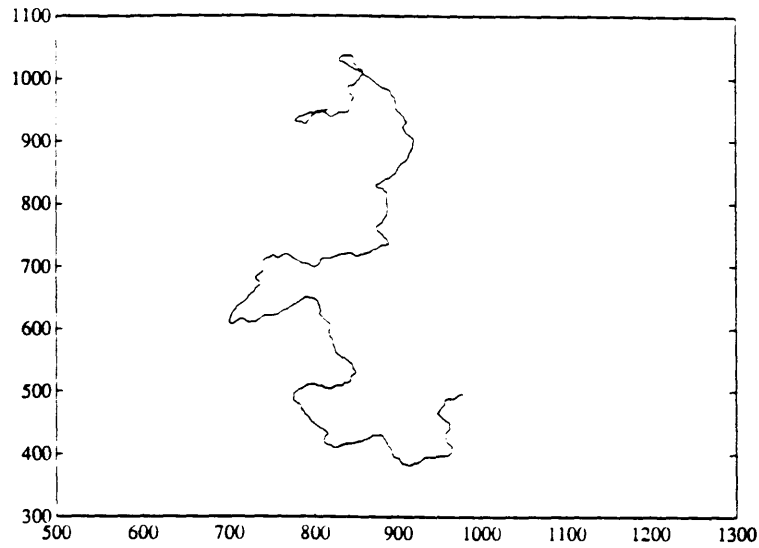
Figure 9.10: Simulated watercourse with first stochastic model. The parameters used in this simulation corresponds to the river shown in Figure 9.9.
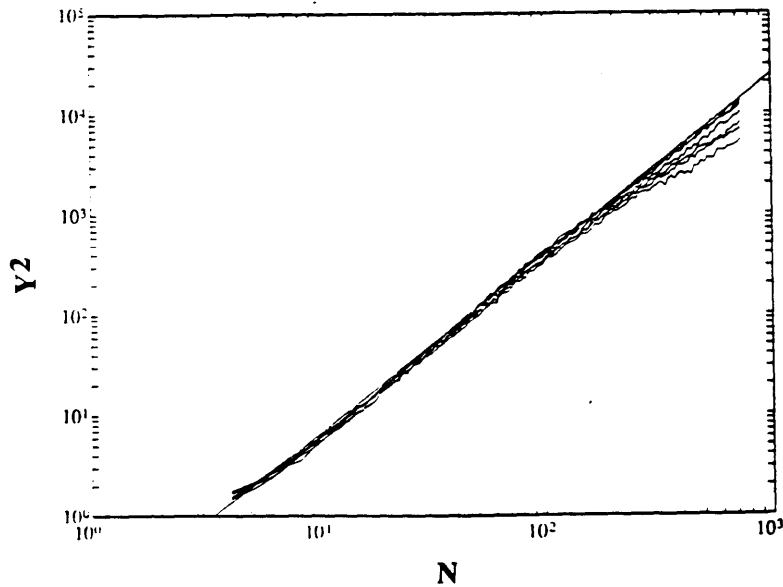
Figure 9.11: Scaling of Y^2 for the simulated channel shown in Figure 9.10. The common scaling slope for different orientations of the axis shows the self-similar character of the curve.

method (Tarboton et al, 1989). Having $\upsilon_x=\upsilon_y$ implies that we are looking at a self-similar fractal. It is easy in fact to appreciate that the tortuosity in Figure 9.10 is isotropic in every direction, unlike actual rivers (compare to Figure 9.9).

The stochastic model can be improved to better reproduce river courses. Our second model works in the following way: flow directions in the grid are indexed $i=1,2,...,8$. At each pixel, the walker has a probability P_j of changing direction given that it has been flowing in direction j. If the river chooses to shift directions, a matrix P_{ijk} gives the probability that the walker changes to direction i given that its current flow direction is j and its last flow direction (without taking into consideration straight segments) was k. Using the probabilities calculated for the actual river in Figure 9.9, we have simulated the river in Figure 9.12. This simulation seems to be a better representation of the actual river. Figure 9.13 shows the scaling in the principal anisotropy axis. The self-affine scaling goes as $\upsilon_x=1.0$ and $\upsilon_y=0.71$ which are similar to the values found in actual rivers (although the value of υ_y is a little low). Notice how in this case the self-affine river appears to be much flatter and oscillations are anisotropically distributed as opposed to the self-similar model of Figure 9.10 where the tortuosity of the river is isotropic in every direction.
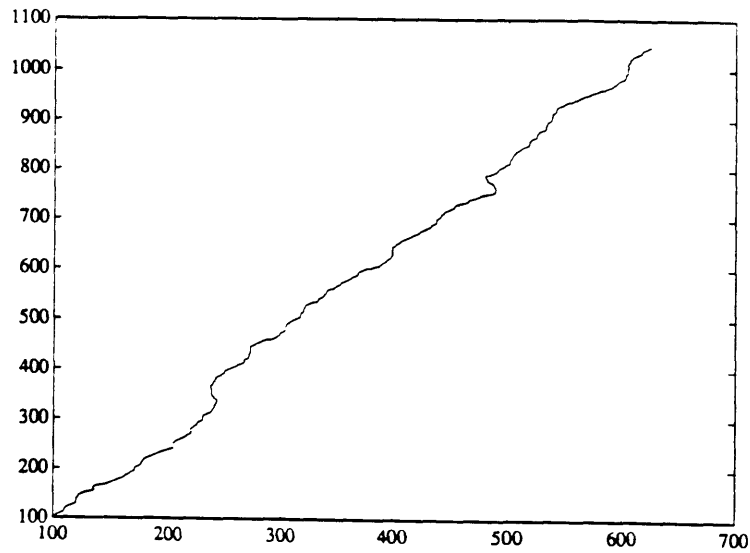
Figure 9.12: Simulated watercourse with second stochastic model. The parameters used in this simulation correspond to the river shown in Figure 9.9.
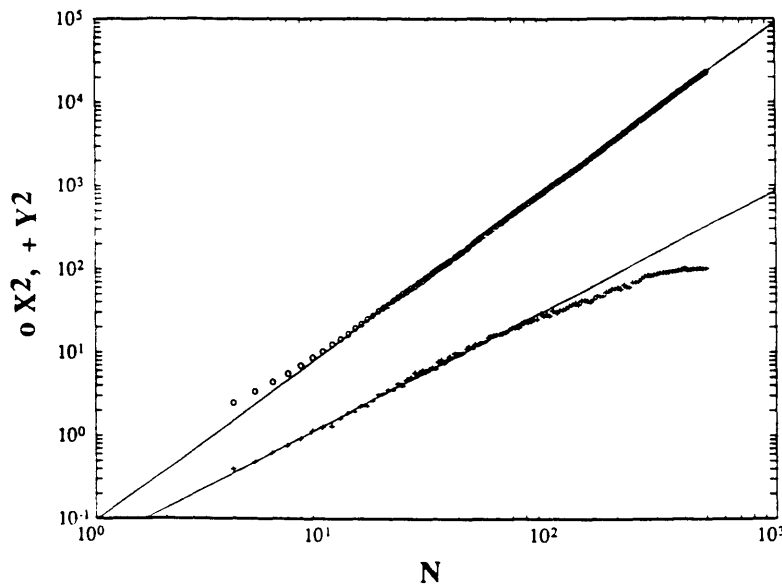
Figure 9.13: Scaling of X^2 and Y^2 along the principal anisotropy axis for the simulated channel shown in Figure 9.12. The fitted scaling lines gives $\upsilon_x=1.0$ and $\upsilon_y=0.71$.

9.7. Summary

In this chapter we studied the scaling properties of the courses of main channels and basin divides identified with the aid of digital elevation maps. Watercourses show anisotropic scaling behavior characteristic of self-affine fractals. The scaling behavior is similar across all the basins analyzed with anisotropic scaling exponents $\upsilon_x=1.0$ and $\upsilon_y=0.75$.

The same analysis was performed on networks simulated with the Slope-Area model using different values of the scaling parameter θ. The variation in θ affects not only the concavity of the river profile but also the overall structure and tortuosity of the network. The measured self-affine scaling for actual rivers is reproduced only when the appropriate value of $\theta=0.5$ is used.

Basin boundaries have been shown to possess self-affine characteristics similar to those of channels but with a larger scaling range. Therefore, although their scaling behavior is similar, rivers and boundaries cannot be considered mirror images of each other.

Finally, we have also presented two simple stochastic models of river courses that graphically illustrate the difference between self-similar and self-affine objects.

The analysis in this chapter has concentrated on the scaling properties of river courses and basin boundaries as

geometrical objects. However, hydrologists are also interested in the spatial distribution of variables like flows, slopes, energy, etc. The next chapter will examine the spatial distribution of these variables on river basins.

Chapter 10

The Multifractal Characterization of River Basins

10.1. Introduction

The spatial distribution of variables in river basins can have large variations. Figure 10.1 shows, as an example, the contributing areas of the tributaries to the main channel of the Brushy Creek basin. Notice the four orders of magnitude of variability in the vertical axis. This large variation had already manifested in the extended range of the power-law cumulative distribution of mass and energy studied in Chapter 4. However, it is also interesting to study not only the distribution of values but also the spatial distribution of these variables and their scaling properties. The goal is to present an integrated picture of the basin, not only geometrically, as was done in Chapter 9, but also through the spatial distribution of mass, energy and slopes.

The multifractal formalism has shown great promise in the understanding of problems similar to the one we are interested in this chapter, especially because of the large spatial variability of the properties to be examined in the basin. The first characterization of multifractals was introduced by Mandelbrot (1982, pp.375-377) and the formalism was developed by Frisch and Parisi (1985), and Halsey et al.
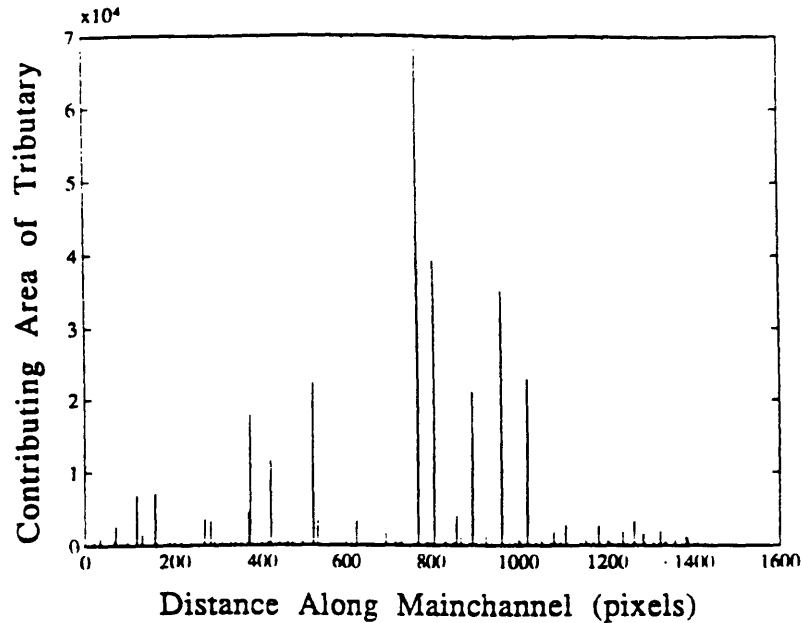
Figure 10.1: Sizes of tributaries draining into main channel of the Brushy Creek basin.

(1986). These ideas have been applied to a number of different phenomena that range from the study of energy dissipation in fully developed turbulence (Menevau and Sreenivasan (1987), Sreenivasan and Menevau (1988), Sreenivasan et al. (1989), Prasad and Sreenivasan (1990)) to the visit frequency of points in chaotic attractors (Halsey et al. (1986), McCauley (1990)), to the growing probability of sites in diffusion limited aggregation (Mandelbrot and Evertsz, 1990), to numerous geophysical processes (Schertzer and Lovejoy, 1991). Good reviews can be found in Paladin and Vulpiani (1987), Mandelbrot (1989) and McCauley (1990).

Section 10.2 presents the general framework of the multifractal formalism. Section 10.3 reviews the mathematical derivation of the method for numerical calculation of the multifractal spectrum. Section 10.4 presents the results of

the multifractal formalism applied to four different variables in nine basins. The first of the variables is the energy expenditure defined as the product of discharge and elevation gradient. The second field of interest is the channel initiation function, a component of the SIBERIA model of basin evolution (Willgoose et al, 1991a-d). This function has the general form $\beta Q^m S^n$ where Q and S are discharge and slope respectively, and β, m and n are constants. This function models phenomena such as surface velocity, shear stress and others that promote channel formation. We will examine this function in more detail in Chapter 11. Finally, discharges and slopes are not only the fundamental components of both energy expenditure and the channel initiation function, but are also themselves key descriptors of the hydrologic response and geometry of the basin. They will also be studied independently within the framework of the multifractal formalism.

10.2. Theoretical Framework

The distribution and spatial organization of a variable of interest (for example, energy expenditure or mass) over a certain set (a river basin) can be studied with the aid of the multifractal formalism. A grid with boxes of size r is superimposed over the set. Every grid box is assigned the value of the integral of the variable over the entire box. This value is properly normalized by the integral of the variable over the entire region. The result obtained in a box

of size r around point x is denoted by $P_r(x)$. The value of $P_r(x)$ measures what proportion of the variable under study is enclosed by the box of size r around x (for example, how much mass can be found in that box). The normalization makes it possible to see $P_r(x)$ also as a probability measure.

The value of $P_r(x)$ depends not only on the location of the box but also on its size r. For example, if a point x is surrounded by points with larger values of the variable then $P_r(x)$ will increase with r as shown in Figure 10.2.a. Figure 10.2.b shows the inverse case where x is surrounded by smaller values. The behavior of $P_r(x)$ with r is directly related to the organization of the variable of interest around x and this behavior can be described by:

$$P_r(x) \sim (r/L)^\alpha \qquad (10.1)$$

where L is the domain size and the scaling exponent α is usually called in the literature the local singularity strength (Halsey et al, 1986). The case shown in Figure 10.2.a has a large value of α while the case in Figure 10.2.b has a small value of α.

Any nontrivial pattern of organization of the measure implies that the growth of $P_r(x)$ on r will depend on the point around which the grid box is centered. Different points may have different values of α. In order to complete the description of the spatial organization of the measure, it is necessary to count the number $N_r(x)$ of grid boxes with common
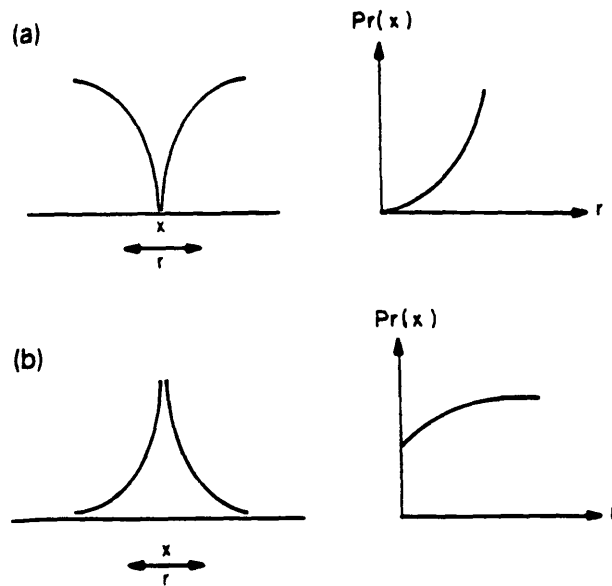
Figure 10.2: Examples of points with (a) large values of α and (b) small values of α. Diagrams of the values of the variable around point x and the increase of $P_r(x)$ with r are presented in each case.

values of α. These grid boxes are mixed and interwoven inside the domain of study. Their number clearly depends on the size r of the grid boxes. This dependence can be described as:

$$N_r(x) \sim (r/L)^{-f(\alpha)} \qquad (10.2)$$

$f(\alpha)$ can be seen as the fractal dimension of the set of boxes with the same α-value, i.e., $f(\alpha)$ measures not only the proportion of points with similar characteristics around them but also the degree of clustering of these points. The curve $f(\alpha)$ vs. α is called the multifractal spectrum (Halsey et al, 1986). This curve provides a synthesized picture of the full complexity of the scaling structure. In general, the variable α takes on values in a range [α_{min}, α_{max}] which corresponds to the scaling of extreme cases similar to the ones shown in

Figure 10.2. $f(\alpha)$ is usually a unimodal function (Paladin and Vulpiani (1987), Tel (1988)).

Clearly not every spatial distribution of a variable has a multifractal spectrum. For example, if the multifractal spectrum of a random field is calculated, it would be found that $P_r(x)$ increases as r^2 with the size of the grid box r for every point x. Therefore, as every grid box has the same value of α, $N_r(x)$ is equal to the total number of boxes and $f(\alpha)=2$. The result of the analysis is not a curve as in multifractal measures but a single point ($\alpha=2$, $f(\alpha)=2$).

10.3. Numerical Calculation of the Multifractal Spectrum

The numerical calculation of the multifractal spectrum based on Equations (10.1) and (10.2) requires large amounts of data and is affected by prelogarithmic factors that depend on the grid size r (Menevau and Sreenivasan, 1989). However, there is a different way of calculating the multifractal spectrum. The basic idea is to separately emphasize regions where the intensity of the variable is high (i.e., α is small) and regions where the intensity of the variable is low (i.e., α is large). This emphasis can be done by studying the cumulants of order q of $P_r(x)$ defined as :

$$C_q(r) = \Sigma_i \, [P_r(x_i)]^q \qquad (10.3)$$

165

where the centers x_i of the boxes have been indexed. It is possible to relate the scaling behavior of $C_q(r)$ with r for different values of q with the multifractal spectrum α vs. $f(\alpha)$. This section will describe the derivation of this relationship following Halsey et al. (1986), Tel (1988) and Feder (1988).

Let us define the function $\tau(q)$ as the exponent at which the cumulant $C_q(r)$ scales with the box size r:

$$C_q(r) \sim (r/L)^{\tau(q)} \qquad\qquad (10.4)$$

The exponents $\tau(q)$ are related to the set of generalized dimensions D_q defined in Grassberger and Procaccia (1983a,b):

$$D_q = \tau(q)/(q-1) \qquad\qquad (10.5)$$

For the case q=0, $C_0(r)$ measures how many boxes of size r are occupied by the measure and D_0 is the fractal dimension of the support set where the variable of interest is studied (if the entire basin is used, then $D_0=2$). There is a discontinuity in the definition of D_1 but taking the limit $q \rightarrow 1$ leads to:

$$-\Sigma_i\ P_r(x_i)\ (\ln P_r(x_i)) \sim D_1\ \ln(1/r) \qquad (10.6)$$

Thus D_1 measures how the information (represented as usual by $\Sigma P \ln P$) required to describe the measure scales with $\ln(1/r)$. A different interpretation of the exponents D_q is presented in Mandelbrot (1988). If the values of D_q are the same for every

value of q, the measure is said to be simple scaling, otherwise it is multiscaling.

It is possible to relate the exponents $\tau(q)$, α and $f(\alpha)$. Following Tel (1988) and Feder (1988), the summation in Equation (10.3) can be replaced by an integral when $r \to 0$. The value of $P_r(x)$ can be replaced using Equation (10.1) and the integral over all boxes can be replaced using Equation (10.2) to integrate over all possible values of α:

$$C_q(r) \sim \int [P_r(x_i)]^q \sim \int \left(\frac{r}{L}\right)^{-f(\alpha)} \left(\frac{r}{L}\right)^{q\alpha} d\alpha \qquad (10.7)$$

Since r is very small, the value of the integral is dominated by the largest value of the integrand. This largest value occurs when $q\alpha - f(\alpha)$ is minimized, i.e. when:

$$df(\alpha)/d\alpha = q \qquad (10.8)$$

Therefore we have:

$$C_q(r) \sim r^{q\alpha(q) - f(\alpha(q))} \qquad (10.9)$$

Notice that the values of $\alpha(q)$ and $f(\alpha(q))$ in the exponent of r are exactly those that minimize the expression $q\alpha - f(\alpha)$. Using Equations (10.4) and (10.9) results in:

$$\tau(q) = q\alpha(q) - f(\alpha(q)) \qquad (10.10)$$

Taking the derivative of $\tau(q)$ with respect to q and using Equation (10.8) we obtain:

$$\frac{d\tau(q)}{dq} = \alpha + q\frac{d\alpha}{dq} - \frac{df}{dq} = \alpha \qquad\qquad (10.11)$$

Equation (10.11) indicates that α is the slope of the tangent to the curve $\tau(q)$ vs. q. Equation (10.10) shows that $f(\alpha)$ is the intercept of that tangent with the $\tau(q)$ axis. Inversely, Equation (10.8) indicates that the slope of a tangent to the curve α vs. $f(\alpha)$ at the point $(\alpha(q),f(\alpha(q)))$ has the value q, and from Equation (10.10) $-\tau(q)$ is the intercept of this tangent with the $f(\alpha)$ axis. Figure 10.3 shows graphically these relationships. It is important to notice also that the right-hand side of the multifractal spectrum corresponds to values of $\alpha(q)$ and $f(\alpha(q))$ with q<0 and the left-hand side to q>0. The maximum of the spectrum corresponds to q=0.

If the measure under study is simple scaling, then all the values of D_q for different q are the same, as was previously stated. Therefore, by replacing (10.5) in (10.11)
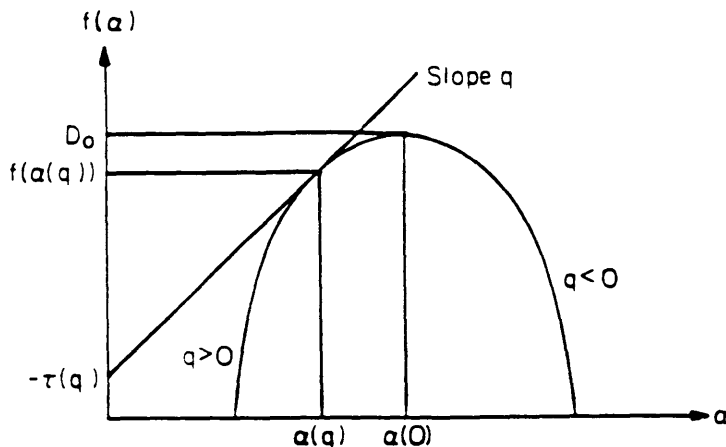
Figure 10.3: Diagram of a typical multifractal spectrum.

it is possible to see that the values of $\alpha(q)$ are the same for every q. Equation (10.10) then shows that $f(\alpha(q))$ is also constant. Simple scaling measures are another example of spatial organization of variables where the curve $\alpha-f(\alpha)$ reduces to a single point.

Summarizing this method, the procedure to calculate the multifractal spectrum has three steps: first, find the cumulants $C_q(r)$ using (10.3); second, find their scaling behavior and calculate $\tau(q)$; finally, use (10.10) and (10.11) to find α and $f(\alpha)$ with the values of $\tau(q)$. Other methods, some of which were used to confirm the results presented in this chapter, appear in Chhabra and Jensen (1989) and Menevau and Sreenivasan (1989).

10.4. Multifractal Spectra in River Basins

10.4.1. Variables under Study

A number of different variables in several river basins will be examined with the aid of the multifractal formalism. These variables are calculated using topographic data from digital elevation maps.

First, we will examine the energy expenditure E_i defined as the product of contributing area (as a surrogate for discharge) multiplied by slope. Second, we will examine the channel initiation function a_i which has the general form $a_i=\beta A_i{}^m S_i{}^n$. This function is an important component of the

SIBERIA model of river basin evolution developed by Willgoose et al. (1991a-d) and represents a variety of processes related to channel initiation. Finally, as key components of the two variables above, we will also examine slopes Si and contributing areas A_i.

10.4.2. Multifractal Spectrum of Energy Expenditure

The calculation of the multifractal spectrum for each of the variables of interest follows the procedure presented in Section 10.3. The multifractal analysis of the energy expenditure E_i is used as an example to illustrate each of the steps. Figure 10.4 shows, for the Buck Creek basin in California, the scaling behavior of the cumulants $C_q(r)$ for different values of q and increasing values of the box size r. The slopes of the fitted lines (in log-log paper) for every value of q in that figure correspond to $\tau(q)$ (i.e., the scaling behavior of $C_q(r)$ with increasing r) as defined in Equation (10.4). Figure 10.5 shows the functions $\tau(q)$ and D_q versus q. The value of D_q is calculated using (10.5). Using Equations (10.10) and (10.11), $\alpha(q)$ and $f(\alpha(q))$ can be numerically calculated and the multifractal spectrum combines these two functions in a single graph.

There are two issues that can be studied at this point regarding the spatial distribution of energy expenditure. First, whether this spatial distribution has a multifractal spectrum; and, second, how the multifractal spectra of energy
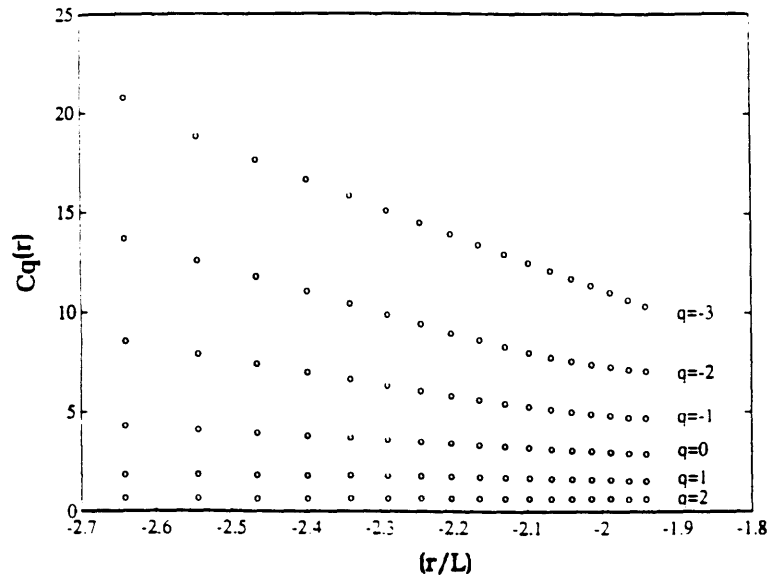
Figure 10.4: Scaling of $C_q(r)$ with the box size r as calculated using Equation (10.3) for energy expenditure in the Buck Creek basin. The fitted slopes for each value of q correspond to $\tau(q)$.
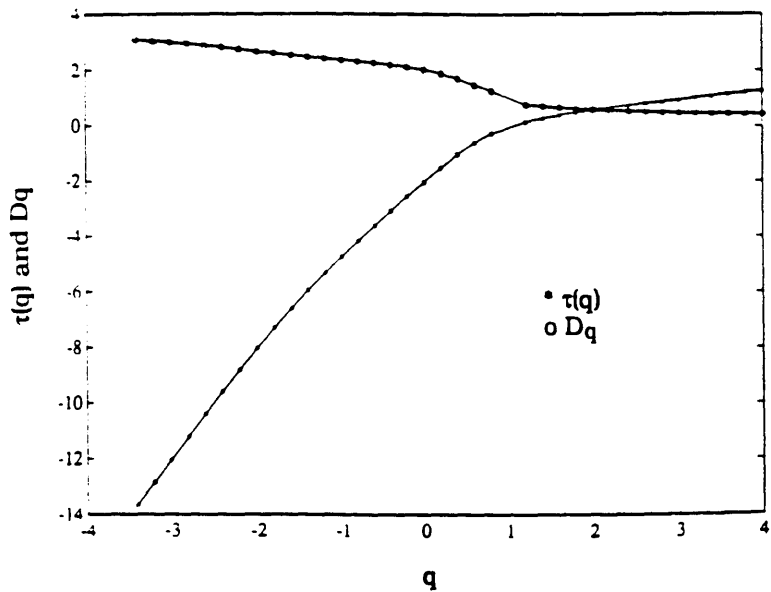
Figure 10.5: $\tau(q)$ and D_q versus q as computed using Equations (10.4) and (10.5) for energy expenditure in the Buck Creek basin.

expenditure for different basins compare. With these two problems in mind, the multifractal spectra of E_i were calculated for nine different basins. The resulting spectra are shown in Figure 10.6. We can see that the spatial organization of energy expenditure has a multifractal distribution which is common across different basins.
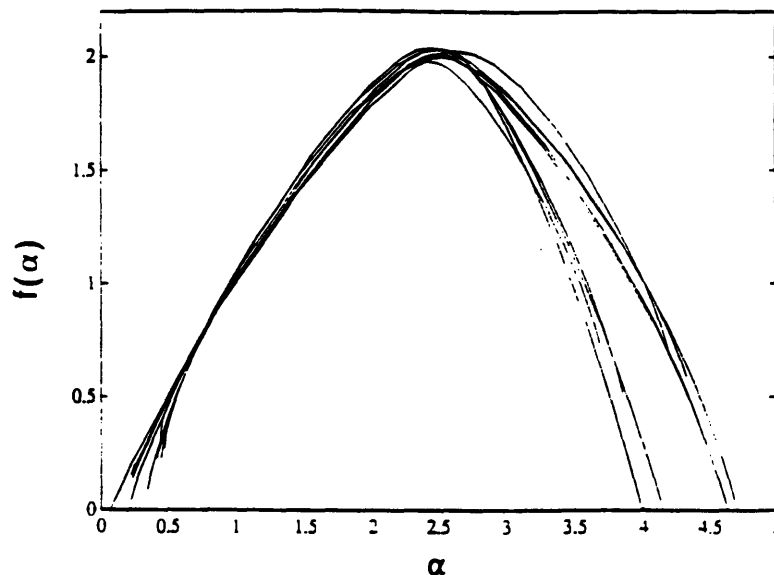
Figure 10.6: Multifractal spectra of energy expenditure E_i for different basins.

The $f(\alpha)$ vs α curves for energy expenditure point towards a common structure and spatial organization of energy dissipation in basins with very different characteristics. The multifractal formalism shows the similarities behind the complex organization of energy dissipation in river basins. The appropriate identification of the multifractal characteristics of energy expenditure in river basins as shown in Figure 10.6 is a first step towards the development of multiplicative cascade models of energy dissipation.

Models of this kind have been constructed to reproduce the flux of energy from larger to smaller scales in turbulent flows (Menevau and Sreenivasan (1987) and Sreenivasan and Menevau (1988)). In turbulence studies, once the multifractal spectrum of energy dissipation is identified, it is possible to extract the underlying multiplicative cascade process which is generating the structure and the spatial distribution of energy dissipation (Chhabra et al, 1989). In geomorphology, the work of Newman and Turcotte (1990) presents a cascade model of erosion to explain fractal features of landscape and is a related approach to the problem of energy dissipation in river basins.

It is clear from Figure 10.6 that the agreement in the multifractal spectra of different basins is very good in the left-hand side of the spectra but there is more variation in the right-hand side. This behavior has also been observed in turbulence studies (Menevau and Sreenivasan, 1987). The problem resides in the presence of noise in the data. The right-hand side of the spectra corresponds to cumulants with large negative values of q (see Figure 10.3). Large values of q<0 emphasize regions of low intensity of the variable where the influence of noise is greater. Confidence intervals (corresponding to the linear fitting to find $\tau(q)$) in Equation (10.4) can be drawn around the spectra. These intervals widen as one moves towards the right in the spectra. The different spectra in Figure 10.6 are statistically indistinguishable.

The domains used in the calculation of the spectra in Figure 10.6 were the largest square boxes entirely contained inside each basin. This was done in order to avoid irregular shapes that, when divided by a regular grid, would leave some grid boxes with a small portion inside the basin and a large portion outside it. The value of α in these boxes would be unrealistically low and the resulting spectra would not measure the true spatial distribution of the variable under study.

Finally, we also investigated the spatial organization of energy expenditure in one-dimensional cuts with different orientations in the basin. Figure 10.7 corresponds to the multifractal spectra calculated along different cuts in the Brushy Creek basin (AL). The different spectra are very similar indicating that the multifractal properties of energy expenditure have directional isotropy.
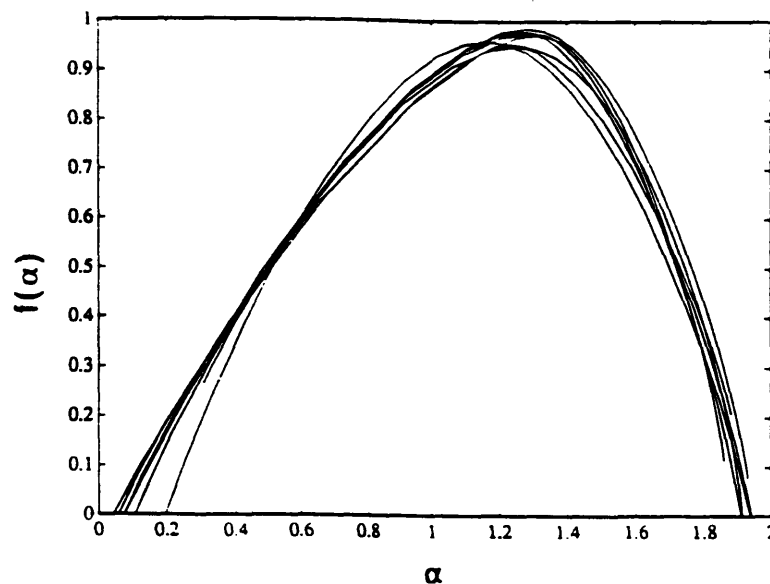
Figure 10.7: Multifractal spectra of energy expenditure measured along 1-D cuts in different directions for the Brushy Creek basin.

10.4.3. Multifractal Spectrum of the Channel Initiation Function

The second variable to be studied is the channel initiation function, an important component of the SIBERIA model of river basin evolution (Willgoose et al, 1991a-d). This model simulates the development of landscapes and river networks as a result of sediment transport processes over geologic time. The model incorporates different transport phenomena for hillslopes and channels. The distinction between channel and hillslope pixels is made through the channel initiation function. A channel advances to any point where the initiation function exceeds a threshold value.

The channel initiation function depends on discharge and slope and has the general form $\beta Q^m S^n$ where β, m and n are constants. This function represents a number of physical processes that are observed to trigger channelization in the field, for example, overland flow velocity, bed shear stress and groundwater sapping. Channel growth is encouraged if discharges or slopes are increased. The channel initiation function depends on the resistance of the catchment to channelization. As usual, contributing area will be used as a surrogate for discharge.

The channel initiation function is analogous to the probability distribution of growth in DLA where high values of the distribution promotes the growth of the DLA network (Feder (1988), Vicsek (1989)). The structure is more likely

to trap the random walkers at the tips. The growth probability measure in DLA studies has been shown to be multifractal (Vicsek (1989), Mandelbrot and Evertsz (1990)) and its multifractal spectrum provides an integrated representation of the spatial fluctuations of the probability of growth. This representation is useful in describing the dynamics of the growth process and screening effects (Ball and Blunt, 1990).

The multifractal properties of two different versions of the channel initiation function were studied, one based on the overland flow criteria where m=1 and n=0.75 and the other corresponding to overland shear stress where m=1 and n=1.17 (Willgoose et al, 1991a-d). Figure 10.8 presents the mean multifractal spectra for both cases along with the energy expenditure case using all the basins. For every value of q,
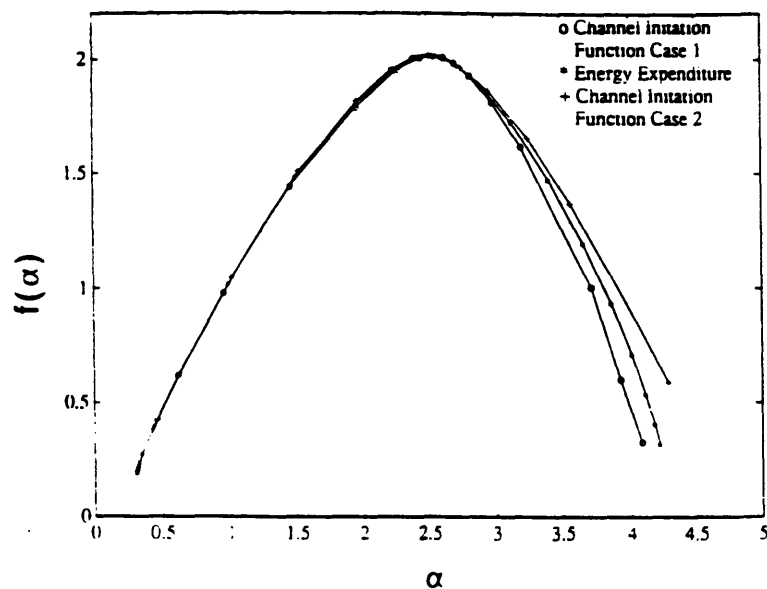
Figure 10.8: Mean multifractal spectra of energy expenditure (A*S) and two forms of the channel initiation function ($A^m S^n$) (based on overland flow criteria n/m=0.75 (case 1) and overland shear stress n/m=1.17 (case 2)).

the mean values of $\alpha(q)$ and $f(\alpha(q))$ across the nine basins studied were used to draw the mean spectra shown in Figure 10.8.

Given that the dependence on discharge for the three measures has the same exponent m=1, the regions of high intensity in these cases will be very similar (i.e., major channels where discharges are very large). On the other hand, when discharges are small and gravity forces (and consequently slopes) become important in the channelization process, some differences, albeit small, appear, as can be appreciated, on the right-hand side of the curves. We will study in more detail the channel initiation function and its possible use in the differentiation between channel and hillslope nodes in DEMs in Chapter 11.

10.4.4. Multifractal Spectra of Slopes and Discharges

Given that discharges and slopes are the variables on which the energy expenditure and the channel initiation function are based, it is of interest to characterize separately the distributions and properties of the measures S_i (normalized drops) and A_i (as a surrogate for discharges). Multifractal spectra for different basins are presented in Figures 10.9 and 10.10 for these two variables. Again, these spectra are very similar for all basins.

The $f(\alpha)$ curves for E_i, A_i and S_i are very different in character even though the three variables are embedded in the
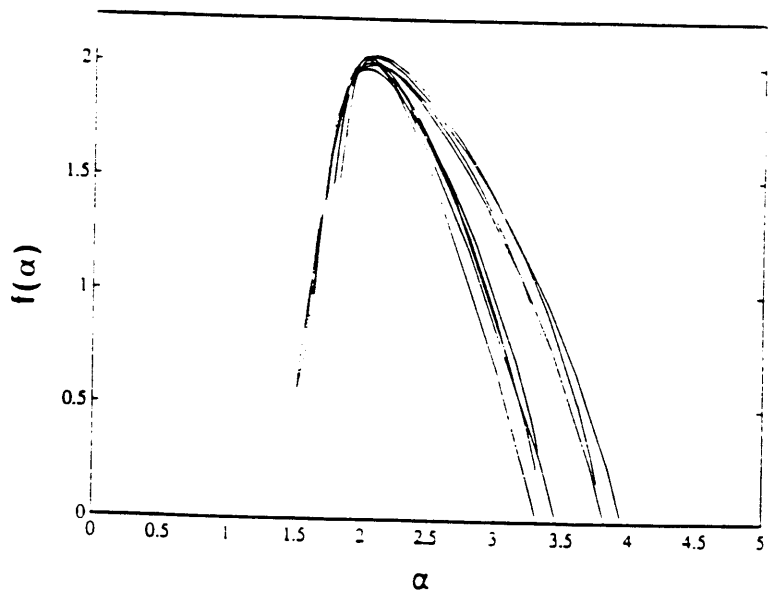
Figure 10.9: Multifractal spectra of slopes S_i for different basins.
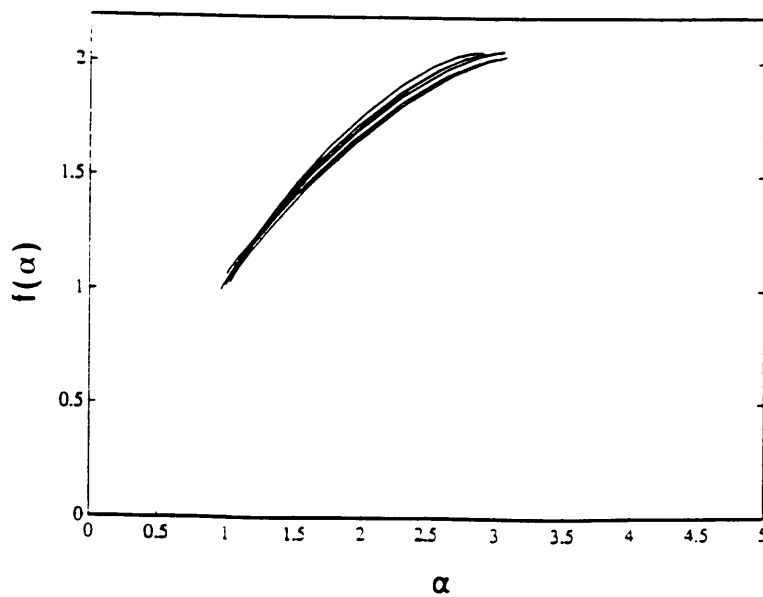
Figure 10.10: Multifractal spectra of contributing areas A_i for different basins.

same domain. Figure 10.11 shows the mean spectra for each of
the three variables calculated, based on the results shown in
previous figures. The spectrum for S_i is much narrower than
the one for E_i. A single point spectrum would indicate simple
scaling (as explained in Section 10.3) while a spectrum like
the one shown in Figure 10.9 corresponds to multiscaling.
This issue is related, although not directly applicable, to
recent work in scaling/multiscaling relationships between
link slopes and discharges (Tarboton et al. (1989a,b), Gupta
and Waymire (1989)).
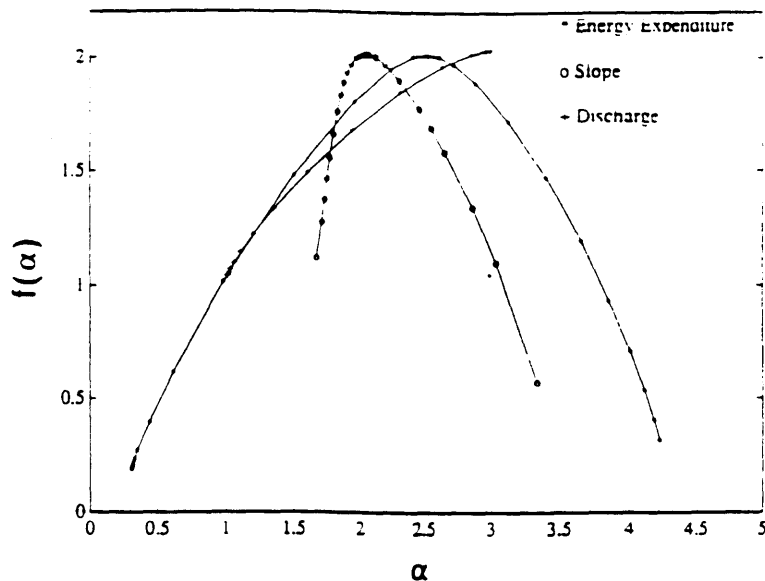
Figure 10.11: Mean multifractal spectra of
energy expenditure E_i, slope S_i and
contributing area A_i.

The strange form of the spectrum for A_i in Figure 10.10
is a result of the spatial configuration of river basins.
Figure 10.12 shows the individual points $(\alpha(q), f(\alpha(q)))$ for
different values of q in the multifractal spectrum for one of
the basins. There are two regions where the values of the

$f(\alpha)$ spectrum for A_i concentrate: around (1, 1.1) for large $q>0$ and around (2,3) for large $q<0$.
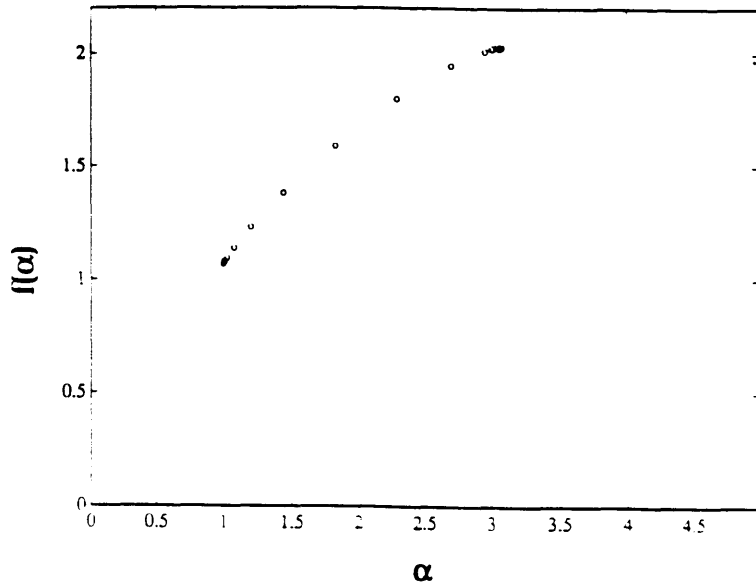
Figure 10.12: Multifractal spectrum of contributing areas A_i for Brushy Creek basin. The individual points $(\alpha(q),f(\alpha(q)))$ are shown for different values of q.

Regions with high values of A_i (i.e., large channels) are emphasized in $C_q(r)$ for large $q>0$. In the most frequent case, boxes with large A_i will be surrounded by boxes with small A_i (i.e., hillslopes) as appears in Figure 10.13.a. The large values of A_i will be approximately equal and the contribution of each box of size r to $C_q(r)$ will grow as $r^{\alpha(q)}$ with $\alpha(q)=1$. The box-counting fractal dimension of this set of boxes is the same as the box-counting fractal dimension of rivers which has been shown to be around 1.1 (Tarboton et al, 1988).

The regions that are emphasized for large $q<0$ correspond to hillslopes near the upper regions of the basin where A_i is
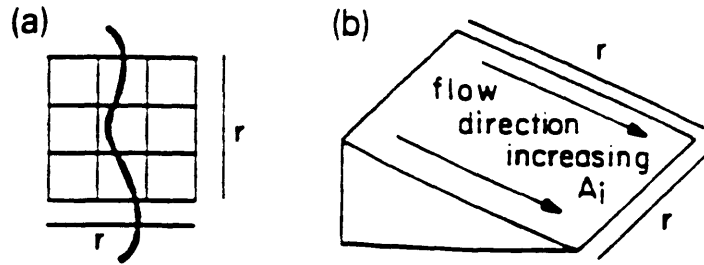
Figure 10.13: Regions with high values of α (large channels) and low values of α (hillslopes) for contributing area.

small. These concentrate on the right-most point $(2,3)$ in the spectrum. In general, these regions can be idealized as appears in Figure 10.13.b. The value of A_i will increase linearly downhill and the value of the integrated variable (contributing area, and not simply area) in a box of size r will be proportional to r^3, giving $\alpha(q)=3$ for $q<0$ large. Hillslopes tend to fill the river basin and therefore the fractal dimension of this set tends towards the value of $f(\alpha(q))=2$.

Now, we can compare the results of multifractal studies of contributing areas in DEMs with traditional morphometric models. One example which has been described previously in this work is Scheidegger's (1967) stochastic model of rivers. Contributing areas of basins draining to the horizontal line at the bottom of the generated network (an example of which was shown in Figure 4.1) were calculated and their multifractal spectrum computed. This spectrum was also calculated by Takayasu and Takayasu (1989) in a model of

particle aggregation with injection which is analogous to Scheidegger's model. The resulting spectrum appears in Figure 10.14 indicated with a continuous line.
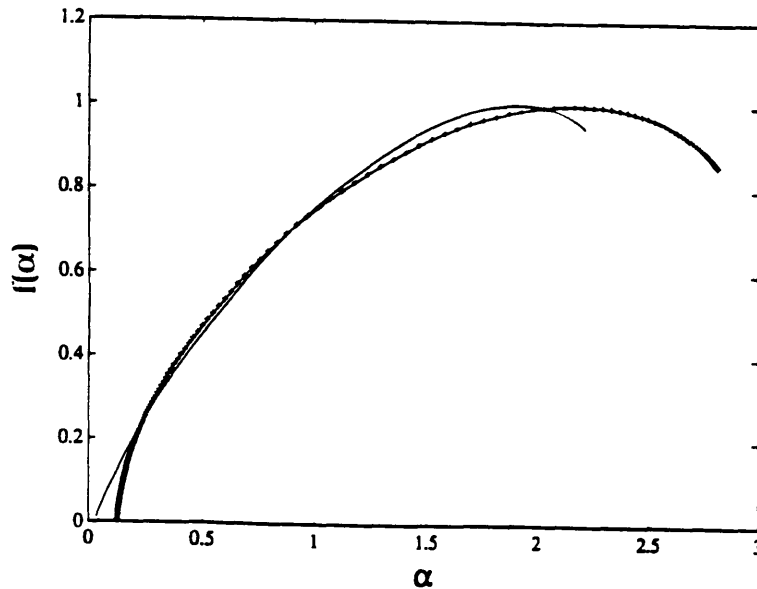
Figure 10.14: Multifractal spectra of contributing areas for bottom line of Scheidegger's (1967) model (continuous line) and pixels adjacent to main channel in Brushy Creek basin (+).

Following the original conceptualization of the model by Scheidegger, this spectrum describes the spatial organization of sizes of tributaries to a large channel. This spatial

organization can also be studied in DEMs. Using the contributing areas of pixels adjacent to the main channel in Brushy Creek, the multifractal spectrum is calculated and appears also in Figure 10.14 represented with (*). The spectra for Scheidegger's model and the actual basin are very similar on the left-hand side of the spectrum. The difference in the right-hand side comes from the different spatial

organization of contributing areas in hillslopes (i.e.,
regions of small A_i). In a DEM the tendency is to have
parallel flows (as shown in Figure 10.13.b) while in
Scheidegger's model there is a tendency for aggregation
regardless of the size of A_i. It is the same kind of
difference in aggregating behavior between channels and
hillslopes that causes the break in the power-law
distribution of contributing areas shown in Figure 4.5.

10.5. Summary

The complexity of the spatial distribution of a number
of variables in river basins was studied with the tools of
the multifractal formalism. The idea was to move one step
beyond the topological and fractal analysis of the
geometrical form of the river network and analyze instead the
distribution, organization and scaling of more physical
variables in river basins.

Four variables were analyzed: contributing area A_i (as a
surrogate for discharge), Slopes S_i, energy expenditure E_i
($A_{i*}S_i$) and the channel initiation function ($\beta Q^m S^n$) of the
SIBERIA model of basin evolution.

These four variables present multifractal
characteristics and they have very similar multifractal
spectra when analyzed in different basins. This shows the
existence of a common underlying structure of organization in
river basins. The identification of a common multifractal

spectrum of energy expenditure is the first step towards the development of multiplicative cascade models of energy dissipation. These models should be able to reproduce the multifractal spectrum that describes the spatial organization and scaling of energy expenditure in river basins.

The multifractal spectra of different forms of the channel initiation function provides a tool to understand the spatial distribution of scaling properties of processes that lead to channel growth and development. These spectra can be used in the verification of models of network growth and basin evolution.

Finally, the multifractal spectrum of contributing areas is useful to understand the organization of flow directions and patterns of organization. The comparison with models of network structure can show differences with real basins which may not be obvious at first. The multifractal spectrum of Scheidegger's (1967) model shows such an example.

Most of the analysis in this work up to this point has looked at the entire landscape of the basin. On various occasions we have found differences in the organization and distribution at large contributing areas (channels) and at small contributing areas (hillslopes). At the same time we have studied in this chapter the behavior of the channel initiation function, a criteria used in the SIBERIA model to differentiate between channels and hillslopes. The following two chapters will gather all the differences in behavior we

have seen in this work and provide a differentiation criterion that could be an option to separate hillslope and channel pixels in digital elevation maps which provide only elevation data.

Chapter 11

The Differentiation Between Hillslope and

Channel Nodes in DEMs: A Hypothesis

11.1. Introduction

Drainage density has been a fundamental concept in geomorphology since its introduction by Horton (1945) who defined it as the ratio between total length of streams and the area of the basin. Drainage density is a measure of the extent to which the channel network occupies and dissects the basin. Such extension depends on a number of geologic and hydrologic factors.

The understanding of the transition between channels and hillslopes is of fundamental importance in the use of Digital Elevation Maps. These maps only provide elevation data for the basin; the differentiation between hillslope and channel grid points is necessary for hydrological applications.

We will examine in this chapter whether a hypothesis presented by Willgoose et al. (1991a) in the development of the SIBERIA model, where channels and hillslopes are differentiated with a channel initiation function, can in fact be observed in DEM data. The idea is to identify different scaling regions of mean slope versus contributing area in the catchment and to find threshold criteria to

separate these regions. Finally, we will present a modified version of the SIBERIA model that is able to reproduce the various scaling regions observed in DEMs.

Section 11.2 presents a review of various threshold criteria for differentiating channels and hillslopes based on the slope-area behavior of points in the basin. Section 11.3 examines DEM data in relationship to the criteria proposed by Willgoose et al. (1991a). Finally, Section 11.4 presents a channel network growth and landscape evolution model that reproduces the slope-area behavior observed in DEMs.

11.2. Threshold Criteria for Differentiating Channels and Hillslopes

On numerous occasions in this work we have shown and used the relationship observed in rivers between slopes and contributing areas:

$$S \sim A^{-\theta} \qquad\qquad (11.1)$$

where θ is approximately 0.5. At very small scales, this relationship cannot hold because it would imply an infinite slope when area tends to zero. Tarboton et al. (1989a) measured slopes and contributing areas for links in channel networks identified with DEMs. They found that Relationship (11.1) breaks down at a certain value of contributing area and they used this value to identify the channel network. A threshold value of contributing area has been used by various

researchers as presented in Chapter 3, but Tarboton et al. (1989a) justify it in terms of sediment transport processes.

Using a modified formulation of the sediment continuity equations proposed by Kirkby (1971) and Smith and Bretherton (1972), Tarboton et al. (1989b,1992) show how changes in contributing area can result in a switch of the dominant sediment transport processes and correspondingly, the slope-area relationship observed. Tarboton et al. (1992) show that when a combination of a mass wasting sediment transport mechanism occurs concurrently with a wash sediment transport process, the slope-area behavior changes from a positive to a negative gradient in a log-log diagram (i.e., from a convex to a concave profile). This switch corresponds to a change in the dominance of the sediment transport mechanism. At small areas, mass wasting diffusive processes (like soil creep and rain splash) dominate, while at large areas, wash processes dominate. Using link-based slopes and areas, Tarboton et al. (1989b) describe techniques to identify the value A_{th} at which the break in slope-area scaling occurs. The criteria proposed then, is if:

$$A < A_{th} \tag{11.2}$$

the grid point is a hillslope point.

In the Smith and Bretherton (1972) criteria channels extend up to the point of break of the slope-area relationship (or equivalently where the dominant sediment

transport process changes from diffusive to fluvial). This implies however, an infinite rilling in the fluvially-dominated portion of the basin, while natural streams are separated by a finite distance in the field. The Smith and Bretherton (1972) criteria also implies the non-existence of convex-concave hillslopes, because the concave portion would be fluvially dominated and hence channelized. On this issue, Dunne and Aubry (1986) and Loewenherz(1991) argue for a stabilizing effect of sheetwash flow. This effect would imply both a finite scale of rill separation and the location of channel heads at values of contributing area larger than the one implied by the Smith and Bretherton (1972) criteria. The movement of the location of channel heads downhill from the break also imply that there may be portions of the unchannelized hillslope with concave profiles where fluvial sediment transport dominates.

Willgoose et al. (1991a-d) use both diffusive and fluvial sediment transport processes in their SIBERIA model, showing a break in the slope-area relationship in the simulated landscape from a positive to a negative gradient. However, they do not consider channels extending up to that break, but use instead a threshold criteria that combines both slopes and areas to distinguish channel and hillslope nodes in the grid. This criteria allows hillslopes to have a convex-concave profile. The criteria is called the channel initiation function and represents processes that are observed to trigger or activate channelization in the field.

Two criteria that can be parameterized by the channel initiation function, which are commonly used in the study of erosion, are overland flow velocity (Henderson, 1966) and overland flow shear stress (Horton (1945), Vanoni (1975), Moore et al. (1988)). Willgoose et al. (1989, 1991a) show how both of these criteria can be represented in the generic form:

$$\beta \; A^{m'} \; S^{n'} > C_{th} \qquad (11.3)$$

for different cross-sections. C_{th} is the threshold value. The channel initiation function criteria (11.3) would be represented as a straight line with gradient n'/m' in a log-log slope-area diagram. The values for n'/m', in the case of a wide channel assumption, are 0.75 for the overland flow velocity criteria and 1.16 for the overland flow shear stress case. We want to examine whether this threshold behavior can be observed in the DEM data.

Threshold criteria combining slopes and areas to identify channelized and unchannelized nodes have also been presented as $AS^2 > C_{th}$ by Montgomery and Dietrich (1988, 1992), and as $A > C_1/S^2 + C_2 S$ by Dietrich et al. (1992).

11.3. Pixel-Based Slope-Area Relationship in DEMs

Using the gridded elevation data provided by the DEM of a basin, it is possible to assign a slope to each pixel in the steepest direction downstream. In order to analyze the average slope behavior, we can group the pixels with the same

contributing area and calculate their mean slope. For large
values of contributing area there are usually not enough
pixels for a meaningful average. In these cases, the pixels
are grouped in bins according to area, such that at least 500
pixels are located within each bin. This procedure is very
similar in spirit to that of Tarboton et al. (1989a), except
that we are using pixels instead of links for the slope
calculations.

Figure 11.1 shows the log-log diagram of the slope-area
relationship for the Brushy Creek basin (AL). Four regions
can be observed in this diagram. At very small areas, the
slope actually increases with contributing area, indicating
the presence of a convex profile on average. This convexity
is the result of diffusive processes and its behavior can be
explained within the framework developed by Tarboton et al.
(1989b, 1992). The slopes begin to decrease as area increases
in Region II, but then they stabilize to an approximately
horizontal behavior in Region III. The slopes continue their
downward trend in Region IV.

Let us first examine the location of the vertical lines
that limit the regions appearing in the slope-area diagram.
The line between Regions I and II is located at the break
between the positive- and negative-gradient behavior of the
slope-area relationship. The location of the line between
Regions II and III coincides with the location of the break
in the power-law behavior of the cumulative distribution of
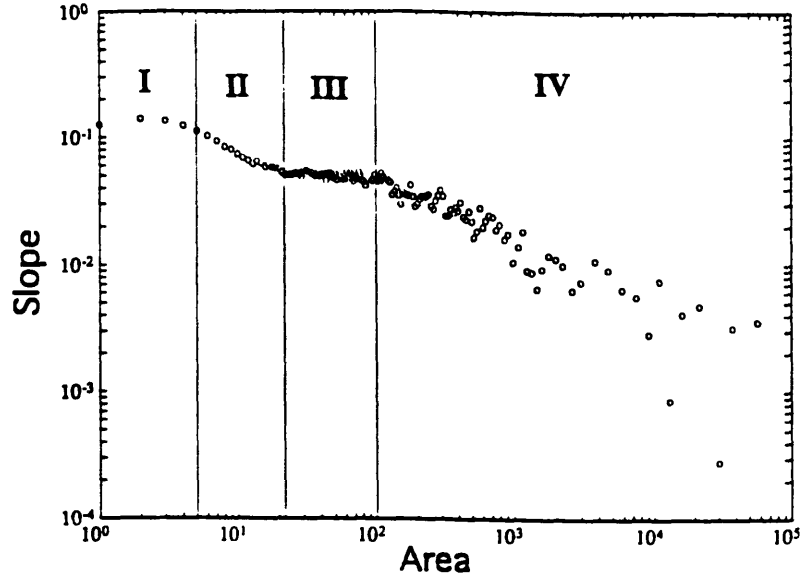
Figure 11.1: Log-log pixel-based slope-area diagram for Brushy Creek basin. Each circle represents the average slope for bins of common contributing area with at least 500 pixels.

contributing areas as discussed in Section 4.4. Figure 11.2 shows the cumulative distribution of areas for the Brushy Creek basin. As will be shown in Chapter 12, this break corresponds to a change in flow organization from a mixed divergent/convergent regime at smaller contributing areas to a purely convergent regime at larger areas. Finally, the location of the line between Regions III and IV approximately coincides with the threshold value of contributing area that can be found using the link-based average slope method described in detail in Tarboton et al. (1989a,b).
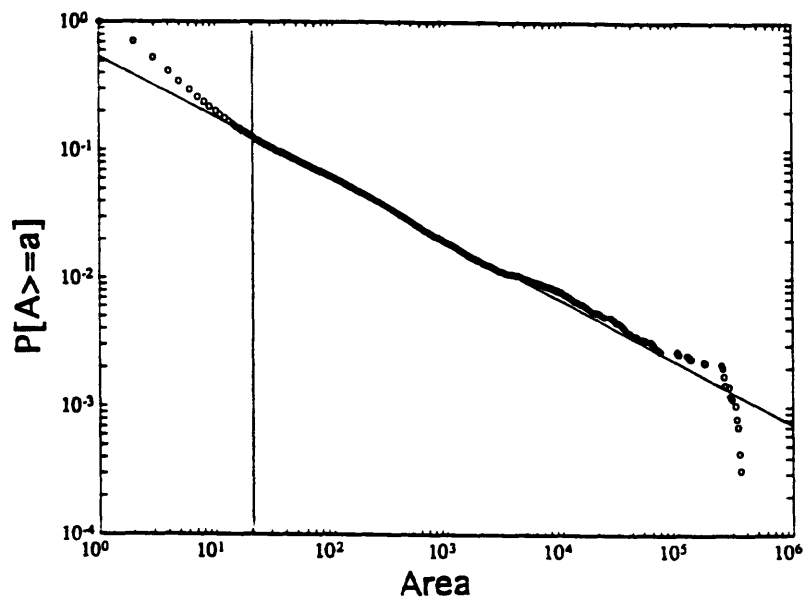
Figure 11.2: Cumulative distribution of
contributing areas for Brushy Creek basin. The
value of area at which the power-law behavior
of the distribution breaks down corresponds to
the location of the boundary between regions
II and III in the slope-area diagram shown in
Figure 11.1.

The approximately horizontal behavior of the slope-area

relationship in Region III appears to be an artifact of the

slope averaging for a given value of the contributing area.

When lines are fit to the slope-area points in Regions II and

IV, it is reasonable to think that the observed mean behavior

in Region III is the result of averaging the two scaling

lines as shown in Figure 11.3. A threshold criteria of the

form proposed by Willgoose et al. (1991a) and shown in Figure

11.3, can be used to distinguish between hillslope and

channel pixels. In the diagram, this threshold criteria

corresponds to the line joining opposite corners of the

quadrilateral formed in Region III. Hillslope pixels are
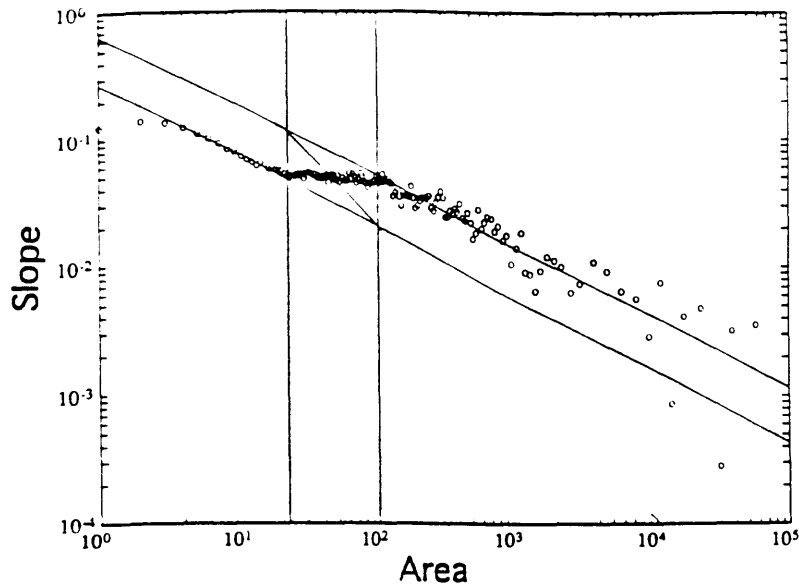
Figure 11.3: Slope-area diagram for Brushy Creek basin with fitted scaling lines for hillslopes and channels, the boundary between regions II, III and IV and the threshold criteria joining opposite corners of the quadrilateral formed.

located to the left and below the threshold line and channel pixels on the opposite side. We would not expect to see, on the average, hillslope pixels in Region IV or channel pixels in Region II because their corresponding scaling relationships cross, by construction, the threshold criteria precisely at the boundary of these regions.

Figures 11.4 and 11.5 show two other examples of slope-area diagrams for the Schoharie Creek basin (NY) and Racoon Creek basin (PA). The boundaries of Region III, the fitted scaling slope-area relationships for channels and hillslopes, and the corresponding threshold lines are shown in these figures. Table 11.1 presents the values of n'/m' (the scaling gradient of the threshold criteria) for various basins across the U.S. The measured gradients of the threshold criteria are approximately equal to the values predicted by the Willgoose
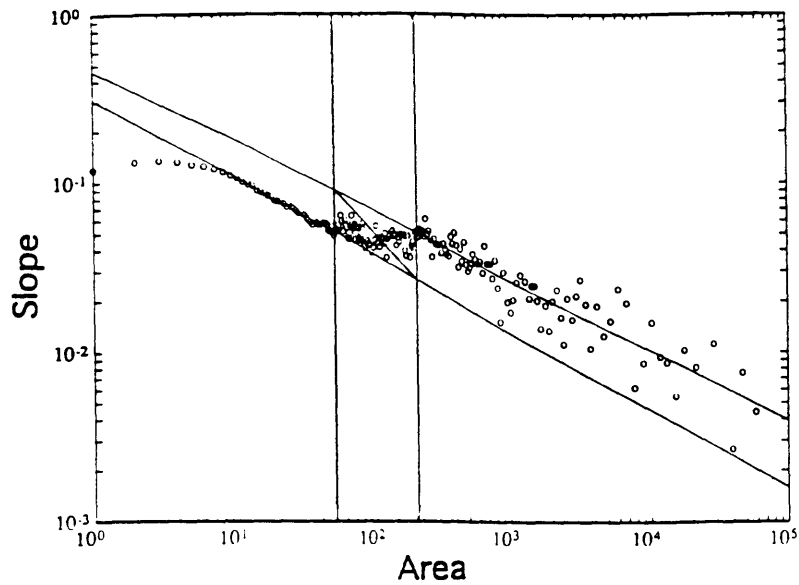
Figure 11.4: Slope-area diagram for Schoharie Creek basin.
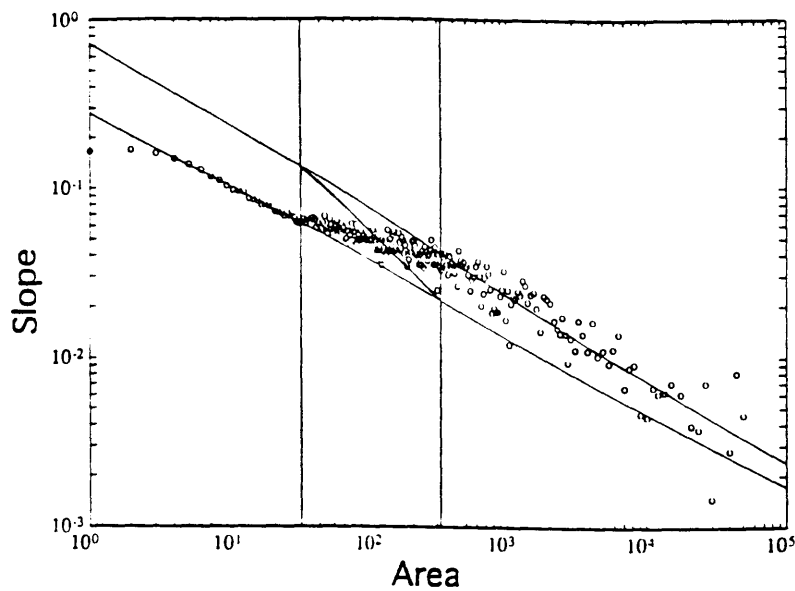
Figure 11.5: Slope-area diagram for Racoon Creek basin.

et al. (1991a) criteria for overland flow velocity in some cases, and for shear stress in others.

Basin	Location	n'/m'
Beaver Creek	PA,OH,MN	0.98
Brushy Creek	AL	1.05
Big Creek	ID	0.62
East Delaware River	NY	0.73
Schoharie Creek Headwaters	NY	0.78
North Fork Cour d'Alene River	ID	0.96
Racoon Creek	PA	0.80
Schoharie Creek	NY	0.83
St. Joe River	MO,ID	0.61

Table 11.1: Scaling gradient n'/m' of the threshold criteria to differentiate channel and hillslope nodes in region III of the slope-area diagram.

Summarizing, we can see four regions in the pixel-based slope-area diagram. Region I corresponds to hillslope points where diffusion processes tend to dominate over fluvial processes. These points correspond to the convex hilltops which have small contributing areas. In Region II we find hillslope pixels, concave in the average, where slopes decrease with increasing area. Region III has a combination of hillslope and channel points that have the same values of contributing area but which may be separated with a threshold criteria of the form suggested by Willgoose et al. (1991a). Finally, as contributing area increases, all the nodes in Region IV are channelized.

11.4. A Channel Network Growth and Landscape Evolution Model

In this section, we will present a modified version of the SIBERIA landscape evolution model with the purpose of simulating a landscape and channel network that would reproduce the slope-area scaling diagram configuration shown in the last section for various basins. We will concentrate our modeling efforts in Regions II, III and IV, as the transition between Regions I and II has been appropriately analyzed in detail elsewhere as a competition between fluvial and diffusive processes (Tarboton et al. (1989a, 1992), Willgoose et al. (1991c)).

The governing equation of the model is:

$$\frac{\partial z_i}{\partial t} = T + \left(Q_{si}^{in} - Q_{si}^{out} \right) \tag{11.4}$$

where z_i is elevation at node i, T is tectonic uplift, and Q_{si}^{in} and Q_{si}^{out} are sediment coming in and out of node i, respectively. The second constitutive equation is:

$$Q_{si}^{out} = Q_{si}^{in} + \begin{cases} \beta_c \ Q_i^{m_c} \ S_i^{n_c} & \text{if node is a channel} \\ \beta_h \ Q_i^{m_h} \ S_i^{n_h} & \text{if node is a hillslope} \end{cases} \tag{11.5}$$

where Q_i and S_i are the discharge and slope at node i and β_c, m_c, n_c, β_h, m_h and n_h are constants. The distinction between channel and hillslope nodes is made with the channel initiation function where, if:

$$Q_i \ S_i^{n_s} > D_{th} \tag{11.6}$$

then node i is a channel. Finally,

$$Q_i = \beta_r A_i \qquad (11.7)$$

where β_r is a constant related to mean rainfall and A_i is the contributing area to node i, which can be recursively calculated as:

$$A_i = \sum_j I_{ij} A_j + a_u \qquad (11.8)$$

where the summation is taken over the eight nodes j neighbor to i, I_{ij} is an indicator function equal to 1 if node j drains into node i, and 0 otherwise, and a_u is the unit area of a single pixel. Drainage directions are defined in the steepest slope direction. The simulations are run with closed flow boundary conditions except at defined outlet nodes. The initial condition is an elevation field with the same mean elevation plus very small random perturbations to properly define flow directions. The outlet is set at a lower elevation. The tectonic input is constant in time and space.

The main difference between this model and the original version of the SIBERIA model is in the way material is removed from each pixel. Ahnert (1976) referred to this difference in modeling slope evolution as point-to-point transfer and direct-removal. In the SIBERIA model the material carried from each point is deposited in the next node downstream. Equivalently, the material carved at each point is equal to the transport capacity of the stream minus the material being carried from uphill (i.e., a point-to-

point transfer). In the modified version, however, the material removed is taken away from the system (i.e., direct removal in Ahnert's terminology). One implication is that the modified version of the model can be used only for basins where deposition is not predominant, and not for deltas or the lower and flat regions of basins. Other models of landscape evolution —such as the slope-area model of Chapter 5 and the models in Kramer and Marder (1992), Takayasu and Inaoka (1992), and Rinaldo et al. (1993)— also remove from the system any material taken away from a point.

Even though the evolution dynamics of the modified version are different from the original SIBERIA model, we will see in this section that it is possible to essentially reproduce the properties of the channel network and landscape at equilibrium with either model. Although the original motivation for developing the modified version of the model was to get around some numerical problems observed in the original version, this new model offers a different approach to landscape evolution that seems to give very similar equilibrium results. Future research should concentrate in analyzing differences between simulated landscapes coming from both models, using new and stronger geomorphological tests not currently available.

The catchment is at dynamic equilibrium when the tectonic input balances the fluvial erosion. At this point it is possible to infer the slope-area relationship and relate

it to the parameters of the model, as in Willgoose et al. (1991c). At dynamic equilibrium for node i:

$$\frac{\partial z_i}{\partial t} = 0 \qquad\qquad (11.9)$$

Therefore, using equations (11.4) and (11.5):

$$T = \beta^* \, Q_i^{m^*} \, S_i^{n^*} \qquad\qquad (11.10)$$

where the multiplicative and power constants β^*, m^*, and n^* depend on the character of node i (hillslope or channel). Replacing Equation (11.7) in (11.10), a log-log linear relationship between slopes and areas is obtained:

$$S_i = \left[\frac{T}{\beta^* \, \beta_r^{m^*}} \right]^{1/n^*} A_i^{-m^*/n^*} \qquad\qquad (11.11)$$

By assuming that the observed DEM is at dynamic equilibrium, it is possible to infer the value (or at least some ratio of values) of the physical parameters of the model. In the log-log diagram, the scaling lines fitted for the hillslope and channel regions (see Figures 11.3 to 11.5) correspond to Relationship (11.11). The slope of the scaling lines would give the ratios m_c/n_c and m_h/n_h. The intercepts of these lines are used to determine the value of the multiplicative prefactors. Notice however, that there are eight unknowns and only four given values (the slopes and intercepts of the scaling lines) which allows certain ratios of the parameters to be determined. Nevertheless, we have found that the network structure and landscape properties

remain approximately the same if we use different values of m* and n*, as long as the ratio m*/n* is kept constant. We will see in Chapter 12 that this is not always the case in other models, where convergence and divergence are taken into consideration.

The meaning of the power exponents m* and n* is not identical to that of the exponents m and n in the original version of the model. The first difference appears in the predicted scaling relationship between slopes and areas in the original SIBERIA model. As already described in Chapter 2, the predicted relationship in the original version is:

$$S \sim A^{(1-m)/n} \qquad\qquad (11.12)$$

which gives the appropriate scaling exponent 0.5 when the values m=2 and n=2, measured in the field for sediment transport capacity of streams (Leopold and Maddock, 1953), are used. However, these field values of m and n do not correspond exactly to m* and n*. The former measure how much sediment can be transported by the current ($\beta Q^m S^n$), while the latter measure how much material is taken away from the node ($\beta^* Q^{m^*} S^{n^*}$). The amount of sediment transported by the current at a point i in the modified model is equal to the sum of sediment taken away from all the nodes upstream from node i. At <u>dynamic equilibrium</u> the sediment transported is precisely equal to TA_i, or equivalently, using Equations (11.10) and (11.7):

$$Q_i^{trans} = A_i \beta^* C_i^{-*} S_i^{n^*} = \beta^* \beta_r^{m^*} A_i^{1+m^*} S_i^{n^*} \qquad (11.13)$$

which suggests a relationship between m, n and m*, n* (e.g. m=2, n=2 would be equivalent to m*=1, n*=2; we have used values around these for the simulations to be shown later in this section). This calculation can be performed only at dynamic equilibrium. In other situations, the way sediment is moved within the system is different for both models in the evolution, although their final equilibrium states are identical under the measures used (the slope-area scaling, for example).

We can use the parameters inferred from the slope-area scaling relationships at the hillslope and channel scale for the Brushy Creek basin shown in Figure 11.3 to run a landscape simulation to dynamic equilibrium. The slopes and intercepts of the scaling lines are used along with Equation (11.11) to determine the parameters of the run. The threshold line is used to find the parameters D_{th} and n_s for the channel initiation function (11.6). The domain size is 50x50 pixels; Figure 11.6 shows an isometric view of the simulated catchment at equilibrium, and Figure 11.7 presents the drainage directions at dynamic equilibrium. The final channel network, determined with the appropriate channel initiation function criteria, is represented in Figure 11.7 with a continuous line.
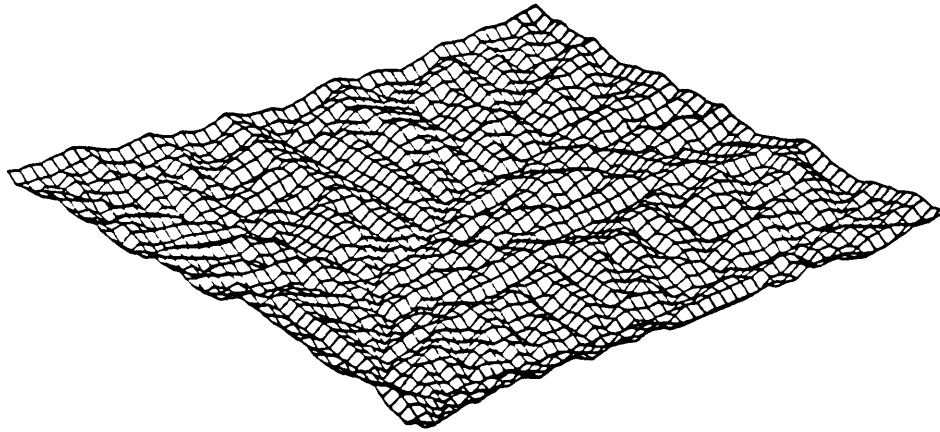
Figure 11.6: Equilibrium landscape simulated
with the modified version of the SIBERIA
model. The parameters of this simulation were
inferred from the slope-area diagram of the
Brushy Creek basin shown in Figure 11.3.
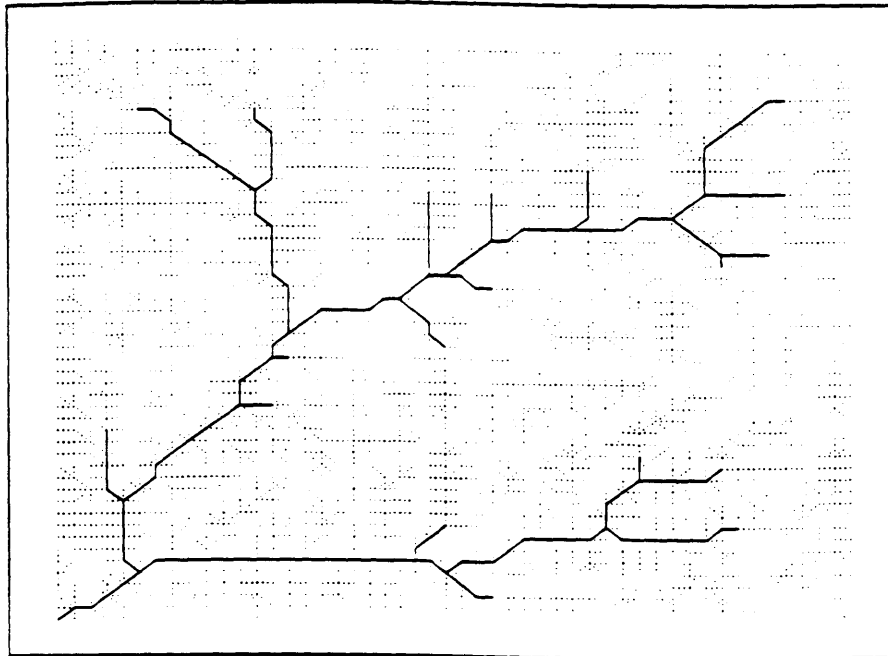
Figure   11.7:   Drainage   directions   at
equilibrium for simulated landscape shown in
Figure 11.6. The channelized nodes, identified
with the appropriate threshold criteria, are
shown with a continuous line.

In order to check that the landscape at dynamic equilibrium indeed presents the expected slope-area scaling relationships at the hillslope and channel scale, Figure 11.8 shows the slopes and areas *for each one* of the pixels in the simulation without averaging or binning. The scaling lines for the Brushy Creek basin (shown in Figure 11.3) are reproduced.
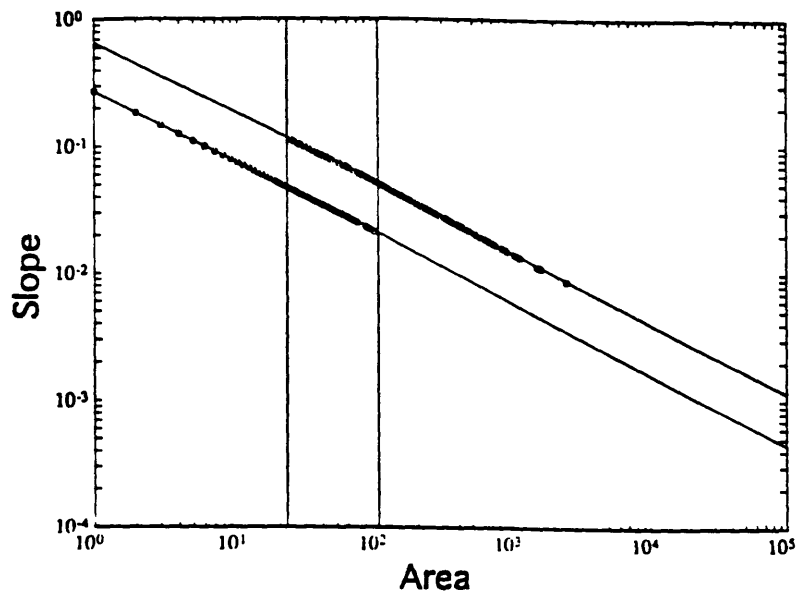
Figure 11.8: Slope-area diagram for simulated landscape at dynamic equilibrium. The slopes and areas for all the 2500 pixels in the 50x50 simulation domain as well as fitted scaling lines are presented. These lines coincide with those of the actual Brushy Creek diagram shown in Figure 11.3.

Finally, to see that the quasi-horizontal behavior observed in Region III of the slope-area diagram may be, in fact, the result of grouping and averaging in bins of common contributing area, we have repeated the procedure with the simulated data. By grouping the pixels in bins and finding the average slope for each bin, we can obtain the slope-area

diagram shown in Figure 11.9. The behavior of the actual slope-area diagram in Region III for the Brushy Creek basin is reproduced.
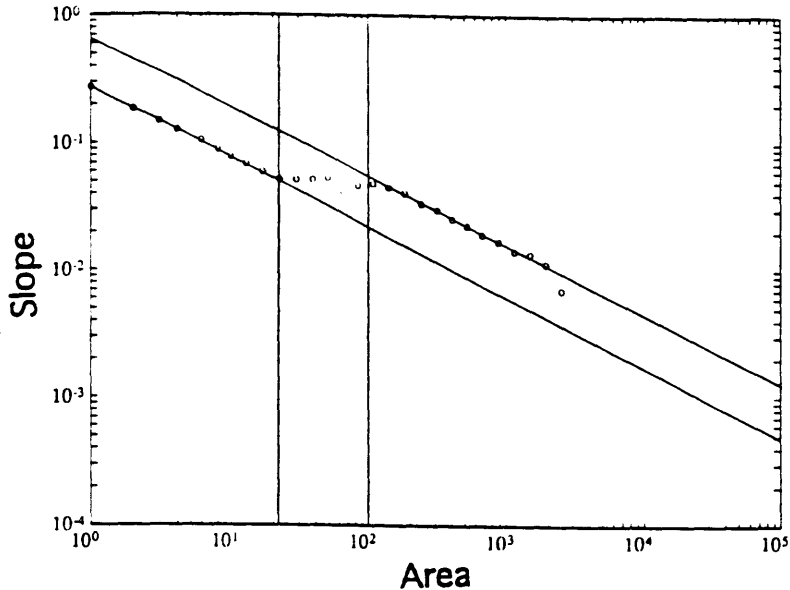
Figure 11.9: Slope-area diagram for simulated landscape at dynamic equilibrium after the bin averaging procedure used in DEM data has been applied. Notice the behavior in region III and its similarity to the corresponding region in the Brushy Creek diagram of Figure 11.3.

In this section, we have presented a modified version of the SIBERIA model developed by Willgoose et al. (1991a-d). The main modification corresponds to the nature of sediment movement from a point-to-point transfer version to a direct-removal method as described by Ahnert (1976). The model can simulate landscapes that evolve to an equilibrium state where the scaling relationships of slope versus area at the hillslope and channel level are reproduced. Furthermore, when bins of contributing area are grouped and their slopes are averaged in the equilibrium landscape, as in DEM analysis,

the actual behavior of the slope-area diagram in Regions II,
III and IV is reproduced. Again, we did not focus our
attention on Region I, as this behavior has been analyzed in
great detail elsewhere (Tarboton et al. (1989a), Willgoose et
al. (1991c)). As a final note, we have found that in only one
of the ten basins in the data set analyzed, Region III does
not behave in the way predicted by the averaging hypothesis
presented in this section. Figure 11.10 presents such
exception.
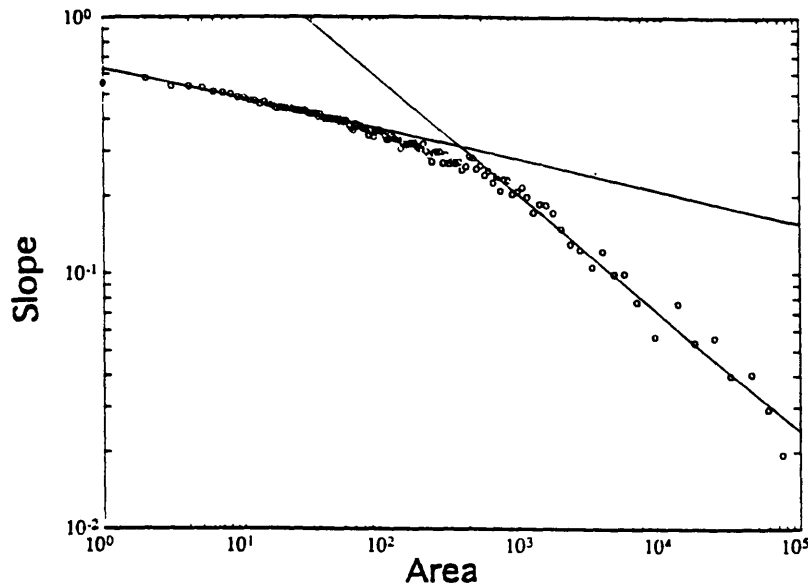
Figure 11.10: Slope-area diagram for Buck
Creek basin. The behavior of the slopes in
region III does not appear to correspond to
the average of the two fitted scaling lines.
This basin is the only exception in our data
set.

11.5 Summary

In this chapter, we have examined the hypothesis that
hillslope and channel nodes could be differentiated based on
their slope-area scaling behavior using a threshold criteria
proposed by Willgoose et al. (1991a). This criteria, called

the channel initiation function, models processes that trigger channelization in the field like overland flow velocity and shear stress. By looking at the mean slope behavior at the pixel scale we were able to identify four regions in the slope-area log-log diagram. In increasing order of contributing area these regions are: Region I, where diffusive sediment transport processes dominate and hillslope profiles are convex; Region II, which has concave hillslope nodes; Region III, where hillslope and channel nodes with the same contributing area coexist but can be differentiated using an appropriate form of the channel initiation function; and Region IV, which has channelized nodes with large contributing area.

A modified version of the SIBERIA model was presented. The model simulates landscapes that evolve towards equilibrium states in which the slope-area diagram observed in actual basins is reproduced. Specifically, the behavior in Region III is shown to be possibly caused by the grouping and averaging in bins of common contributing area performed in the DEM data.

The use of a threshold criteria like the channel initiation function, in which a combination of areas and slopes is used to differentiate between channel and hillslope nodes in a DEM, is not without problems. The advantage of a threshold area criteria is that a continuous network is always obtained. The introduction of slopes in the threshold

adds noise to the criteria and a disconnected network is commonly found. Research along these lines should continue and the channel initiation function criteria may help some of these efforts.

One problem with the modified version of the SIBERIA model presented in this chapter, the Slope-Area model presented in Chapter 5, and most other models of landscape simulation and channel network growth, is their tendency to aggregation and convergence down to the lowest scales (see Figure 11.7 in this chapter, or Figure 7.6 for the Slope-Area model). This feature translates into a cumulative distribution of contributing areas that follows a power-law down to the lowest values (see Figure 5.4 for the case of the Slope-Area model). However, we know that the power-law behavior breaks down at a value of contributing area that approximately coincides with the boundary line between Regions II and III in the slope-area diagram as shown in this chapter. In Chapter 12, we will examine the relationship between this break and the convergent/divergent nature of hillslopes as opposed to the convergent and collecting character of channels.

Chapter 12

Convergence and Divergence in the Basin Landscape

12.1. Introduction

The channel network is a collecting structure in which its members aggregate into larger branches to deliver water and sediment out of the basin in an optimal configuration as examined in Chapter 6. Hillslopes, on the other hand, are not necessarily aggregating structures. They are three-dimensional objects with varied forms as shown in Figure 12.1 from Ruhe (1975). The form of the hillslope has a direct effect on runoff and erosion as shown by Young and Mutchler (1969). The effect on runoff has been recently incorporated in the analysis of DEMs using new algorithms for calculating contributing area. The effect on erosion has been less studied from the modeling point of view. The importance of the form of hillslopes on the location of channel heads in the field has recently been noted by Dietrich et al. (1992).

The spatial flow organization of the basin is directly related to the cumulative distribution of contributing areas. We will examine in this chapter the relationship between the observed break in this distribution and the different flow organizations at the hillslope and channel scales. We will present an evolution model in which the contributing area and
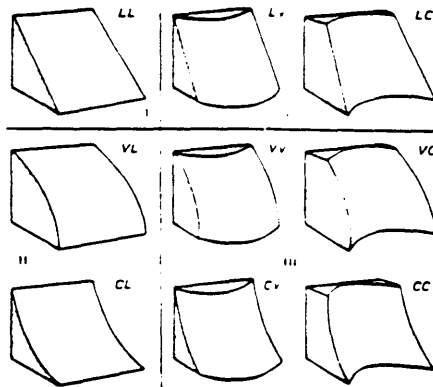
Figure 12.1: Different forms of hillslopes when considered as three-dimensional objects (from Ruhe, 1975).

sediment transport take into account the existence of divergent hillslopes. This model will also help us to understand the way divergent and convergent hillslopes organize in space.

12.2. Convergence and Divergence in a Landscape Evolution Model

The issue of convergence and divergence in hillslopes and their influence on flow paths and other variables of digital elevation maps, mainly contributing area, has been recently studied by various researchers (Fairfield and Leymarie (1991), Freeman (1991), Quinn et al. (1991), Cabral and Burges (1992)). The idea is to use algorithms where multiple flow directions are used to handle divergent landscapes which cannot be properly analyzed using a single flow direction for each pixel. Analogously, in landscape evolution models where a single flow direction is defined in

the steepest slope, the model generates landscapes in which
the aggregation goes down to the smallest scales with no
consideration for divergent features.

In this section we will implement the algorithm proposed
by Quinn et al. (1991) to calculate the contributing area in
a landscape evolution model and proceed to study the
influence of the spatial organization of flows on the
simulated landscape. Quinn et al. (1991) propose to
distribute the contributing area downhill proportionally to
the values of the slopes downhill from each node, i.e.:

$$A_{ij} = A_i \frac{S_{ij} \ C_{ij} \ I_{ij}}{\sum_k S_{ik} \ C_{ik} \ I_{ik}} \qquad (12.1)$$

where A_{ij} is the portion of contributing area passed from node
i to node j, A_i is the total area of node i, S_{ij} the slope
from node i to node j, C_{ij} a contour length measured normal to
the flow (equal to 0.5 in the orthogonal directions and 0.354
in the diagonal directions; for details see Quinn et al.
(1991)) and I_{ij} is an indicator function equal to 1 if node j
has a lower elevation than node i and 0 otherwise. The
summation in the denominator is done over the eight nodes
around node i. The idea with this procedure is to allow the
contributing area to diffuse, if a node has more than one
neighbor downhill. The algorithm is able to handle divergent
landscapes and hillslopes not strictly aligned with the
orthogonal or diagonal directions. Finally, notice that the

contributing areas are not necessarily integers when calculated using (12.1).

The total contributing area to each node is then calculated as:

$$A_i = \Sigma_k \, A_{ki} + a_u \qquad (12.2)$$

where the summation is performed over the areas A_{ki} passed from nodes k, with higher elevation, located next to node i and a unit value a_u for the area of the pixel.

Once the contributing areas to each node are calculated it is possible to use the landscape evolution model described in Chapter 11. As our interest in this chapter is focused on the analysis of convergent and divergent regions, we will use, for simplicity, a single slope-area relationship in the model. This implies that only one set of parameters (β, m and n) will be used for the sediment removal from node i:

$$Q_{si}^{out} = Q_{si}^{in} + \beta \, Q_i^m \, S_i^n \qquad (12.3)$$

12.3. Simulated Landscapes and their Cumulative Distribution of Contributing Areas

The purpose of the modified version of the model introduced in the last section is two-fold. First, we are interested in simulating divergent and convergent hillslopes. One important characteristic of landscape models is their aggregation behavior at all scales. Visually, landscapes

simulated with these models look too "rough" because they lack the roundness of divergent hillslopes. Second, we want to study the influence of different flow organizations on the cumulative distribution of areas with the purpose of reproducing the observed behavior in actual basins.

What we have found in simulations with the convergent/divergent model is that, in this new version, the size of the diverging hillslopes and the form of the cumulative distribution of areas are directly affected by the values of m and n. This is unlike the version of the model analyzed in Chapter 11 where the actual values of m and n did not influence the overall structure of the landscape as long as m/n was constant.

In order to show this effect, we will use as an example the Brushy Creek basin (AL). To find the proper ratio m/n, the gradient of the hillslope slope-area relationship shown in Figure 11.3 can be used as seen in Equation (11.11). Three different simulations were run with the same ratio m/n=0.56. The difference between the simulations was in the values of m and n: 1.68 and 3.00 for case 1, 0.56 and 1.00 for case 2, and 0.112 and 0.2 for case 3. Figures 12.2 to 12.4 show the cumulative distribution of contributing areas for cases 1, 2 and 3 respectively. In each figure the actual distribution of areas for the Brushy Creek basin is shown with a continuous line while the distribution for the simulated basin is shown with circles. The first case has a power-law distribution
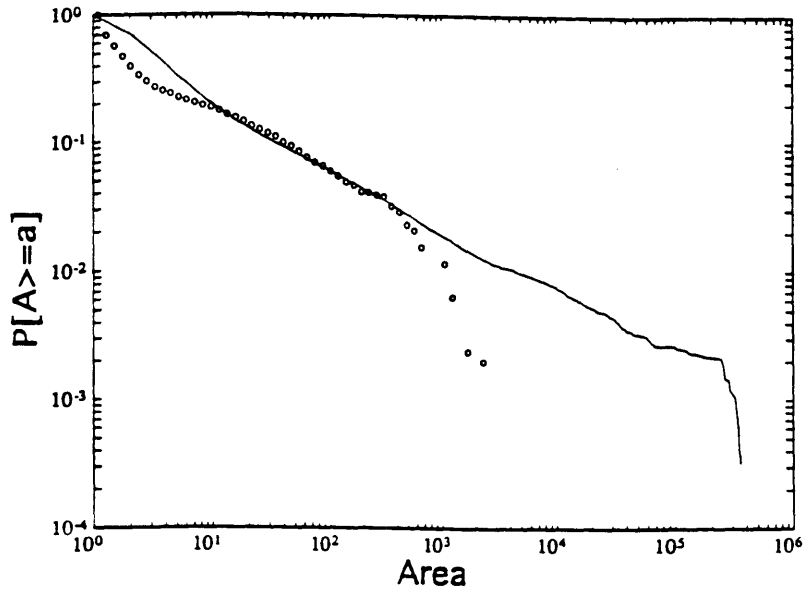
Figure 12.2: Cumulative distribution of areas for simulation with m=1.68, n=3.00, m/n=0.56.
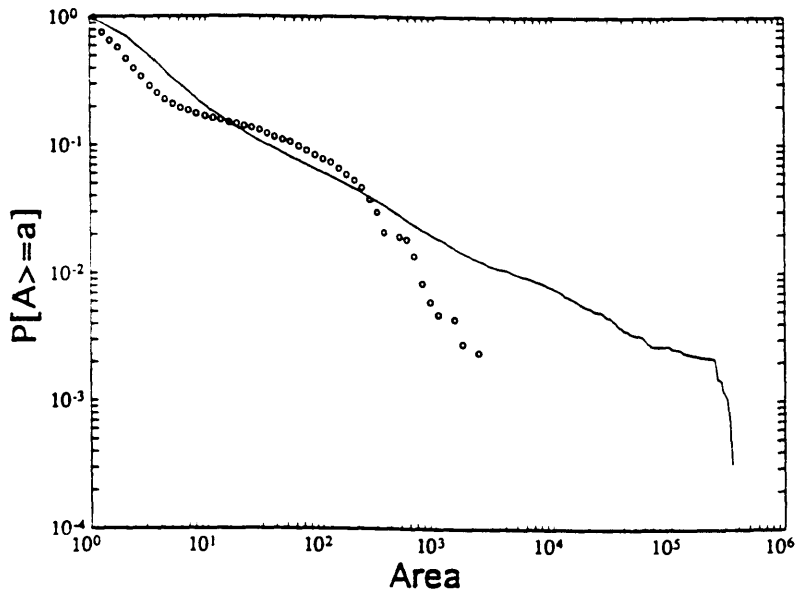
Figure 12.3: Cumulative distribution of areas for simulation with m=0.56, n=1.00, m/n=0.56.
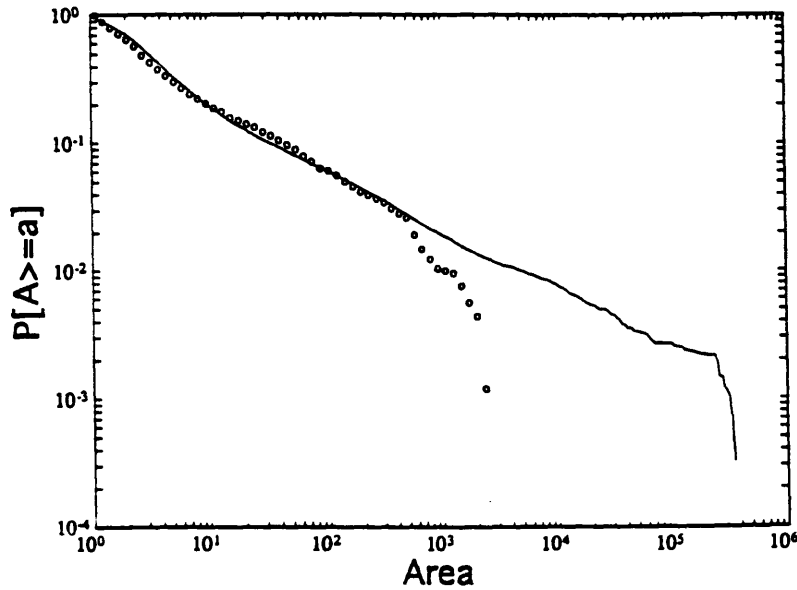
Figure 12.4: Cumulative distribution of areas for simulation with m=0.112, n=0.20, m/n=0.56.

that extends down to the lowest scale. As we will see in the resulting network, the aggregation also begins at the lowest scale. In the third case, the actual cumulative distribution is well approximated by the simulation. Notice that the distribution of areas in the simulated basins breaks down before the real basin does because of its much smaller domain size.

Now we can proceed to look at other properties of the landscape using Cases 1 and 3. Figures 12.5 to 12.7 and 12.8 to 12.10 show the landscape, contour, and averaged flow directions for the cases m=1.68 and n=3.00, and m=0.112 and n=0.2 respectively. The landscape in Figure 12.8 appears more natural than the one in Figure 12.5 because it is not dissected to the lowest scale. Something similar can be said about the contour maps in Figures 12.6 and 12.9. The
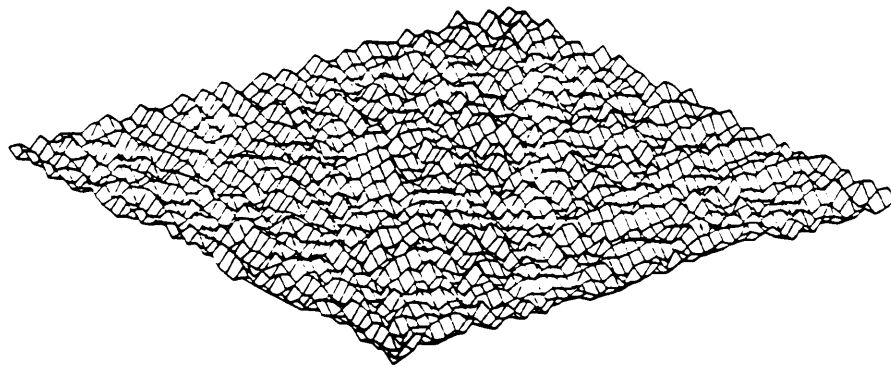
Figure 12.5: Equilibrium landscape at dynamic equilibrium for simulation with m=1.68, n=3.00.
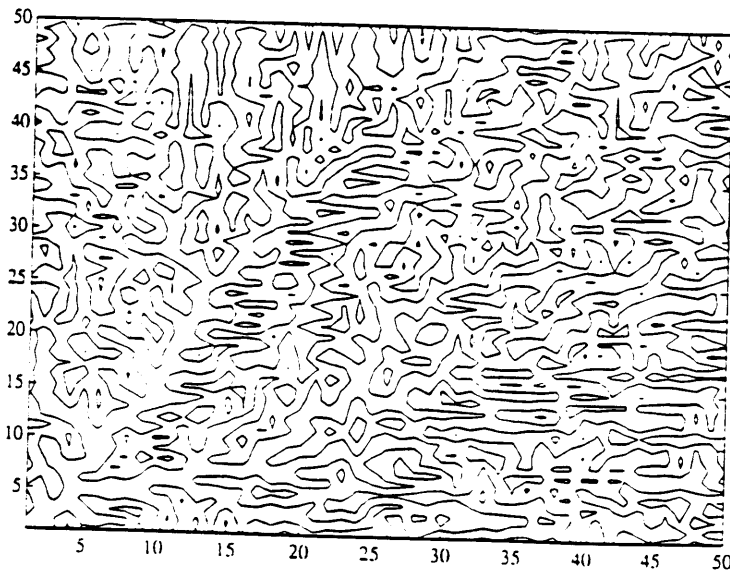
Figure 12.6: Contours of elevation at dynamic equilibrium for simulation with m=1.68, n=3.00.
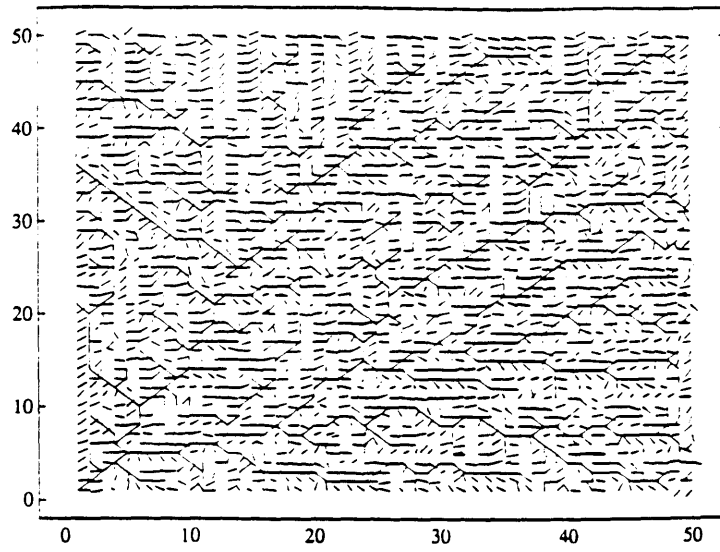
Figure 12.7: Averaged flow direction at dynamic equilibrium for simulation with m=1.68, n=3.00.
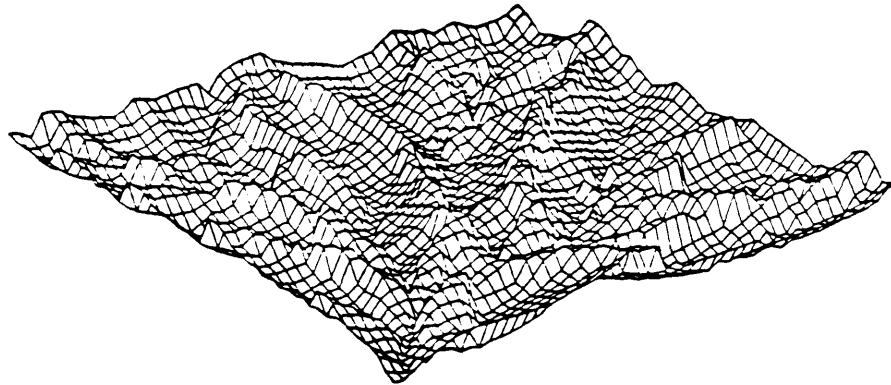
Figure 12.8: Equilibrium landscape at dynamic equilibrium for simulation with m=0.112, n=0.2.
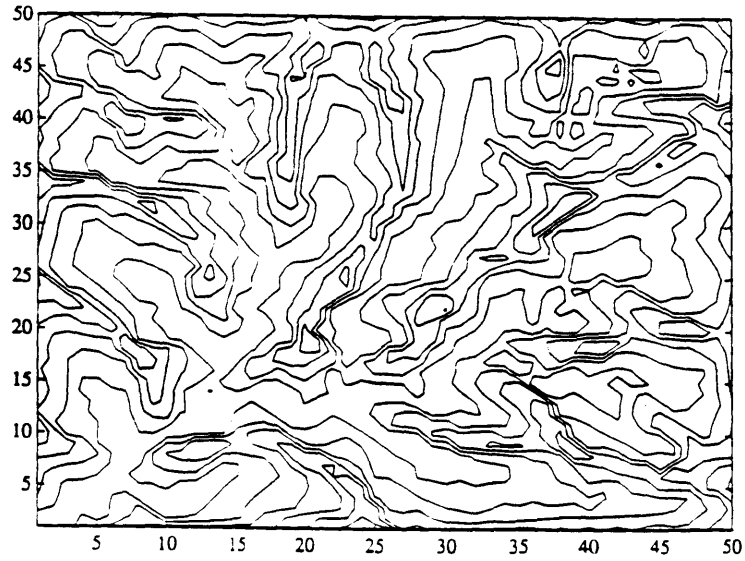
Figure 12.9: Contours of elevation at dynamic equilibrium for simulation with m=0.112, n=0.2.
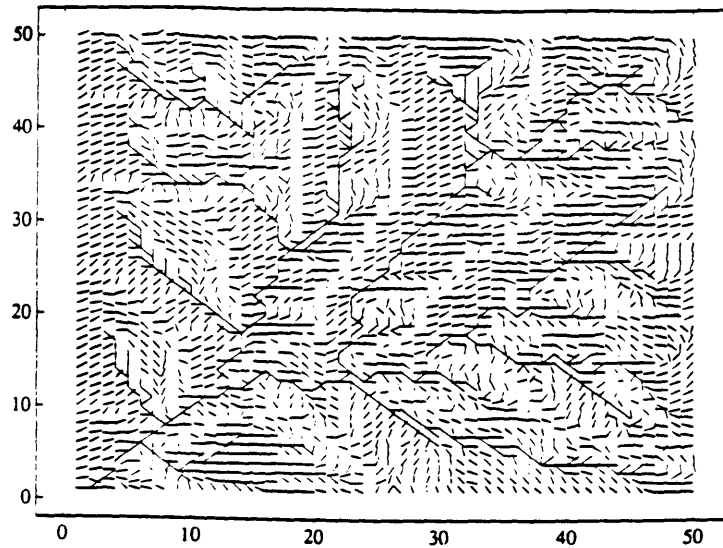
Figure 12.10: Averaged flow direction at dynamic equilibrium for simulation with m=0.112, n=0.2.

landscape in Figure 12.5 is very similar to landscapes generated with models in which contributing areas are calculated using a single flow direction.

Figures 12.7 and 12.10 present how the flow directions organize within the basin. To do that we have taken the value of contributing area at which the power-law behavior of the distribution breaks down, as an indicator of the boundary below which divergence exists. This value can be read from Figures 12.2 and 12.4 (3 for Case 1 and 15 for Case 3). For nodes with areas below the break, Figures 12.7 and 12.10 show an averaged flow direction where the weights used in the averaging are those used in (12.1). In this way a graphical sense of divergence in the planar representation of the basin can be conveyed. To help the eye identify the collecting network, we used the principal flow direction for nodes with areas above the break.

All the figures above show from different perspectives, the relationship between the actual values of m and n, the size of diverging hillslopes, and the location of the break in the power-law behavior of the cumulative distribution of areas.

One final point about the diffusive effect of moving contributing area to more than one neighbor downhill as is done in the model through equation (12.1) needs to be discussed. This diffusive effect is very different from the diffusion term used in the SIBERIA model by Willgoose et al.

(1991a-d), where the purpose was to simulate the convex tops of hills in Region I of the slope-area diagram. The flow directions in the simulated diffusive-dominated regions tend to be parallel, and the vertical profile is convex. In the model presented in this chapter, some of the hillslopes are divergent (not just planar with parallel flow as generated by the diffusion sediment transport term) and they are concave because they are fluvially dominated. It is reasonable to think that even more realism can be added to the simulated landscape by including diffusion. The added diffusion would round the tops of the hills, and would better simulate the region of the slope-area diagram with positive gradient for very small contributing areas in DEMs. Such extension is currently under development by G. Moglen (private communication).

12.4. Summary

A landscape evolution model was developed in order to examine the hypothesis that the break in the power-law behavior of the cumulative distribution of areas in river basins is caused by the change, in flow organization, from an essentially collecting and aggregating structure at the channel level to a combination of convergent and divergent features at the hillslope scale. The only change in this model, compared to the version shown in Chapter 11, is the way in which contributing areas are calculated. Instead of moving area downhill only in the steepest direction, the

contributing area is distributed to all nodes downhill proportionally to the slopes in their corresponding directions in the new model. In this way the modified version is able to simulate divergent hillslopes using the feedback provided by the diffusion of the contributing area dispersed downhill and the diffusion's effect on sediment movement. The parameters m and n of the model directly influence the size of the divergent hillslopes and hence the location of the break point where the cumulative distribution of areas changes its power-law nature. The inclusion of the diffusive processes is a point where the model can still be improved, and the development of measures to study and understand the organization of divergent features in the landscape will be necessary in the near future. Also, the representation of the sediment movement in hillslopes (especially those that are divergent) used in the model presented in this chapter is crude at best and better formulations are required.

Chapter 13

Conclusions

13.1. Summary of Results

The main questions addressed in this work and the results presented will be summarized in this section. The data used came from Digital Elevation Maps (DEMs) which give elevations in a gridded system. The data structure and programs used to analyze the elevation field were those developed by Tarboton et al. (1989b). Chapter 3 gives the main physiographic characteristics of the basins analyzed.

In Chapter 4, the distributions of mass and energy in river basins were examined. These distributions were found to follow a power-law with common scaling exponents of 0.43 and 0.9 respectively across different basins. The value of 0.43 for areas can be compared against the 1/3 obtained for Scheidegger's model of random river networks. This difference illustrates the possible use of this property as a test for simulated networks. The power-law distribution and fractal organization in space is one of the properties of self-organized critical (SOC) systems. These systems evolve towards a state with fractal distributions in space and time. Motivated by the possibility of describing the evolution of river basins as a SOC system, a simple model of channel network growth was developed in Chapter 5.

One of the objectives of developing a simple model of landscape evolution was the possibility of simulating landscapes in a domain large enough to allow the study of the spatial and temporal fluctuations of the geomorphic process over various orders of magnitude. At the same time, the model has enough realism in its formulation to reproduce many of the common geomorphological statistics used to analyze channel networks. The Slope-Area model developed in Chapter 5 uses the scaling relationship between slopes and areas observed in river basins as the basic component of the algorithm. It was shown that the cumulative distribution of areas (a spatial feature) follows a power-law with an exponent similar to that of actual basins. The lifetimes of the family of sub-basins and the growth of perturbations, which are temporal characteristics, also follow power-laws. These three properties are common to SOC systems.

Chapter 6 presents three principles of energy expenditure proposed by Rodriguez-Iturbe et al. (1992b) from which the average behavior of the local geometric features at the link level (width, depth, slope and velocity) versus flow can be derived. The implications of a global principle of minimum energy expenditure in the network were examined after developing an optimization algorithm capable of finding the Optimal Channel Network (OCN) draining a given basin area. It was shown that OCNs reproduce common geomorphological statistics like Horton's laws and the power-law behavior of the cumulative distribution of areas.

A problem with the optimization algorithm developed in Chapter 6 is its computer intensive nature. The largest size it can handle is about two orders of magnitude smaller than the typical size of basins in DEMs at the scale of resolution available. A plausible way to predict the optimum level of energy for a basin at the DEM scale was presented in Chapter 7. The idea is to use the Slope-Area model as an intermediate tool in the process. In the first step we showed that the levels of total energy expenditure in OCNs and in Slope-Area networks constructed in small domains that could be handled by the optimization algorithm were very similar. Then, using the actual boundary and outlet location of river basins identified from DEMs, the Slope-Area model was used to grow drainage networks in these domains. The actual network and the simulated one were shown to have very similar values of energy for the various basins studied. This evidence, along with the tests presented in Chapter 5, tends to indicate that river basins appear to evolve towards states of optimum energy expenditure.

Furthermore, by showing the equivalence between total energy expenditure and the sum of elevation in the basin (a measure of the available potential energy), a possible mechanism by which the network evolves towards states of minimum energy was proposed in Chapter 7. In this way, a connection was made between OCNs (which does not consider the evolution process which basins must go through in order to arrive at states of minimum energy expenditure) and evolution

models that do not have any optimality requirements in their formulation. It was also shown in this chapter how certain equilibrium landscapes are unstable even though the slope-area scaling relationship is present. These unstable landscapes were shown to be states with very high total energy expenditure and to be unsustainable under perturbations.

Chapter 8 examines the implications of minimum energy expenditure on the shape of competing drainage sub-units that try to optimally allocate space among them in order to drain a given area more effectively. Using a controlled geometry as reference, it was shown that river basins tend to elongate with size. OCNs reproduce what is known in geomorphology as "Hack's law" with the scaling exponent observed in actual basins. Also, motivated by a small-scale erosion experiment in a circular domain which showed six main branches in its drainage organization around a center outlet, it was shown that OCNs and the Slope-Area model indeed reproduced this behavior while other models based on DLA and random networks did not.

Chapter 9 presented a method for describing the geometric complexity of river courses and their scaling behavior. Although rivers have been usually considered as self-similar fractal lines, this chapter presents evidence pointing towards the possibility that river courses are not self-similar but self-affine fractals. The difference is the

anisotropy that exists in the scaling of the oscillations present in the planar form of rivers. The scaling behavior was found to be similar across different basins. The same self-affine fractal analysis was performed in networks simulated with the Slope-Area model. It was observed that by varying the value of the scaling exponent θ between slopes and areas, not only were the vertical profiles of rivers was affected, but the form of the network structure and the tortuosity of individual rivers were as well. It was shown that the self-affine scaling observed in actual rivers was reproduced only when the appropriate value of $\theta=0.5$ was used in the model. This relationship shows the connection between the three-dimensional organization of the basin, the energy optimization at the local level and the planar organization of the river network along with the tortuosity of its individual members.

Instead of looking only at the geometrical form of the network or the individual channels, Chapter 10 analyzes the scaling properties of more physical variables like energy, slope, area and the channel initiation function (a measure of mechanisms known to trigger channelization in the basin) using the multifractal formalism. The interwoven scales in the spatial organization of these variables were shown to have a multifractal distribution which was found to be common across different basins. These multifractal distributions are directly related to multiplicative models that could be developed in geomorphology. Using the multifractal spectrum

of the contributing areas in river basins as an example, the way this spectrum can provide information about the spatial organization of key variables in the river basin, was shown.

In Chapter 11 we analyzed a threshold hypothesis previously used to separate hillslopes and channels in DEMs. Up to this point, most of the analysis was performed using the entire basin landscape, but it is also important for the hydrologist to be able to distinguish whether a pixel in a DEM is a channel or a hillslope because of their different hydrologic properties. The threshold criteria proposed by Willgoose et al. (1991a) in the context of their SIBERIA model of landscape evolution and channel network growth, was studied in DEMs. By looking at the mean slope behavior versus area at the pixel scale, we were able to identify four regions in the slope-area log-log diagram. In increasing order of contributing area these regions can be described as: a region I where diffusive sediment transport processes dominate and hillslope profiles are convex, a region II of concave hillslope nodes, a region III where hillslope and channel nodes with the same contributing area coexist but which can be differentiated using a threshold of the form proposed by Willgoose et al. (1991a), and a region IV of channelized nodes with large contributing areas.

In Chapter 11 we also presented a modified version of the SIBERIA model that shows how the landscape can evolve towards an equilibrium state where the observed slope-area

diagram is reproduced. The differences between this and the original model in terms of sediment transport are discussed in this chapter.

One of the problems of all landscape models presented up to this point was the fact that they tend to aggregate and form a convergent network down to the lowest scales. However, it is clear that at the hillslope scale we find convergent as well as divergent features. Furthermore, it was found that the cumulative distribution of contributing areas, when observed at the pixel scale instead of the link scale, shows a break in its power-law behavior at small scales which would indicate a change in flow organization. A modification to landscape models is proposed in Chapter 12 where contributing areas are calculated using more than one flow direction as opposed to the single-direction constraint in previous models. In this way, diverging hillslopes were simulated in the model and the break in the power-law behavior of contributing area was reproduced.

13.2. Suggestions for Future Research

13.2.1. Three Problems in Channel Networks and the Basin Landscape

In this section we will propose three research problems which are extensions of the results previously presented in this work. The first problem examines growth modes different from the headward growth mechanism present in the SIBERIA and

Slope-Area models. The idea is to examine the implications of various growth modes on the structure of the network and on measures like the cumulative distribution of areas. The second problem looks at the improvement of stochastic branching network models previously proposed in the literature by including some of the network properties found in the present work. Finally, we will examine a possible formulation of a modified version of OCNs where a measure of the cost of construction (and not only operation and maintenance as presented in Chapter 6) is added into the optimization with the goal of including effects from the initial topography. The presentation on these areas of research is in the very preliminary stages of discussion and the results shown should not be considered final.

In the second sub-section more general lines of research and open lines of inquiry that may use some of the results and methodologies presented will be described.

13.2.1.1. Different Growth Modes in Drainage Network Development

Various idealized models of network growth have been presented in the literature. At one extreme we have Horton's (1945) model which suggested that on a steep surface a series of parallel rills will form and, through micropiracy, a network will develop. At the other extreme, we have the headward growth model (Howard, 1971a) where the network is fully developed right up to the edge of the dissected area.

Once the boundary of capture has passed a region, the drainage network is established and, aside from a decrease in elevation, no other changes in flow direction occur. In between these two models we have the one proposed by Glock (1931) where major channels rapidly cut the basin area and then smaller tributaries fill the space. Figure 13.1 (from Schumm et al, 1987) shows schematically the differences between the three models. Glock's mode of growth was observed in the erosion experiments performed at CSU although the stages proposed by him (elongation, elaboration, integration) occurred simultaneously in different parts of the domain (Schumm et al, 1987).

The SIBERIA model developed by Willgoose et al. (1991a) as well as the Slope-Area model introduced in the present work belong to the headward growth class of network development models. Once the network captures a certain area, the flow directions are largely fixed for the rest of the evolution.

The headward growth mode has implications on the overall form of the network that develops in a given area. We have found that, although the simulated networks look reasonable and reproduce common geomorphological statistics, they still appear to be more elongated than the actual networks. This difference can be appreciated in Figures 7.10.a and 7.10.b where a Slope-Area network is grown in the same domain of a basin at the DEM scale.
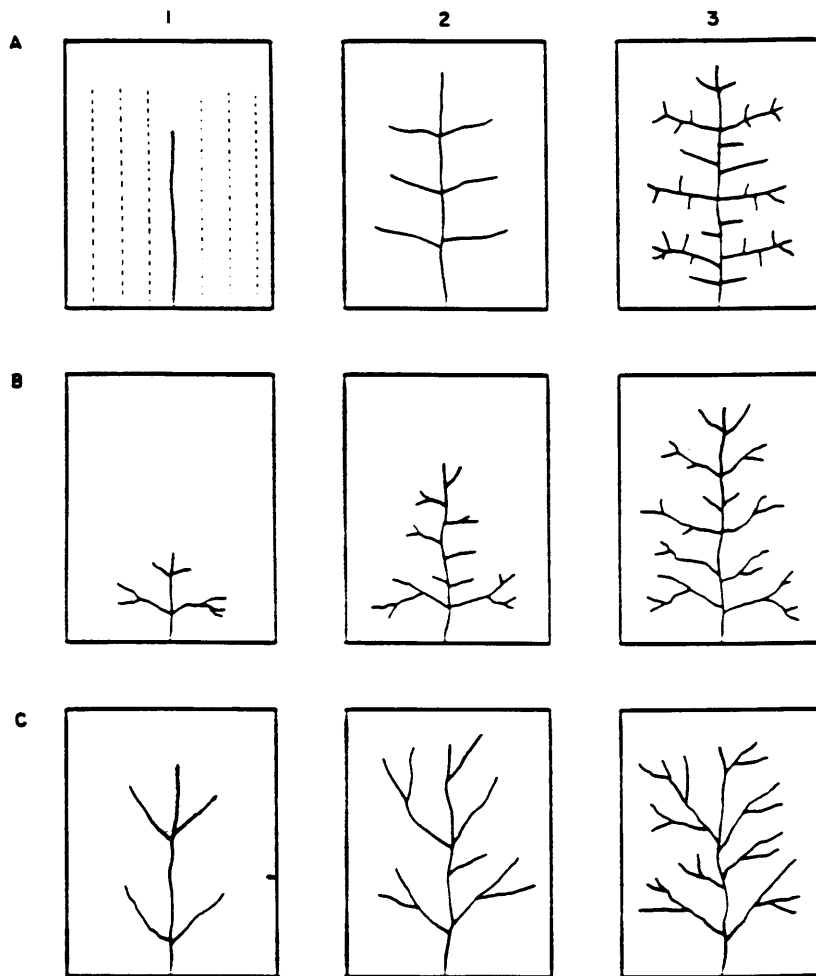
Figure 13.1: Models of drainage network growth. (a) Horton's model, (b) Headward growth model and (c) Glock's model. (From Schumm et al, 1987).

In this section, we will propose a modified version of the Slope-Area model that tries to account for different growth modes by parameterizing the speed to equilibrium of different points in the basin. The difference between the headward growth model and Glock's model is that in the former model large channels, small tributaries and hillslopes pick their flow directions and evolve towards equilibrium at similar speeds. In Glock's model, on the other hand, large channels which have higher erosive power grow much faster than small streams, cut the drainage area quickly and are followed only at a later time by smaller tributaries.

In the original Slope-Area model, every point captured by the network is immediately relaxed to the value of slope that is indicated by the slope-area scaling relationship. Instead it could be possible to add to the captured network only the N_v pixels in the boundary of capture with the largest power (defined as A*S). The slope relaxation would then be applied only to those points that belong to the network. In the next iteration a new set of N_v pixels is added and so on. The purpose of choosing only a set of pixels at the boundary is to represent and enhance, in a very crude way, the growth preference of points with largest erosive power. The goal is to observe the influence of this effect on the network structure. With a very large N_v we get back the original Slope-Area model because every point in the boundary of capture is added to the network.

Figure 13.2 shows the effect on the resulting network (drawn with a threshold area of 20 in a 50x50 domain) as the value of N_v is decreased. We can clearly see how the elongation is reduced in the network, the inter-valley distance is increased and the drainage density (for the same threshold area) is reduced. Not only do the networks look more natural, but also the scaling exponent of the power-law distribution of contributing areas increases to values more in line with those observed, as Figure 13.3 illustrates. Preliminary results indicate that there may even be a small decrease in total energy expenditure at an intermediate value of N_v.

The modified Slope-Area model presented in this section is still a crude discrete representation of different growth models in drainage network development, but it shows that it is possible to improve the current models in order to better simulate networks, reduce their elongation and obtain a value of the scaling slope of the power-law distribution of areas more in line with the actual one. A continuous formulation, based on a better representation of sediment transport and its temporal average, used within the framework of the SIBERIA model would be a better modeling tool for this purpose.
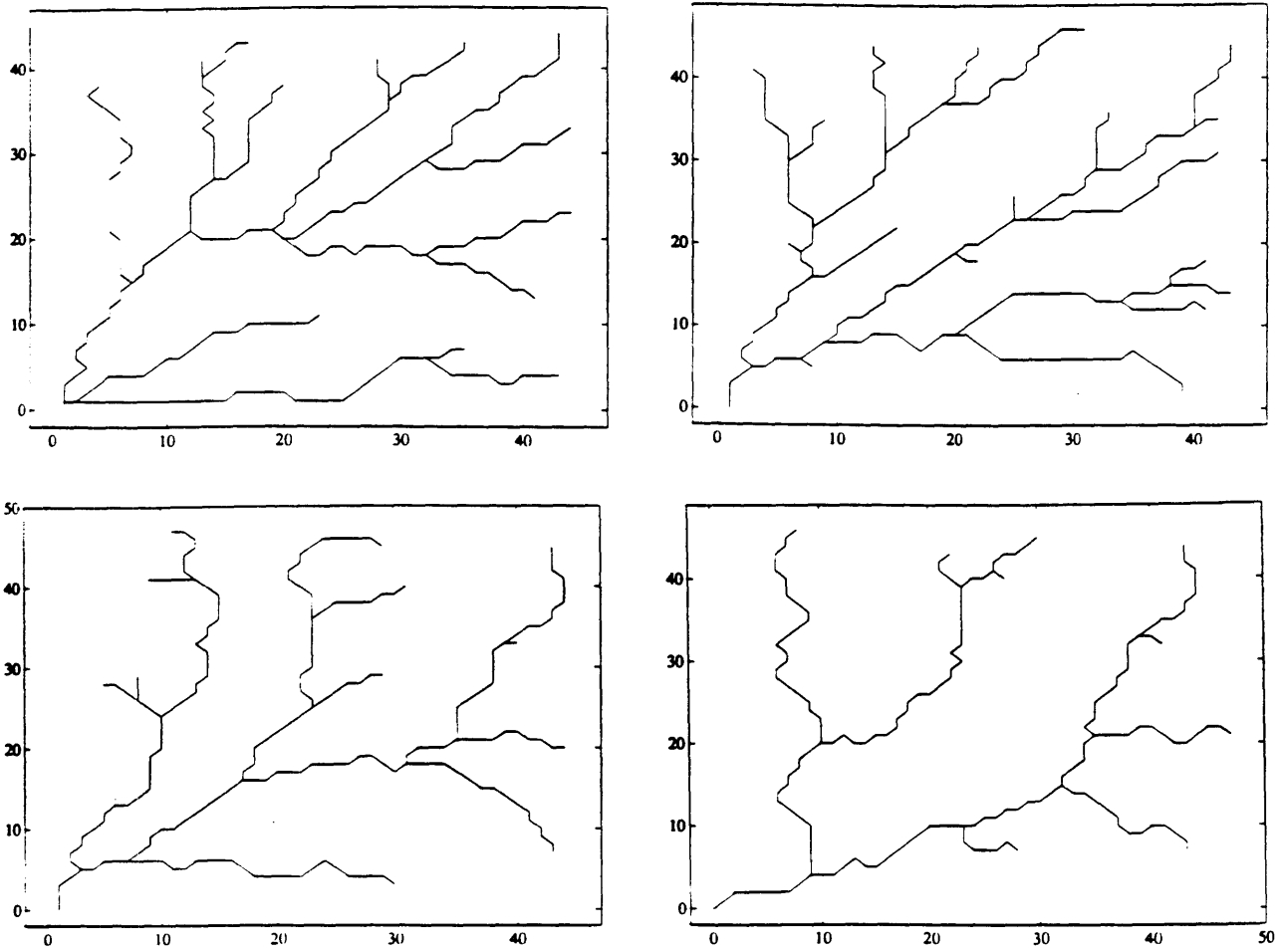
Figure 13.2: Networks generated with the modified version of the Slope-Area model as the value of N_V decreases. The first network is equivalent to the original slope-area model.

234
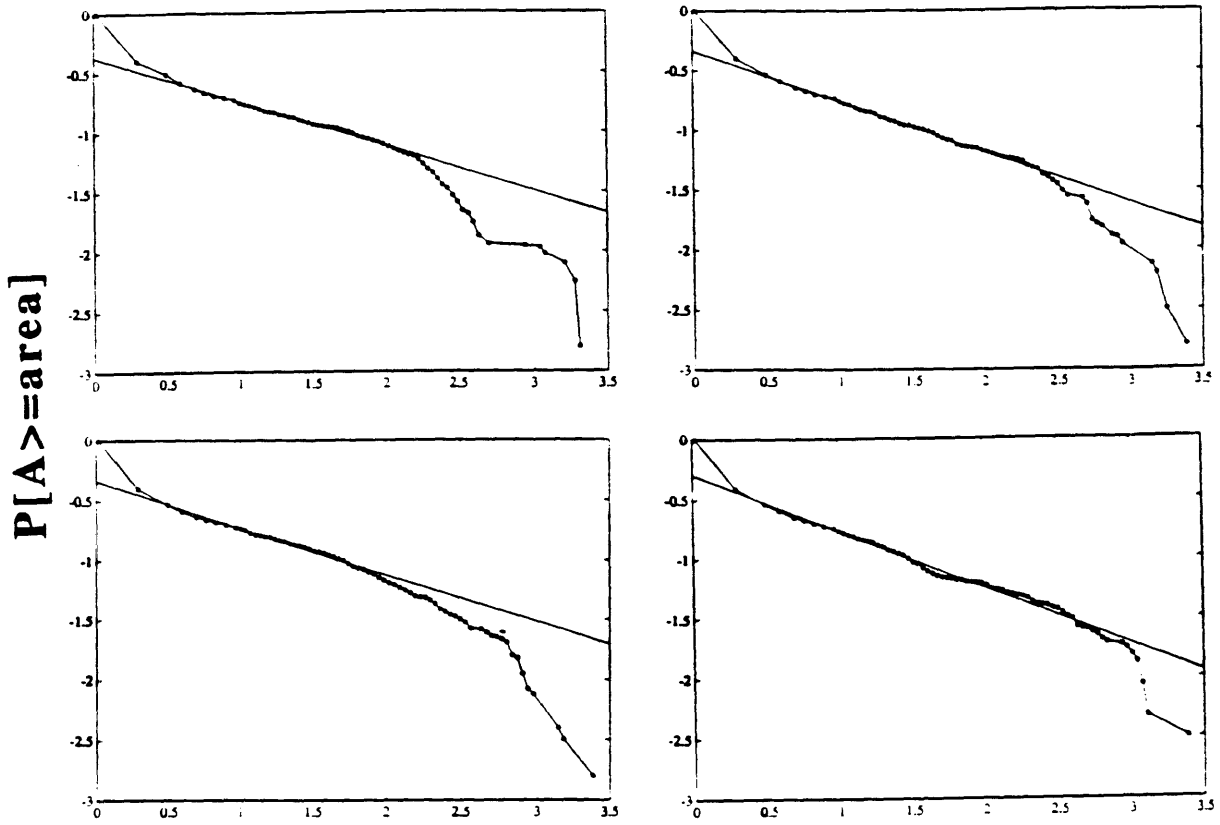
Area

Figure 13.3: Power-law cumulative distribution of contributing areas for the networks shown in Figure 13.2. The scaling slopes are: 0.40, 0.42, 0.44, 0.47.

13.2.1.2 Stochastic Branching Models of Drainage Networks

Hydrologists have recently looked at the ensemble average linear hydrologic response of families of stochastic networks with common properties. This average response can hopefully be used in ungauged basins. The first attempt was the Geomorphologic Instantaneous Unit Hydrograph (GIUH) introduced by Rodriguez-Iturbe and Valdes (1979) and restated by Gupta et al. (1980). The GIUH is the ensemble average of a family of networks that share stream properties like Horton's laws. Gupta and Waymire (1983) argue that the Strahler ordering is a coarse characterization and propose to use links instead of streams. The key tool in their approach is the width function. Mesa (1986) and Troutman and Karlinger (1984, 1985, 1986) studied the ensemble average of the width function for a family of networks coming from a birth and death process.

In the birth and death process, a network is constructed from a single element (a link). Each element can bifurcate or die with equal probability and its length comes from an exponential distribution. The ensemble average can be found by conditioning the family of networks on their magnitude or diameter. The average width function was compared in Mesa (1986) against that of actual basins. The model worked well for small basins but appeared to underpredict the width function for larger basins. However, the comparison was made

between the predicted average of the ensemble and a single basin realization without presenting an estimate of the variance.

Stochastic birth and death processes do not have power-law distribution for properties of their members, (see Figure 13.4 for the cumulative distribution of stream lengths). This differs dramatically from the power-law distribution of actual basins (Tarboton et al, 1988).
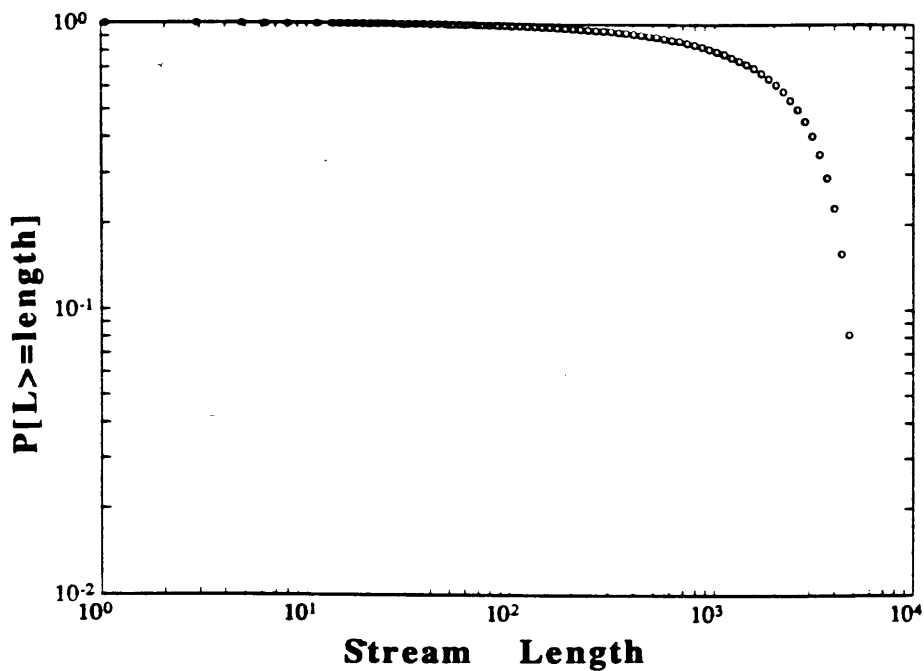
Figure 13.4: Cumulative distribution of stream lengths for a network simulated with a stochastic birth and death model.

DEMs provide a data set with large enough basins to carry ensemble averages of the width function of subbasins with common properties. For example, we can take all subbasins with a given diameter within a basin and find their average width function. Figure 13.5 shows the result for two
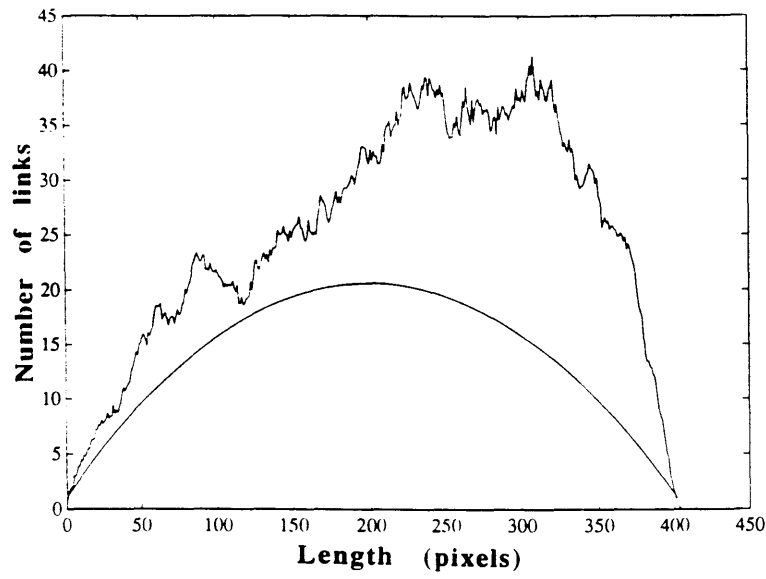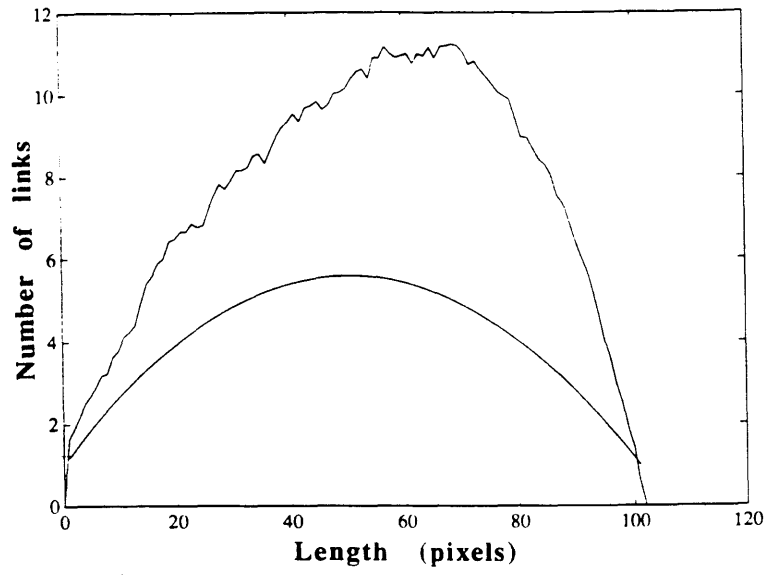
Figure 13.5: Average width function predicted by birth and death model (lower parabola) and actual average calculated from a DEM for subbasins with (a) 100 and (b) 200 pixels.

values of diameter (100 and 400 pixels). The lower parabola in each case is the predicted average width function from the stochastic birth and death model using the appropriate value of the parameters calculated from the DEM data. In this case, we can be more certain of the under-prediction of the model because we are comparing it with an ensemble _average_ of actual basins. The situation is similar with conditioning on magnitude, as shown in Figure 13.6. In this case, we see that the birth and death process tends to overpredict the diameter of the network.
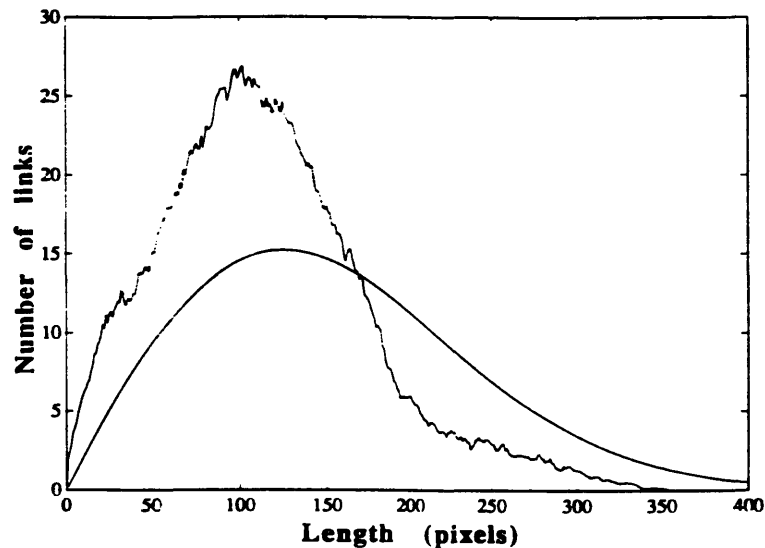
Figure 13.6: Average width function predicted by birth and death model (lower curve) and actual average calculated from a DEM for subbasins with magnitude 300.

It is possible to formulate a stochastic model in which the distribution of areas follows a power-law. The model we propose here as a preliminary idea was originally inspired by multiplicative processes (Menevau and Sreenivasan, 1987). The idea is to use the contributing area as a key variable.

Starting with the total area of the basin at the outlet and moving upward, a portion of the area is broken away from the main channel creating a tributary at each step. The value of the area taken away comes from a distribution that follows a power-law of the form observed in actual networks. The area of the tributary is also constrained to be less or equal to half of the area carried by the main channel. The process is iterated until the entire area is broken away from the main channel. The result is analogous to Figure 10.1 where the sizes of the tributaries draining into the main channel of the Brushy Creek basin were shown. The network is completed by repeating the breaking process in each one of the tributaries until the entire area in each of the channels has been used.

Preliminary results indicate that this power-law break model generates a width function more in line with those of actual basins. This behavior appears to be a consequence of the presence of larger tributaries coming out of the main channel. Stochastic birth and death processes seem to generate networks with very long main channels and small tributaries coming into them. This would explain the under-prediction in the peak and the over-prediction in the diameter observed in Figure 13.6.

The proposed power-law break model is not independent of the multifractal spectrum. Preliminary results indicate that only when the appropriate scaling slope of the power-law

distribution of area is used, is the multifractal spectrum reproduced. Figure 13.7 shows with (+) the actual multifractal spectrum of the contributing areas of tributaries coming into the main channel of the Brushy Creek basin which was already shown in Figure 10.14. The continuous lines show the spectra from simulations coming from the power-law break model with different scaling slopes of the distribution. The actual spectrum is reproduced when the slope is 0.45. The differences on the right-hand side of the spectrum come from hillslope nodes which are not represented in the stochastic model.
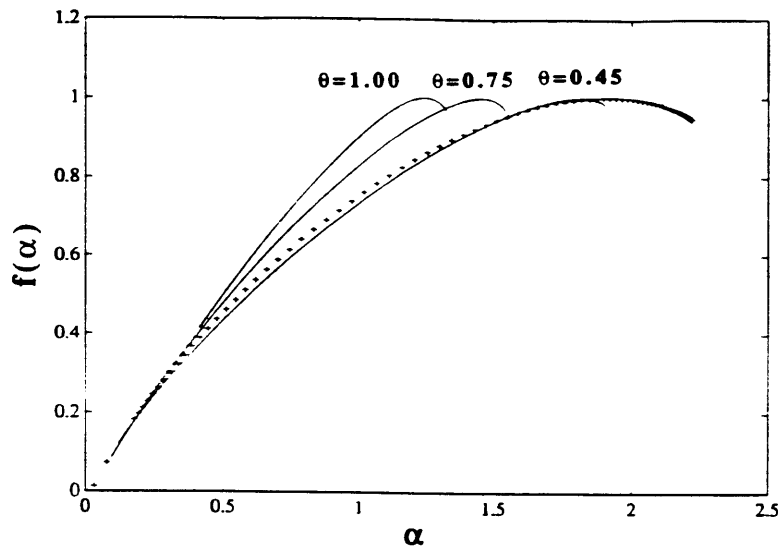
Figure 13.7: Multifractal spectrum of sizes of tributaries coming into main channel of Brushy Creek basin (+). Multifractal spectra of sizes of tributaries from a network simulated with the power-law beak model using different values of the scaling slope of the cumulative distribution of areas (continuous lines).

Many points still remain to be investigated with the power-law break model: how well is it able to reproduce ensemble averages of the width function as well as other properties of channel networks?; how can hillslope effects be included?; how can the networks be tied to a physical space and introduce space-filling constraints? On this last point two papers may be of interest: the work on cis-trans links (James and Krumbein, 1969) and more recent work on levels of sets (Takayasu, 1993) in which a test to study the spatial organization of variables, which appears to be stronger than the multifractal spectrum, is presented.

One advantage of using area as the key variable of the power-law break model is its linkage with many other geomorphic variables. The clearest example is the third dimension which can be introduced through the slope-area relationship and can provide a link to energy organization and measures like the link concentration function.

Finally, it is important to note that the ensemble approach to the hydrologic response of the basin underpredicts the peaks of the individual width functions of the family. This is analogous to the distortion and flattening of a unit hydrograph calculated by averaging ordinates of a given time. Other measures (like peak, size, time to peak, etc.) should also be considered in the ensemble analysis.

13.2.1.3. OCNs with a Modified Cost Function

The three principles of energy expenditure in river basins originally proposed by Rodriguez-Iturbe et al. (1992b) included energy costs for "operation" and "maintenance" of the channel network. However, no "construction" cost was included. This implies that no matter what the initial topography is, the network would carve its way to an absolute optimal state. Nevertheless, it is probable that the network prefers to make a trade-off in its development. Absolute optimality may be constrained as the network encounters areas of very high elevation or non-easily erodible material. It might be interesting to study these effects on OCNs as a possible explanation of some sub-optimal local features observed in actual basins.

Another consideration in this area of research is the fact that OCNs have straight channels because if no construction costs are included, it is optimal to do so. However, we have shown in Chapter 9 that this is not the case and actual river courses are self-affine curves. A possible way of reconciling these two observations may be to include a measure that accounts for inhomogeneities in topography or material. Furthermore, the relationship between θ (the scaling exponent between slopes and area which can be derived from the local energy principles) and the self-affine character of river courses indicate that such reconciliation may be feasible.

A first attempt to include construction costs might be to include a weighted term in the energy expenditure expression. As shown in Chapter 7, the energy expenditure in the original OCN formulation can also be seen as the sum of elevations $k\Sigma_i Z_i$. The cost of excavating down to this elevation field may be crudely parameterized as $\gamma\Sigma_i Z^e_i$ where $Z^e_i = Z^o_i - Z_i$ is the material excavated at node i and Z^o_i is the original elevation at that point.

It is then possible to study the effects of different values of γ in the modified expression for total energy $k\Sigma_i Z_i + \gamma\Sigma_i Z^e_i$. In this case, the optimization would use not only the area to be drained but also the original topography (in order to calculate the excavation costs).

As the value of γ compared to k is reduced, the network tends more and more towards the original OCN organization because minimizing operation costs is then more important than minimizing construction costs. Figure 13.8 shows a sequence of optimal networks with decreasing values of γ from $\gamma=k$ (in which case construction and operation costs are the same) down to $\gamma=0$ (the original OCN). All simulations were started with a random elevation field. As an initial network for the optimal search algorithm we used the network shown in Figure 13.8.a. The lower edge is open.

In the first case of Figure 13.8, given that $\gamma=k$, any network has the same cost $k\Sigma_i(Z_i+Z^e_i) = k\Sigma_i Z^o_i$ so the search algorithm stays in the initial condition. As γ goes down, the
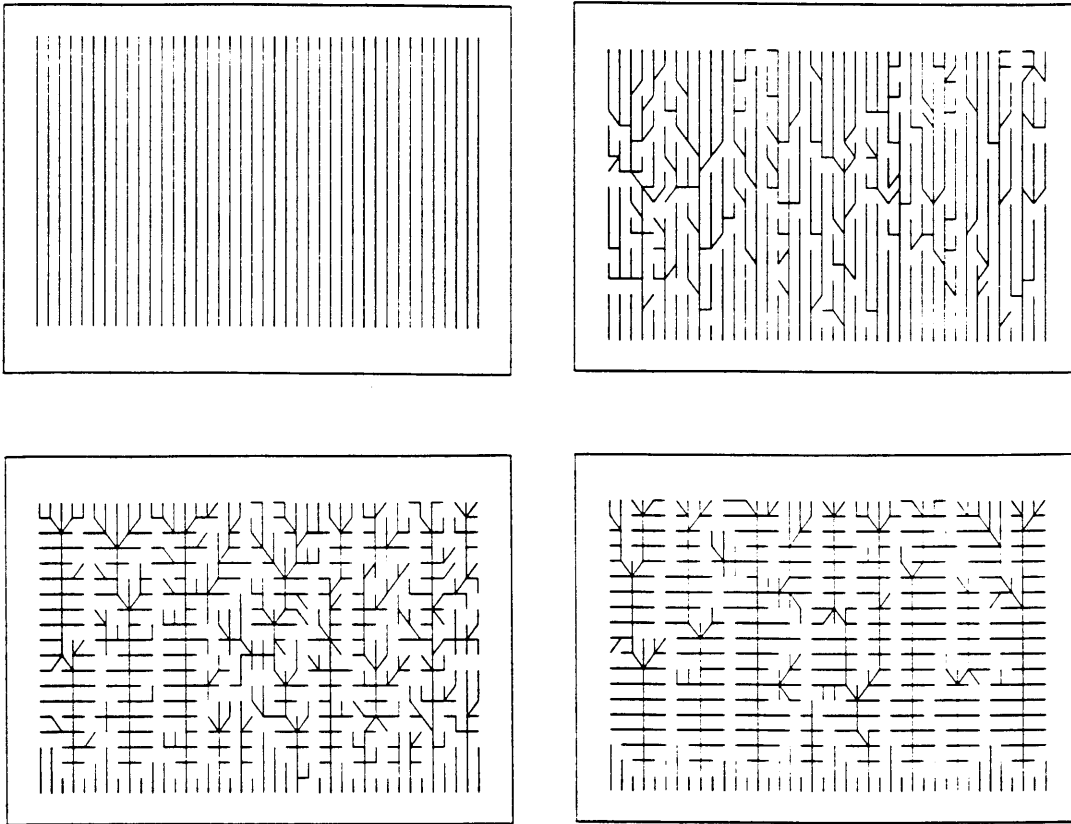
Figure 13.8: Optimal networks with construction costs included. The value of γ is decreased from $\gamma=k$ to $\gamma=0$.

network starts making a trade-off between construction and operation costs. Figure 13.8 shows that sequence.

Other formulations could be more realistic but this simple model illustrates some of the research questions that might be studied.

13.2.2. Other Research Questions in River Networks

In this section we will discuss some research avenues which are still not as clearly defined as those formulated in previous sections. Most of these avenues come from unanswered

questions left by the present work as well as improvements on many of the concepts presented.

The characterization of the basin landscape and the channel network should be improved with new and stronger measures. This work has taken some small steps in this direction, moving away from Horton's laws which are a coarse topological measure. Every new measure usually requires a modeling improvement in order to match these observations, as has been shown in the present work.

Further understanding of the contributing area mapping that assigns to each node the area draining through it is very important, especially for analytical work. Given that the contributing area may be used as a surrogate for flow, which is a key variable in the evolution of the landscape and the organization of the basin, it is necessary to have a good handle on the area mapping. Three problems that require the ability to understand and work with the area mapping are:

1) Understanding of screening effects in the growth of the network. The relationship with growth potential (probably in the form of the channel initiation function discussed in Chapter 11) is essential. Analogous research questions in the context of DLA are studied in Halsey and Leibig (1992).

2) Formulation of a theoretical relationship between θ and the tortuosity of river courses measured through their self-affine scaling. This problem as well as problem (1), may

be tackled by looking at only a small region around the boundary of capture, which is where all the action is occurring in headward growth models, as discussed in Section 13.2.1.1. By analyzing how randomness in topography (or inhomogeneities in the terrain) are processed by the evolution dynamics and transformed into a drainage structure, a new understanding of network growth may be developed.

3) Theoretical prediction of the scaling slope of the power-law distribution of areas. One of the very few SOC systems that has been studied analytically is Scheidegger's stochastic river model because of its simplicity. To move to higher-order models like the Slope-Area model or other models of landscape evolution and to be able to predict the SOC exponents is an interesting theoretical problem.

A great portion of the analysis presented in this work deals with the observed mean behavior of different variables. One example is the slope-area analysis, where only the average slope for groups of pixels with the same contributing area are observed. It might be important to consider the entire distribution of slopes. This study could lead to better understanding of the nature of randomness in the basin, improved landscape models and maybe a better modeling of runoff production mechanisms like saturation from below, which depend on both slopes and areas. Some work has been done in this direction (Tarboton et al, 1989a). To visually illustrate the importance of the random distribution of

slopes, Figure 13.9 shows the profile of the main channel of the Racoon Creek basin. The profile is very reminiscent of the Devil's staircase (Feder, 1988) related to multifractal processes and multifractal distributions.
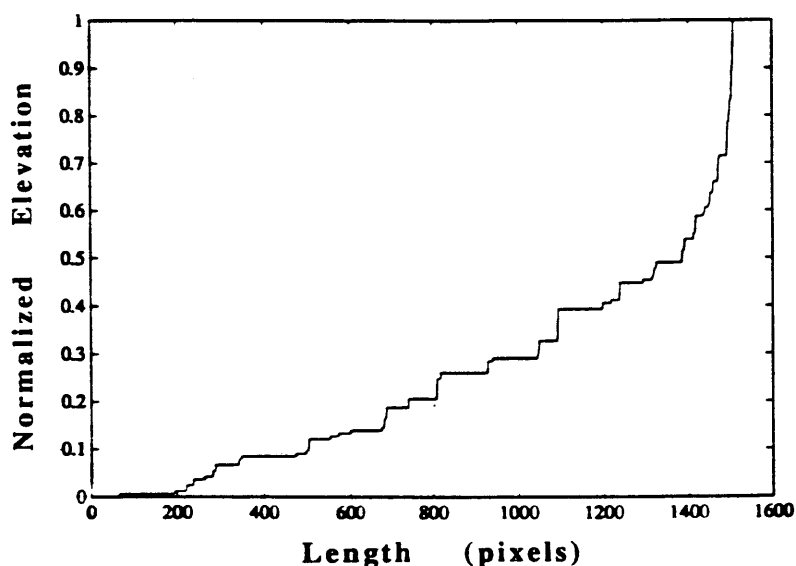
Figure 13.9: Normalized stream profile of main channel in Racoon Creek basin.

The discussion between different sediment transport modes (point-to-point or direct removal as described in Chapter 11) is still open. We have concentrated in this work only on the properties of equilibrium landscapes in which no major differences have been observed between the original and the modified SIBERIA model, with the exception of a little more elongation in the latter model. Stronger measures are needed to understand these differences in the final network. However, the greatest difference between both models resides in the evolution process. They get to similar equilibrium landscapes but through different paths. Further study of the

evolution of the landscape, a revision of the dynamic equilibrium hypothesis and field verification might be required in this line of research.

Two other problems in landscape modeling are the inclusion of small and medium-scale catastrophic events and the modeling of the widening of valleys. Given the restriction of single-flow direction in our current models, floods that move large amounts of sediment and alter significantly the local structure of the network cannot be modeled. This effect may be another way in which local defects are corrected in the search of the basin for states with lower energy expenditure, in the same spirit as the experiments shown in Section 7.5. The single-flow direction also does not allow the widening of valleys observed in actual basins. This process may require, however, the inclusion of different sediment transport mechanisms.

Further understanding and a better representation of the mixed convergent/divergent features at the hillslope scale are required. By locally adjusting analytical surfaces to DEMs it may be possible to perform second-order analysis and study the spatial organization of the convergent and divergent hillslopes and their interlocking behavior (Papo and Gelbman, 1984). Furthermore, in the modeling of landscapes one should notice that runoff production in convergent hillslopes is very different from runoff production in divergent hillslopes (Young and Mutchler

(1969), Dietrich et al. (1992)). This behavior has clear implications for the evolution of the landscape, which might require a revision in the way hillslope evolution is treated in Chapter 12.

Most of the landscape evolution work at the hillslope scale has been in 1-D form and very few researchers have looked at the three-dimensional structure and the convergent/divergent features. The way in which these hillslopes evolve (along with the ease of measuring their evolution in controlled experiments because of their size) may be a feasible avenue of research. The linkage with the channel as boundary condition and the corresponding interactions should not be set aside.

Chapter 12 showed a possible way of inferring the independent values of the parameters m and n of the sediment transport equation in the landscape evolution model by looking at the mixed convergent/divergent nature of hillslopes. Previously, only the ratio m/n was available from the scaling parameter θ between slopes and areas. The results in Chapter 12 are an example of how processes and parameter values might be inferred from form. Another problem still open is the coefficient of the slope-area relationship in equation (11.11) where tectonics, rainfall and the multiplicative factor of the sediment transport expression are joined in a single ratio. How to infer their independent

values from the form of the landscape using DEM data is still an open question.

Finally, field verification of many of the underlying hypotheses of sediment transport, landscape evolution, network adjustment, channel head location and randomness are required.

All of the proposed avenues of research in this chapter can be encompassed in six areas: the relationship between form and processes, the hydrologic response of the basin, scales in the basin (hillslope versus channel), runoff production, field verification and the study of the river basin in the context of non-linear dynamical systems. This work has barely touched upon some of these areas and many research questions remain unexplored.

References

Abrahams, A.D. Channel networks: a geomorphological perspective. Water Resources Research. 20(2):161-168, 1984.

Ahnert, F. Brief description of a comprehensive three-dimensional process-response model for landform development. Zeitschrift fur Geomorphologie.N.F. Supplement. 25:29-49, 1976.

Alstrom, P. Self-organized criticality and fractal growth. Physical Review A. 41(12):7049-7052, 1990.

Alstrom, P., P.A. Trunfio and H.E. Stanley. Spatiotemporal fluctuations in growth phenomena: Dynamical phases and 1/f noise. Physical Review A. 41(6):3403-3406, 1990.

Arneodo, A., A. Argoul, E. Bacry, J.F. Muzy, and M. Tabard. Golden mean arithmetic in the fractal branching of diffusion-limited aggregates. Physical Review Letters 68(23):3456-3459, 1992.

Bak, P. and K. Chen Self-organized criticality. Scientific American. 264(1):46-53, 1991.

Bak, P. and C. Tang Earthquakes as a self-organized critical phenomenon. Journal of Geophysical Research. 94:15635-15637, 1989.

Bak, P., C. Tang and K. Wiesenfeld. Self-organized criticality: An explanation of 1/f noise. Physical Review Letters. 59:381-384, 1987.

Bak, P., C. Tang and K. Wiesenfeld. Self-organized criticality. Physical Review A. 38:364-374, 1988.

Baker, V.R. Geological fluvial geomorphology. Bulletin, Geological Society of America. 100:1157-1167, 1988.

Ball, R.C. Diffusion-limited aggregation and its response to anisotropy. Physica A. 140:62-69, 1986.

Ball, R.C. and M. Blunt. Dynamical screening in multifractal growth. Physical Review A. 41:582-589, 1990.

Band, L.E. Topographic partition of watersheds with digital elevation models. Water Resources Research. 22(1):15-24, 1986.

Band, L.E. A terrain-based watershed information system. Hydrologic Processes. 3:151-162, 1989.

Berge, P., Y. Pomeau and C. Vidal. Order within Chaos Wiley, France, 1984.

Brush, L.M. Drainage basins, channels and flow characteristics of selected streams in central Pennsylvania, US Geological Survey Professional Paper 282-F, 1961.

Buldyrev, S.V., A.-L. Barabasi, F. Caserta, S. Havlin, H.E. Stanley and T. Vicsek. Anomalous interface roughening in porous media: Experiment and models. Physical Review A. 45(12):8313-8316, 1992.

Cabral, M. and S.J. Burges. DEMON: a new method for the automated extraction of contributing areas and drainage networks from rectangular DEMs. EOS. 73(43):202, 1992.

Calver, A., M.J. Kirkby and D.R. Weyman. Modeling hillslope and channel flows. IN: R.J. Chorley, ed. Spatial Analysis in Geomorphology. London: Methuen, pp.197-218, 1972

Carson, M.A. and M.J. Kirkby. Hillslope Form and Processes. Cambridge University Press, 1972.

Chhabra, A.B. and R.V. Jensen. Direct determination of the $f(\alpha)$ singularity spectrum. Physical Review Letters. 62(12):1327-1330, 1989.

Chhabra, A.B., R.V. Jensen and K.R. Sreenivasan Extraction of underlying multiplicative processes from multifractals via the thermodynamic formalism. Physical Review A. 40(8):4593-4611, 1989.

Chorley, R.J., D.E.G. Malm and H.A. Pogorzelski. A new standard for estimating drainage basin shape. American Journal of Science 255:138-141, 1957.

Cordova, J.R., I. Rodriguez-Iturbe and P. Vaca. On the development of drainage networks, in Recent developments in the explanation and prediction of erosion and sediment yield, ed. by D.E. Wallings, pp.19-30, Exeter, U.K., 1982.

Culling, W.E.H. and M. Datko. The fractal geometry of the soil covered landscape. Earth Surface Processes and Landforms. 12:369-385, 1987.

Derrida, B. and V. Hakim. Needle models of Laplacian growth. Physical Review A. 45(12):8759-8765, 1992.

Dhar, D. and R. Ramaswany. Exactly solved model of self-organized critical phenomena. Physical Review Letters. 63:1659-1662, 1989.

Dietrich, W.E., C.J. Wilson, D.R. Montgomery, J. McKean and R. Bauer. Erosion thresholds and land surface morphology. Geology. 20:675-679, 1992.

Dunne, T. and B.A. Aubry. Evaluation of Horton's theory of sheetwash and rill erosion on the basis of field experiments, in Hillslope Processes ed. by A.D. Abrahams, pp.31-53, Allen and Umwin, Boston, 1986.

Eagleson, P.S., Dynamic Hydrology, Mc Graw Hill, New York, 1970.

Fairfield, J. and P. Leymarie. Drainage networks from digital elevation models. Water Resources Research. 27(5):709-717, 1991.

Family, F. and T. Vicsek. Scaling of the active zone in the Eden process on percolation networks and the ballistic deposition model. Journal of Physics A. 18:L75-L81, 1985.

Feder, J. Fractals. Plenum Press, New York, 1988.

Feuerecker, G., A. Hubler and E. Luscher. Pattern formation of metallic particles in electric and magnetic-fields. Biological Cybernetics. 56(2/3):151-154, 1987.

Flint, J.J. Stream gradient as a function of order, magnitude and discharge. Water Resources Research 10(5):969-973, 1974.

Freeman, T.G. Calculating catchment area with divergent flow based on a regular grid. Computers and Geosciences. 17(3):413-422, 1991.

Frisch, U. and G. Parisi, Fully developed turbulence and intermittency. In: M. Ghil, R. Benzi and G. Parisi (Eds.) Turbulence and Predictability in Geophysical Fluid Dynamics. North Holland, Amsterdam, pp.71-88, 1985.

Glock, W.S. The development of drainage systems: a synoptic view. Geographical Review. 21:475-482, 1931.

Grassberger, P. and I. Procaccia. Characterization of strange attractors. Physical Review Letters. 50:346-349, 1983a.

Grassberger, P. and I. Procaccia. Measuring the strangeness of strange attractors. Physica D. 9:189-208, 1983b.

Grey, D.M., Interrelationships of watershed characteristics, Journal of Geophysical Research 66:1215-1223, 1961.

Gupta, V.K. and E. Waymire. On the formulation of an analytical approach to hydrologic response and similarity at the basin scale. Journal of Hydrology. 65:95-123, 1983.

Gupta, V.K. and E. Waymire. Statistical self-similarity in river networks parameterized by elevation. Water Resources Research. 25(3):463-476, 1989.

Gupta, V.K., E. Waymire and C.T. Wang. Representation of an instantaneous unit hydrograph from geomorphology. Water Resources Research. 16(5):855-862, 1980.

Hack, J.T., Studies of longitudinal stream profiles in Virginia and Maryland, U.S. Geological Survey Professional Paper. 294-B: 45-97, 1957.

Halsey, T.C., M.H. Jensen, L.P. Kadanoff, I. Procaccia and B.I. Shraiman. Fractal measures and their singularities: characterization of strange sets. Physical Review A. 333(2):1141-1151, 1986.

Halsey, T.C. and M. Leibig. Theory of branched growth. Physical Revuew A. 46(12):7793-7809, 1992.

Henderson, P.M. Open Channel Flow. McMillan, New York, 1966.

Hjelmfelt, A.T., Fractals and the river-length catchment area ratio. Water Resources Bulletin. 24:2455-459, 1988.

Holden, A.V. Chaos. Princeton University Press, Princeton, 1986.

Horton, R.E. Drainage basin characteristics. Transactions American Geophysical Union 13:350-361, 1932.

Horton, R.E. Erosional development of streams and their drainage basins; hydrophysical approach to quantitative morphology. Geological Society of America Bulletin. 56:275-370, 1945.

Howard, A.D. Simulation of stream networks by headward growth and branching. Geographical Analysis. 3:29-50, 1971a.

Howard, A.D. Optimal angles of stream junction: geometric stability to capture and minimum power criteria. Water Resources Research. 7:863-873, 1971b.

Howard, A.D.   Theoretical model of optimal drainage networks.   Water Resources Research   26(9):2107-2117, 1990.

Huber, G.   Scheidegger's rivers, Takayasu's aggregates and continued fractions.   Physica A.   170:463-470, 1991.

Ijjasz-Vasquez, E.J., R.L. Bras and I. Rodriguez-Iturbe. Self-organized criticality in river basins.   EOS. 72(44):202, 1991.

Ijjasz-Vasquez, E.J., R.L. Bras, I. Rodriguez-Iturbe,   On the multifractal characterization of river basins. Geomorphology.   5:297-310, 1992a.

Ijjasz-Vasquez, E.J., R.L. Bras and G. Moglen.   Sensitivity of a basin evolution model to the nature of runoff production and to initial conditions.   Water Resources Research.   28(10):2733-2741, 1992b.

Ijjasz-Vasquez, E.J., R.L. Bras, I. Rodriguez-Iturbe, R. Rigon and A. Rinaldo.   Are river basins optimal channel networks?   Advances in Water Resources.   16:69-79, 1993a.

Ijjasz-Vasquez, E.J., R.L. Bras and I. Rodriguez-Iturbe. Hack's relation and optimal channel networks.   Geophysical Research Letters.   20(15):1583-1586, 1993b.

Ijjasz-Vasquez, E.J., R.L. Bras and I. Rodriguez-Iturbe. Self-affine scaling of fractal river courses and basin boundaries.   Submitted to Physica A.   1993c.

Ijjasz-Vasquez, E.J., R.L. Bras and I. Rodriguez-Iturbe. Implications of minimal energy expenditure on the shape of river basins.   Submitted to Journal of Physics A, 1993d.

James, W.R. and W.C.K. Krumbein.   Frequency distribution of stream link lengths.   Journal of Geology.   77:544-565, 1969.

Jenson, S.K. and J.O. Domingue.   Extracting topographic structure from digital elevation data for geographic information system analysis.   Photogrammetric Engineering and Remote Sensing.   54(11):1593-1600, 1988.

Johnsons, D.   More approaches on the travelling salesman guide.   Nature.   330(10):525, 1987.

Kardar, M., G. Parisi and Y.-C. Zhang.   Dynamic scaling of growing interfaces.   Physical Review Letters 56(9):889-892, 1986.

Kardar, M. and Y.-C. Zhang   Scaling of directed polymers in random media. Physical Review Letters 58(20):2087-2090, 1987.

Kennedy, B.A.   Hutton to Horton: views of sequence, progression and equilibrium in geomorphology. Geomorphology.   5:231-250, 1992.

Kirkby, M.J.   Hillslope process-response models based on the continuity equation, in Slopes, Forms and Processes, Institute of British Geographers. Special Publication No. 3, 1971.

Kirkby, M.J.   Tests of the random network model and its application to basin hydrology.   Earth Surface Processes. 1:197-212, 1976.

Kondoh, H., Y. Fukuda and M. Matsushita. Self-affinity of Scheidegger's river patterns. Journal of the Physical Society of Japan. 56(6):1913-1915, 1987.

Kramer, S. and M. Marder. Evolution of river networks. Physical Review Letters. 68:205-208, 1992.

La Barbera, P. and R. Rosso. On the fractal dimension of stream networks. Water Resources Research 25(4):735-741, 1989.

Lee, J., S. Havlin, H.E. Stanley and J.E. Kiefer. Hierarchical model of the multifractality of diffusion-limited aggregation. Physical Review A. 42(8):4832-4837, 1990.

Lee, J., P.K. Snyder and P.F. Fisher. Modeling the effect of data errors on feature extraction from digital elevation models. Photogrammetric Engineering and Remote Sensing. 58(10):1461-1467, 1992.

Leopold, L.B. and W.L. Langbein. The concept of entropy in landscape evolution. U.S. Geologic Survey Professional Paper 500-A, 1962.

Leopold, L.B. and T. Maddock. The hydraulic geometry of stream channels and other physiographic implications. U.S. Geological Survey Professional Paper 252, 1953.

Leopold, L.B. and J.P. Miller. Ephemeral streams-hydraulic factor and their relation to the drainage net. U.S. Geological Survey Professional Paper 282-A, 1956

Leopold, L.B., M.G. Wolman and J.P. Miller. Fluvial Processes in Geomorphology. W.H.Freeman, New York, 1964.

Lin, S. Computer solutions for the traveling salesman problem. Bell Systems. tech. J. 44, 2245-2269, 1965.

Liu, T. Fractal structure and properties of stream networks. Water Resources. Res. 28(11):2981-2988,1992.

Loewenherz, D.S. Stability and the initiation of channelized surface drainage: a reassessment of short wavelength limit. Journal of Geophysical Research 96(B5):8453-8464, 1991.

Luke, J.C. Special solutions for nonlinear erosion problems. Journal of Geophysical Research. 79:4035-4040, 1974.

Mackin, J.H. Concept of the graded river. Bulletin, Geological Society of America. 59:463-512, 1948.

Malinverno, A. A simple method to estimate the fractal dimension of a self-affine series. Geophysical Research Letters 17(11):1953-1956, 1990.

Mandelbrot, B.B. Fractals: Form, Chance and Dimension. W.H. Freeman, New York, 1977.

Mandelbrot, B.B., The Fractal Geometry of Nature. W.H. Freeman, New York, 1982.

Mandelbrot, B.B. An introduction to multifractal distribution function. In: H.E. Stanley and N. Ostrowsky (Eds.) Fluctuations and Pattern Formation, Kluwer, Dordrecht-Boston, pp.345-360, 1988.

Mandelbrot, B.B. Multifractal measures, especially for the geophysicist. Pure and Applied Geophysics. 131(1/2):5-42, 1989.

Mandelbrot, B.B. and C.J.G. Evertsz. The potential distribution around growing fractal clusters. Nature. 348:143-146, 1990.

Mandelbrot, B.B. and J.W. Van Ness Fractional Brownian motion, fractional noises and applications. SIAM Review 10:442-437, 1968.

Mandelbrot, B.B. and J.R. Wallis. Noah, Joseph and operational hydrology. Water Resources Research. 4:909-918, 1968

Mark, D.M. Automated detection of drainage networks from digital elevation models. Cartographica. 21:168-178, 1984.

Mark, D.M. and P.B. Aronson. Scale-dependent fractal dimension of topographic surfaces: an empirical investigation with applications in geomorphology and computer imaging. Mathematical Geology. 16(7):671-683, 1984.

Matsushita, M. and S. Ouchi. On the self-affinity of various curves. Physica D. 38:246-251, 1989.

Matsushita, M., S. Ouchi and K. Honda. On the fractal structure and statistics of contour lines on a self-affine surface. Journal of the Physical Society of Japan. 60(7):2109-2112, 1991.

McCauley, H.L. Introduction to multifractals in dynamical systems theory and fully developed turbulence. Physics Reports. 189(5):225-266, 1990.

Meakin, P. The growth of self-affine fractal structures. Physica D. 38:252-259, 1989.

Meakin, P. An Eden model for the growth of adaptive networks. Physica A 179:167-178, 1991a.

Meakin, P. Fractal aggregates in Geophysics. Reviews of Geophysics. 29:317-354, 1991b.

Meakin, P., J. Feder and T. Jossang. Simple statistical models for river networks. Physica A. 176:409-429, 1991.

Menevau, C. and K.R. Sreenivasan. Simple multifractal cascade model for fully developed turbulence. Physical Review Letters. 59(13):1424-1427, 1987.

Menevau, C. and K.R. Sreenivasan. Measurement of $f(\alpha)$ from scaling of histograms and applications to dynamic systems and fully developed turbulence. Physics Letters. 137A:103-112, 1989.

Menevau, C., K.R. Sreenivasan, P. Kailasnath and M.S. Fan. Joint multifractal measures: theory and applications to turbulence. Physical Review A. 41(2):894-913, 1990.

Merte, B., P. Gaitzsch, M. Fritzenwanger, W. Kropf, A. Hubler and E. Luscher. Stable stationary dendritic patterns with minimal dissipation. Helvetica Physica Acta. 61(1/2):76-79, 1988.

Mesa, O.J. Analysis of channel networks parameterized by elevation. University of Mississippi, PhD dissertation, Dept. of Civil Engineering, 1986.

Miller, V.C. A quantitative geomorphic study of drainage basin characteristics in the Clinch Mountain area, Virginia and Tennessee: Dept. of Geology, Columbia Univ., New York, Tech. Report no. 3, Office of Naval Research, 1953.

Mock, S.J. A classification of channel links in stream networks. Water Resources Research. 7:1558-1566, 1971.

Montgomery, D.R. and W.E. Dietrich. Source areas, drainage density and channel initiation. Water Resources Research. 25:1907-1918, 1988.

Montgomery, D.R. and W.E. Dietrich. Channel initiation and the problem of landscape scale. Science. 255:826-830, 1992.

Moore, I.D., G.J. Burch and D.H. Mackenzie. Topographic effects on the distribution of surface soil water and location of ephemeral gullies. American Society of Agricultural Engineers. Transactions. 31:1098-1107, 1988.

Moore, I.D., E.M. O'loughlin and G.J. Burch. A contour based topographic model for hydrological and ecological applications. Earth Surface Processes and Landforms. 13:305-320, 1988.

Morisawa, M.E. Measurement of drainage-basin outline form. Journal of Geology 66:587-591, 1958.

Morisawa, M. Development of quantitative geomorphology. Geological Society of America, Centennial Special Volume 1: 79-107, 1985.

Morisawa, M. The Geological Society of America Bulletin and the development of quantitative geomorphology. Bulletin, Geological Society of America. 100:1016-1022, 1988.

Morris, D.G., and R.G. Heerdegen. Automatically derived catchment boundaries and channel networks and their hydrological applications. Geomorphology. 1:131-141, 1988.

Murray, C.D. The physiological principle of minimum work, I, The vascular system and the cost of blood volume. Proceedings National Academy of Sciences. USA. 12:207-214, 1926.

National Research Council, Committee on Opportunities in the Hydrologic Sciences. Opportunities in the Hydrologic Sciences. National Academy Press, Washington D.C., 1991.

Newman, W.I. and D.L. Turcotte. Cascade model for fluvial geomorphology. Geophysics Journal International. 100:433-439, 1990.

Nikora, V.I. Fractal structures of river planar forms. Water Resources Research 27(6):1327-1333, 1991.

O'Callaghan, J.F. and D.M.Mark. The extraction of drainage networks from digital elevation data. Computer Vision and Graphics Image Processing. 28:323-344, 1984.

Palacios-Velez, O.L. and B. Cuevas-Renaud. Automated river-course, ridge and basin delineation from digital elevation data. Journal of Hydrology. 86:299-314, 1986.

Paladin, G. and A. Vulpiani. Anomalous scaling laws in multifractal objects. Physics Reports. 156(4):147-225, 1987.

Papo, H.B. and E. Gelbman. Digital terrain models for slopes and curvatures. Photogrammetric Engineering and Remote Sensing. 50(6):695-701, 1984.

Parker, R.S. Experimental study of drainage basin evolution and its hydrologic implications. PhD thesis, Colorado State University, Fort Collins, Colorado, 1977.

Peitgen, H.-O. and D. Saupe. The Science of Fractal Images. Springer-Verlag, New York, 1988.

Perlsman, E. and M. Schwartz. Ultrametric tree structure in the directed polymer problem. Europhysics Letters 17(1):11-16, 1992.

Peucker, T.K. and D.H. Douglas. Detection of surface-specific points by local parallel processing of discrete terrain elevation data. Computer Graphics and Image Processing. 4:375-387, 1975.

Prasad, R.R. and K.R. Sreenivasan Quantitative three-dimensional imaging and the structure of passive scalar fields in fully turbulent flows. Journal of Fluid Mechanics. 216:1-34, 1990.

Prasad, R.R. C. Menevau and K.R. Sreenivasan. Multifractal nature of the dissipation field of passive scalars in fully turbulent flows. Physical Review Letters. 61(1):74-77, 1988.

Procaccia, I. and R. Zeitak. Shape of fractal growth patterns: exactly solvable models and stability considerations. Physical Review Letters 60(24):2511-2514, 1988.

Quinn, P., K. Beven, P. Chevallier and O. Planchon. The prediction of hillslope flow paths for distributed hydrological modelling using digital terrain models. Hydrological Processes. 5:59-79, 1991.

Rinaldo, A., I. Rodriguez-Iturbe, R. Rigon, R.L. Bras, E.J. Ijjasz-Vasquez, and A. Marani, Minimum energy and fractal structures of drainage networks. Water Resources Research. 28:2183-2195, 1992.

Rinaldo, A., I. Rodriguez-Iturbe, R. Rigon, E.J. Ijjasz-Vasquez, and R.L. Bras, Self-organized fractal river networks Physical Review Letters. 70:822-825, 1993.

Rigon, R., A. Rinaldo, I. Rodriguez-Iturbe, R.L. Bras, and E.J. Ijjasz-Vasquez. Optimal Channel Networks: A framework for the study of river basin morphology. Water Resources Research. 29:1635-1646, 1993.

Ritter, D.F. Landscape analysis and the search for geomorphic unity. Bulletin, Geological Society of America. 100:160-171, 1988.

Robert, A. and A.G. Roy. On the fractal interpretation of the mainstream length-drainage area relationship. Water Resources Research. 26:839-842, 1990.

Rodriguez-Iturbe, I., E. Ijjasz-Vasquez, R.L. Bras and D.G. Tarboton. Power-law distribution of discharge, mass and

energy in river basins. Water Resources Research 28(4):1089-1093, 1992a.

Rodriguez-Iturbe, I., A. Rinaldo, R. Rigon, R.L. Bras, A. Marani, and E.J. Ijjasz-Vasquez. Energy dissipation, runoff production and the three-dimensional structure of river basins. Water Resources Research. 28:1095-1103, 1992b.

Rodriguez-Iturbe, I., A. Rinaldo, R. Rigon, R.L. Bras, E.J. Ijjasz-Vasquez, and A. Marani. Fractal structures as least energy patterns: the case of river networks. Geophysical Research Letters. 19:889-892, 1992c.

Rodriguez-Iturbe, I. and J.B. Valdes. The geomorphologic structure of hydrologic response. Water Resources Research. 15(6):1409-1420, 1979.

Roth, G., F. Siccardi and R. Rosso. Hydrodynamic description of the erosional development of drainage patterns. Water Resources Research. 25(2):319-332, 1989.

Roy, A.G. Optimal angular geometry models for river branching. Geographical Analysis 15:87-96, 1983.

Ruhe, R.V. Geomorphology. Houghton Mifflin, Boston, 1975.

Sack, D. New wine in old bottles: the historiography of a paradigm change. Geomorphology. 5:251-264, 1992.

Scheidegger, A.E. A stochastic model for drainage patterns into an intramountane trench. Bulletin Association of Scientific Hydrology 12:15-20, 1967.

Scheidegger, A.E. Theoretical Geomorphology. Springer Verlag, Berlin, 1970.

Scheidegger, A.E. Systematic Geomorphology. Springer-Verlag, Vienna, 1987.

Schertzer, D. and S. Lovejoy. Non-linear Variability in Geophysics. Kluwer, Netherlands, 1991.

Schumm, S.A. The evolution of drainage systems and slopes in badlands at Perth Amboy. Bulletin of the American Geological Society 67(5):597-646, 1956.

Schumm, S.A., M.P. Mosley and W.E. Weaver. Experimental Fluvial Geomorphology. Wiley, New York, 1987.

Shreve, R.L. Statistical law of stream numbers. Journal of Geology. 74:17-37, 1966.

Shreve, R.L. Infinite topologically random channel networks. Journal of Geology. 75:178-186, 1967.

Shreve, R.L. Stream lengths and basin areas in topologically random channel networks. Journal of Geology. 77:397-414, 1969.

Smart, J.S. and C. Werner. Applications of the random model of drainage basin composition. Earth Surface Processes. 1:219-233, 1976.

Smith, T.R. and F.P. Bretherton Stability and the conservation of mass in drainage basin evolution Water Resource research 8(6):1506-1529, 1972

Snow, R.S. Fractal sinuosity of channels. Pure and Applied Geophysics. 131:99-109, 1989.

Sreenivasan, K.R. and C. Menevau. Singularities of the equations of fluid motion. Physical Review A. 38(12):6287-6295, 1988.

Sreenivasan, K.R., R.R. Prasad, C. Menevau and R. Ramshankar. The fractal geometry of interfaces and the multifractal distribution of dissipation in fully turbulent flows. Pure and Applied Geophysics. 131(1/2):43-60, 1989.

Stark, C.P. An invasion percolation model of drainage network evolution. Nature 352:423-425, 1991.

Stevens, P.S., Patterns in Nature, Little, Brown and Co, Boston, 1974.

Strahler, A.N. Davis' concepts of slope development viewed in the light of recent quantitative investigations. Annals, Association of American Geographers. 40:209-213, 1950.

Strahler, A.N. Hypsometric (area-altitude) analysis of erosional topography. Bulletin, Geological Society of America. 63:1117-1142, 1952.

Strahler, A.N. Quantitative/dynamic geomorphology at Columbia 1945-60: a retrospective. Progress in Physical Geography. 16(1):65-84, 1992.

Surkan, A.J. Synthetic hydrographs: effects of network geometry. Water Resources Research. 5(1):112-128, 1968.

Takayasu, H. and H. Inaoka. New type of self-organized criticality in a model of erosion. Physical Review Letters. 68:966-969, 1992.

Takayasu, H., I. Nishikawa and H. Tasaki. Power-law mass distribution of aggregation systems with injection. Physical Review A. 37:3110-3117, 1988.

Takayasu, M. Characterization of violent fluctuations by interval distributions of level sets. Physica A. 197:371-378, 1993.

Takayasu, M. and H. Takayasu. Apparent independence of an aggregation system with injection. Physical Review A. 39(8):4345-4347, 1989.

Tarboton, D.G., R.L. Bras, and I. Rodriguez-Iturbe, The fractal nature of river networks. Water Resources Research. 24:1317-1322, 1988.

Tarboton, D.G., R.L. Bras and I. Rodriguez-Iturbe. Scaling and elevation in river networks. Water Resources Research 25(9):2037-2051, 1989a.

Tarboton, D.G., R.L. Bras, and I. Rodriguez-Iturbe, The analysis of river basins and channel networks using digital terrain data. Report 326, Ralph M. Parsons Lab., Massachusetts Institute of Technology, Cambridge, 1989b.

Tarboton, D.G., R.L. Bras and I. Rodriguez-Iturbe A physical basis for drainage density Geomorphology 5(1/2) 59-76, 1992.

Taylor, A.B. and H.E. Schwarz, Unit hydrograph lag and peak flow related to basin characteristics. Transactions AGU. 33:235-246, 1952.

Tel, T. Fractals, multifractals and thermodynamics. Z. Naturforsch. 43a:1154-1174, 1988.

Tinkler, K.J.   A Short History of Geomorphology.   Barnes and Noble, New Jersey, 1985.

Tribe, A.   Automated recognition of valley heads from digital elevation models.   Earth Surface Processes and Landforms.   16:33-49, 1991.

Tribe, A.   Automated recognition of valley lines and drainage networks from grid elevation models: a review and a new method.   Journal of Hydrology.   139:263-293, 1992.

Troutman, B.M. and M.R. Karlinger.   On the expected width function for topologically random channel networks.   Journal of Applied Probability.   21:836-884,1984.

Troutman, B.M. and M.R. Karlinger.   Unit hydrograph approximation assuming linear flow through topologically random channel networks.   Water Resources Research.   21(5):743-754, 1985.

Troutman, B.M. and M.R. Karlinger.   Averaging properties of channel networks using methods in stochastic branching theory.   In: V.K. Gupta, I. Rodriguez-Iturbe and E.F. Wood.   (Eds.) Scale Problems in Hydrology.   Dordrecht, Holland: D. Reidel, 1986.

Vanoni, V.A.   Sedimentation Engineering.   ASCE, New York, 1975.

Vicsek, T.   Fractal Growth Phenomena.   World Scientific, Singapore, 1989.

Wejchert, J.   Optimally collecting networks.   Europhysics Letters.   9(6):503-508, 1989.

Werner, C.   Several duality theorems for interlocking ridge and channel networks.   Water Resources Research 27(12):3237-3247, 1991.

Willgoose, G., R.L. Bras and I. Rodriguez-Iturbe.   A physically-based channel network and catchment evolution model.   Report 322, Ralph M. Parsons Laboratory, Massachusetts Institute of Technology, Cambridge, 1989.

Willgoose, G., R.L. Bras and I. Rodriguez-Iturbe.   A coupled channel network growth and hillslope evolution model, 1. Theory.   Water Resources Research   27(7):1671-1684, 1991a

Willgoose, G., R.L. Bras and I. Rodriguez-Iturbe.   A coupled channel network growth and hillslope evolution model, 1. Non-dimensionalization and applications..   Water Resources Research   27(7):1685-1696, 1991b

Willgoose, G., R.L. Bras and I. Rodriguez-Iturbe   A physical explanation of an observed link area-slope relationship.   Water Resources Research 27(7):1697-1702, 1991c.

Willgoose, G., R.L. Bras and I. Rodriguez-Iturbe.   Results from a new model of river basin evolution.   Earth Surface Processes and Landforms   16:237-254, 1991d.

Wittman, R., T. Kautzky, A. Hubler and E. Luscher.   A simple experiment for the examination of dendritic river systems.   Naturwissenschaften.   78:23-25, 1991.

Woldenberg, M.J.   Spatial order in fluvial systems – Horton's laws derived from mixed hexagonal hierarchies of drainage basin areas.   Geological Society of America Bulletin.   80:97-112, 1969.

Woldenberg, M.J. and K. Horsfield.   Relation of branching angles to optimality for four cost principles.   Journal of Theoretical Biology.   122:204, 1986.

Wolman, M.G.   The natural channel of Brandywine Creek, Pennsylvania, US.   US Geological Survey Professional Paper 271, 1955

Yang, C.T.   Potential energy and stream morphology.   Water Resources Research 7(2):311-322, 1971.

Yang, C.T. and C.C.S. Song   Theory of minimum rate of energy dissipation.   Journal of the Hydraulics Division, ASCE, 105:769-784, 1979.

Young, R.A. and C.K. Mutchler.   American Society of Agricultural Engineers. Transactions.   12(2):231-239, 1969.

Zavoianu, I.   Morphometry of Drainage Basins.   Editura Academici, Bucharest, 1985.